UNIVERSITÉ DE MONTRÉAL

# STREAMWISE FLUIDELASTIC INSTABILITY OF TUBE ARRAYS SUBJECTED TO TWO-PHASE FLOW

STEPHEN OKOTH OLALA

DÉPARTEMENT DE GÉNIE MÉCANIQUE

ÉCOLE POLYTECHNIQUE DE MONTRÉAL

THÈSE PRÉSENTÉE EN VUE DE L'OBTENTION

DU DIPLÔME DE PHILOSOPHIAE DOCTOR

(GÉNIE MÉCANIQUE)

AOÛT 2016

UNIVERSITÉ DE MONTRÉAL

ÉCOLE POLYTECHNIQUE DE MONTRÉAL

Cette thèse intitulée :

STREAMWISE FLUIDELASTIC INSTABILITY OF TUBE ARRAYS SUBJECTED TO TWO-PHASE FLOW

présentée par : OLALA Stephen Okoth

en vue de l'obtention du diplôme de : Philosophiae Doctor

a été dûment acceptée par le jury d'examen constitué de :

M. REGGIO Marcelo, Ph. D., président

M. MUREITHI Njuki William, Ph. D., membre et directeur de recherche

M. GOSSELIN Frédérick, Doctorat, membre

M. MOHANY Atef, Ph. D., membre externe

# ACKNOWLEDGEMENTS

First and foremost I would wish to thank my research supervisor, Prof. Njuki W. Mureithi, for his support, motivation and encouragement. Without his constant feedback and guidance, this Ph.D. would not have been achievable.

I would also like to express my gratitude to the staff at Polytechnique Montréal who offered various technical assistance. Mr. Noor Aimène for instrumentation of the strain gauges and Mr. Benedict Bésner for helping with the electronic devices installation and configuration; his immense knowledge on instrumentation and National Instrument data acquisition systems is commendable. Special mention goes to Mr. Thierry Lafrance, currently of Mekanic inc., for his guidance on technical design and modification of the test section.

I cannot forget the contribution of Teguewinde Sawadogo, currently at CNL, for sharing his experience on experimentation at the initial stages of the Ph.D. project.

I am grateful to the BWC/AECL/NSERC Industrial Chair of Fluid-Structure Interaction (FSI) for the financial support to pursue the Ph.D. program. Special recognition is due to the members of the FSI lab, especially Abdallah Hadji and Hao Li for their availability, encouragement and criticism, and Cedric Benguin for his help in the translation process of “Résumé”.

To all the friends who helped me remain focused during the Ph.D. program, I say a big thank you.

Finally, I convey my deepest sense of gratitude and respect to my wife Florence and children, Imani, Adley and Marlone for their encouragement and unfailing love in spite of enduring my absence during the Ph.D journey.

# RÉSUMÉ

Les vibrations induites par les écoulements est une préoccupation majeure pour les concepteurs et les opérateurs des échangeurs de chaleur. Parmi les nombreux mécanismes d'excitation, l'instabilité fluide-élastique a été identifiée comme la source la plus catastrophique de défaillance de tube à court terme dans les faisceaux. Par conséquent, un certain nombre de théories ont été mis au point pour sa prédiction. Cependant, toutes ces théories ont été développées principalement pour l'écoulement de monophasique, même si les faisceaux de tubes dans les générateurs de vapeur fonctionnent principalement en écoulement diphasique.

L'objectif principal de ce projet de recherche est donc d'étendre les modèles théoriques de l'instabilité fluide-élastique aux écoulements diphasique, en particulier, par l'instabilité fluide-élastique dans le sens de l'écoulement avec de multiples tubes flexibles. Le modèle quasi-statique a été étudié dans le cadre du projet de recherche en cours. L'étude a été réalisée pour un faisceau de tube triangulaire tourné.

Premièrement, des tests expérimentaux ont été réalisés afin de déterminer les forces quasi-statiques sur une grappe de tubes soumis à un écoulement diphasique transverse eau-air. Les tests ont été effectués pour une série de taux de vide et un nombre de Reynolds (en fonction de la vitesse inter tubé), $\mathrm{Re} = 7.2 \times 10^4$. Les forces obtenues et leurs dérivés spatiales en fonction de la position du tube central de la grappe ont ensuite été utilisées pour effectuer une analyse quasi-statique de l'instabilité fluides-élastiques. Les vitesses prévues d'instabilité ont été jugés en assez bon accord avec les tests de stabilité dynamique. La stabilité du faisceau de tubes a été trouvée en fonction du nombre et de l'emplacement des tubes flexibles. Entant donné que l'effet du déphasage a été ignoré à ce stade, l'analyse a confirmé la prédominance du mécanisme contrôlé par la rigidité pour provoquer une instabilité fluide-élastique dans le sens de l'écoulement. L'effet de désaccorder dans les fréquences naturelles des tubes sur le seuil d'instabilité a aussi été exploré. On a constaté que cet effet a en général un effet stabilisant. Cependant, pour un grand écart initial dans une population de fréquences, il a été constaté qu'un plus petit échantillon tiré de la population plus large puisse parfois avoir un écart inférieur ou supérieur résultant d'une grande dispersion des valeurs possibles de la constante de stabilité.

Deuxièmement, les forces fluides instationnaires ont été mesurées sur la même grappe de tubes lorsque le tube central oscille dans la direction d'écoulement. Il a été trouvé que l'amplitude de la force de fluide instationnaire est une fonction dépendant uniquement de la vitesse réduite, et que pour des valeurs élevées de la vitesse réduite, elle est indépendante de la vitesse réduite. Les forces fluides induites sur les autres tubes ont cependant montré une dispersion importante probablement en raison de la faiblesse de la cohérence entre le mouvement du tube central et ces forces induites.

Les forces fluides instationnaires et les forces quasi-statiques obtenues dans la première série d'expériences ont ensuite été utilisées pour estimer, d'une part, le retard (déphasage) entre le mouvement du tube central et les forces de fluide sur lui-même et d'autre part, le retard entre le mouvement du tube central et les forces de fluide produites sur les tubes adjacents. Ce décalage temporel a été extrait pour chacun des tubes et le paramètre de retard et obtenu pour les taux de vide compris entre 60% et 90%. Ce paramètre de retard a montré une dépendance importante à la position du tube et au taux de vide.

Troisièmement, la masse ajoutée et l'amortissement indépendant de la vitesse de l'écoulement sur un tube contraint de vibrer seulement dans la direction de l'écoulement ont été déterminés expérimentalement. Il a été observé que la masse ajoutée diminue avec le taux de vide. L'amortissement d'autre part, augmente presque linéairement avec le taux de vide jusqu'à environ un taux de vide de 40%, puis reste relativement constant jusqu'à un taux de vide de 70%, puis enfin diminue à mesure que l'écoulement se rapproché d'un écoulement monophasique de gaz.

Finalement, avec tous les paramètres nécessaires obtenus, le modèle quasi-statique a été utilisé pour prédire la vitesse critique d'instabilité fluide-élastique dans le sens de l'écoulement pour de multiples combinaisons de tubes flexibles au sein d'un réseau de tube triangulaire tourné soumis à un écoulement diphasique. L'utilisation du paramètre de retard déterminé expérimentalement n'affecte pas de manière significative la prédiction de la vitesse critique d'instabilité fluide-élastique pour les multiples configurations analysées. Les résultats obtenus avec le modèle quasi-statique, lorsque le paramètre de retard a été omis, étaient toujours en assez bon accord avec les données expérimentales.

La présente analyse a, en particulier, démontré le potentiel du modèle quasi-stationnaire pour la prédiction du seuil d'instabilité fluides-élastiques dans le sens de l’écoulement dans des faisceaux de tubes soumis à un écoulement transverse diphasique.

# ABSTRACT

Flow induced vibration is a major concern to designers and operators of tube-and-shell heat exchangers. Among the several excitation mechanisms, fluidelastic instability has been identified to be the most catastrophic source of tube failure in the short term in tube bundles. Consequently, a number of theories have been developed for its prediction. However, all these theories were developed primarily for single phase flow even though tube arrays in steam generators operate mostly in two-phase flow.

The main goal of this research project is therefore, to extend the theoretical models for fluidelastic instability to two-phase flow, particularly, streamwise fluidelastic instability of multiple flexible tube arrays in two-phase flow. The quasi-steady model has been studied in the scope of the current research project. The study was conducted for a rotated triangular array of pitch-to-diameter ratio , $P/D = 1.5$.

Firstly, experimental tests were performed to determine the quasi-steady forces on a kernel of tubes subjected to two-phase air-water cross-flow. The tests were done for a series of void fractions and a Reynolds number (based on the pitch velocity), $\mathrm{Re} = 7.2 \times 10^4$. The forces obtained and their derivatives with respect to the static streamwise displacement of the central tube in the cluster were then used to perform a quasi-steady fluidelastic instability analysis. The predicted instability velocities were found to be in fairly good agreement with dynamic stability tests. Array stability was found to depend on the number and location of the flexible tubes. Since the effect of the time delay was ignored at this stage, the analysis confirmed the predominance of the stiffness-controlled mechanism in causing streamwise fluidelastic instability.

The effect of frequency detuning on the streamwise fluidelastic instability threshold was also explored. It was found that frequency detuning has, in general, a stabilizing effect. However, for a large initial variance in a population of frequencies, a smaller sample drawn from the larger population was found to sometimes have lower or higher variance resulting in a large scatter in possible values of the stability constant.

Secondly, the unsteady fluid forces on the same kernel of tubes were measured when the central tube was oscillated in the flow direction. The measured unsteady streamwise fluid force coefficient magnitude was found to be a single valued function of the reduced velocity, and

showed no dependence on the reduced velocity for high values of the reduced velocity. The cross-coupling fluid force phase, however, showed scatter possibly due to weak coherence between the central tube motion and the induced forces. The unsteady fluid forces together with quasi-steady forces obtained in the first set of experiments were then used to estimate, firstly, the time delay between the central tube motion and fluid forces on itself and secondly, the time delay between the central tube motion and the fluid forces generated on the adjacent tubes. The time lag/lead was extracted for each of the tubes and the time delay parameter obtained for void fractions between 60%-90% due to test loop limitations. The time delay showed significant dependence on tube position and void fraction.

Thirdly, the hydrodynamic mass and flow independent damping on a tube constrained to vibrate only in the streamwise direction in the array were experimentally determined. The hydrodynamic mass was observed to decrease with void fraction. The damping on the other hand, was found to increase almost linearly with void fraction till about 40% void fraction, remained fairly constant till 70% void fraction, then decreased as the flow approached single phase gas flow.

Finally, with all the necessary parameters obtained, the quasi-steady model was used to predict the critical velocity for streamwise fluidelastic instability of multiple flexible tubes in a rotated triangular tube array subjected to two-phase flow. The use of the experimentally determined time delays was found not to significantly affect the reduced critical velocity for streamwise fluidelastic instability of the multiple flexible tubes configurations analyzed. The results obtained with the quasi-steady model were in fairly good agreement with experimental data.

The present analysis has, in particular, demonstrated the potential of the quasi-steady model in predicting streamwise fluidelastic instability threshold in tube arrays subjected to two-phase cross-flow.

# TABLE OF CONTENTS

# LIST OF TABLES

# LIST OF FIGURES

# LIST OF SYMBOLS AND ABBREVIATIONS

| | |
|---|---|
| $A$ | Cross sectional area ($m^2$) |
| $[\mathbf{C}]$ | Damping matrix |
| $C_D$, $C_L$ | Drag coefficient, Lift coefficient |
| $C_{sh}$ | Dimensionless stiffness coefficient |
| $C_F$ | Unsteady fluid force coefficient |
| $C_{dh}$ | Dimensionless damping coefficient |
| $D$ | Tube diameter (m) |
| $E$ | Modulus of elasticity ( $N / m^2$ ) |
| FEI | Fluidelastic instability |
| $F_B$ | Buoyancy force (N) |
| $F_D$, $F_L$ | Corrected drag, lift force (N) |
| $F_{DM}$, $F_{LM}$ | Measured drag, lift force (N) |
| $F_{LS}$ | Measured lift force in stationary liquid (N) |
| $F_{measured}$ | Measured fluid force per unit length |
| $F_{Uns}$ | Unsteady fluid force per unit length |
| $F_{Uns\_cc}$ | Cross-coupling unsteady fluid force per unit length |
| $F_x$ | Streamwise quasi-steady force per unit length |
| $g$ | Gravitational acceleration ($m/s^2$), frequency dependent time delay parameter |
| $I$ | Moment of inertia ( $m^4$ ) |
| $[I]$ | Identity matrix |
| $j$ | $=\sqrt{-1}$ |
| $[\mathbf{K}]$ | Stiffness matrix |
| $K$ | Connors constant |

| | |
|---|---|
| $L$ | Tube length, distance between rows (m) |
| $l_s$ | Unsupported span length ( $m$ ) |
| $[\mathbf{M}]$ | Mass matrix |
| $m_s$ | Mass of tube per unit length |
| $m_h$ | Hydrodynamic mass per unit length |
| $P$ | Pitch between tubes (m) |
| $Q_g, Q_l$ | Gas, liquid volumetric flow rate ($m^3/s$) |
| $S$ | Distance between tubes (m), velocity slip ratio |
| SG | Steam generator |
| $U_\infty$ | Free-stream velocity (m/s) |
| $U, U_p$ | Pitch velocity (m/s) |
| $U_{eq}, U_c$ | Equivalent pitch velocity, critical velocity (m/s) |
| $U_r,$ | Relative velocity (m/s) |
| $x, y$ | Tube position in drag and lift direction (m) |
| $\mathbf{q}$ | Generalized coordinates vector |
| $\bar{\mathbf{x}}$ | Dimensionless displacement with respect to D |
| $\{\bar{\mathbf{x}}\}$ | Dimensionless displacement vector |
| $\tilde{\mathbf{x}}$ | Eigenvector |
| $f_n$ | Tube natural frequency (Hz) |
| $m, m_a$ | Structural, hydrodynamic mass per unit length (kg/m) |
| $t$ | Time (s) |
| $\rho_h, \rho_g, \rho_l$ | Two-phase, gas and liquid density ($kg/m^3$) |
| $\alpha, \beta$ | Void fraction |
| $\sigma$ | Standard deviation |
| $\delta$ | Logarithmic decrement of damping |

| | |
|---|---|
| $\mu$ | Dynamic viscosity, time delay parameter |
| $\phi_F$ | Phase angle |
| $\chi$ | Dimensionless displacement, drag direction |
| $\eta$ | Dimensionless displacement, lift direction |
| $\tau$ | Dimensionless time, time delay |
| $\zeta$ | Damping ratio |
| $\lambda$ | Eigenvalue, dimensionless frequency factor |
| $\omega, \omega_n, \omega_d$ | Circular frequency, undamped natural frequency, damped natural frequency (rad/s) |

# CHAPTER 1 INTRODUCTION

In a nuclear power plant, steam generators are used to convert liquid water to steam for purposes of driving turbines to produce electricity. Each of the steam generators contains thousands of tubes to maximize heat transfer. The "U" bend region of a recirculating-type nuclear steam generator experiences two-phase cross-flow that may induce structural vibrations and instability. Excessive vibrations could cause tube failure due to fatigue and fretting wear at the supports. These failures ordinarily lead to unscheduled plant shutdown and possible leakage of radioactive materials resulting in accidents and economic loss. Three mechanisms have been identified to be responsible for flow-induced vibrations in these components (Pettigrew & Taylor, 1991): turbulent buffeting which results from the unsteady forces developed on a tube due to exposure to the random pressure perturbations in the flow field, vortex shedding (flow periodicity) that leads to vibrations due to vortices shed when a fluid flows over a bluff body, and fluidelastic instability which is a self-excited mechanism in which vibrations result from the competition between energy input by the fluid and energy expended by the tubes. Of these vibration mechanisms, fluidelastic instability is the most dominant cause of tube failure in the short term, hence a major design consideration. As the flow velocity is increased, large tube vibrations occur. The larger the amplitude of the oscillation, the larger the resulting fluid dynamic force, leading to a rapid rise in oscillation amplitude with velocity. The velocity at which the fluidelastic forces balance the damping forces, characterized by a sharp increase in vibration amplitude, defines the threshold of fluidelastic instability and is referred to as the critical velocity. It is this critical velocity that is of importance to designing against fluidelastic instability.

Several theoretical models have been developed to deepen the understanding of fluidelastic instability phenomenon and estimate the critical velocity. These include the jet-switch model (Roberts, 1962), the quasi-static model (Blevins, 1974; Connors, 1970), the quasi-steady model (Price & Paidoussis, 1982, 1983), the unsteady model (Chen, 1983a, 1983b; Tanaka & Takahara, 1980), the semi-analytical model (Lever & Weaver, 1982, 1986a), the quasi-unsteady model (Granger & Paidoussis, 1996) and numerical models (Marn & Catton, 1990, 1991). Since these models were developed for single phase flow whereas most heat exchangers operate in two-phase flow, there is a need to extend and validate them in two-phase flow. All these models are carefully reviewed in this study.

Most of the reported flow-induced vibration experimental studies in two-phase flow have been done using air-water mixtures due to the high cost of operating steam-water loops. This raises the question of the validity of experimental results for tubes in a steam generator that, in practical situations, operate in steam-water mixtures. To overcome this problem, some researchers have used Freon due to the close proximity of its liquid/vapor density ratio to that of water/steam (Pettigrew & Taylor, 2009). However, Sawadogo (2016) recently demonstrated that there is no significant difference in the critical velocities obtained with both Freon and air-water mixtures. Air-water mixture is used in the present study.

Among the aforementioned fluidelastic instability models, the quasi-steady model (Price & Paidoussis, 1982, 1983) was chosen for the current study. This is due to the model's ability to overcome the challenges posed by the other models, namely: the complexity of the two-phase flow making the implementation of the semi-analytical model (Lever & Weaver, 1982, 1986a, 1986b) cumbersome; enhanced experimental effort required by the unsteady model (Chen, 1983b; Tanaka & Takahara, 1980), the apparent multi-valued functional relation between the unsteady fluid force coefficient and the reduced velocity (Inada et al., 2002; Mureithi et al., 2002) and weak correlation between the tube displacement and the resulting unsteady fluidelastic forces (Mureithi et al., 2002) in two-phase flow. The computational fluid dynamic capabilities, at present, still rely on the other theoretical models and are confined to low Reynolds numbers.

Studies conducted at the Fluid-Structure Interactions laboratory at École Polytechnique de Montréal by Shahriary et al. (2007) and Sawadogo & Mureithi (2014a, 2014b) successfully employed the quasi-steady model to investigate fluidelastic instability of tube bundles subjected to two-phase cross-flow. This model not only allowed the prediction of the critical velocity for instability but also the vibrational response of the cylinder as a result of fluid excitation.

The most important input parameters for the quasi-steady model are the quasi-steady forces and the time delay between tube displacement and the fluid forces generated thereby. Presently, the model has only been verified for vibration of a single flexible tube within a rotated triangular tube array in the transverse direction to the flow.

Until recently, most of the analysis on fluidelastic instability had been conducted for the direction transverse to the flow, after initial studies showed that fluidelastic instability occurred predominantly in that direction. However, recent tube failures at San Onofre Nuclear Generating

Station (SONGS) in U.S.A. (S.C.E., 2013) confirmed the possibility of fluidelastic instability occurring in the streamwise direction.

## 1.1 Objectives

The main goal of this Ph.D research project is to extend the existing knowledge on fluidelastic instability phenomenon in two-phase flows and validate the quasi-steady model for streamwise fluidelastic instability analysis. This is achieved by obtaining the necessary fluid force data through experimentation and employing the quasi-steady model to predict the critical velocity for streamwise fluidelastic instability of tubes in a rotated triangular array of $P/D = 1.5$.

To realize the global objective the project is divided into three phases. In the first phase, the flow direction quasi-steady fluid forces are experimentally determined for a central cluster of tubes in a rotated triangular array subjected to air-water two-phase flow. The derivatives of these forces are also obtained relative to the displacement of the central tube and, as a first approximation, the time delay is ignored. A stability analysis is then performed in the framework of the quasi-steady model to study the influence of the cross-coupling forces on the streamwise fluidelastic instability of the tube array under investigation. The effect of frequency detuning is also investigated in this phase. The quasi-steady fluid forces from this phase are passed on to the second phase to be used in the estimation of the time delay.

In phase two, the unsteady fluid forces on the kernel of tubes are measured to obtain the fluid force phases necessary for the estimation of the time delay. This is done for various excitation frequencies and void fractions. A wide range of flow velocities and frequencies are necessary to satisfy the assumption of the quasi-steady model whose input parameters are to be obtained. The method adopted for the extraction of the time delay requires the unsteady fluid forces and the corresponding quasi-steady fluid forces including their derivatives. The time delay parameters obtained in this phase are passed on to phase three.

Phase three is the analysis stage. Additional experiments are conducted to determine the flow independent damping and the hydrodynamic mass which are additional fluid-structure system characteristics. The parameters obtained in the previous phases are used to perform fluidelastic instability analysis for different configurations of the flexible tubes in the array. The results are then compared with dynamic test results in the literature to validate the model in two-phase flow.

## 1.2 Outline of the Thesis

The thesis begins with an introduction which includes the project objectives, methodology and the thesis outline. A detailed literature review follows in Chapter 2, focusing on flow induced vibration excitation mechanisms, theoretical models for fluidelastic instability and two-phase flow models.

The results are presented in the form of journal articles (Chapter 3-5). The first paper presented in Chapter 3 mainly focusses on the quasi-steady fluid forces. The second paper (Chapter 4) introduces the unsteady fluid forces and the time delay while the third paper (Chapter 5) presents the complete fluidelastic instability analysis using all the input parameters obtained in the previous papers/chapters. Model validation is also done in this chapter by comparing the model results with dynamic experiments' data.

Finally, a general discussion of the results is made in Chapter 6 and recommendations for future work introduced in the Conclusion.

# CHAPTER 2 LITERATURE REVIEW

## 2.1 Flow induced excitation mechanisms

Vibrations induced by fluid flow can be classified into three broad categories (Naudascher & Rockwell, 2005) namely forced vibrations, self-controlled vibrations and self-excited vibrations. Four excitation mechanisms have been identified for tube bundles subjected to cross–flow (Gorman, 1976; Pettigrew et al., 1991; Weaver, 1993): turbulent buffeting which is a forced vibration mechanism, vorticity shedding (Strouhal periodicity), and acoustic resonance which are self-controlled mechanisms, and fluidelastic instability, a self-excited mechanism. Figure 2-1 represents a typical vibratory response of a tube in a bundle subjected to cross-flow as a function of flow velocity (Blevins, 1990).

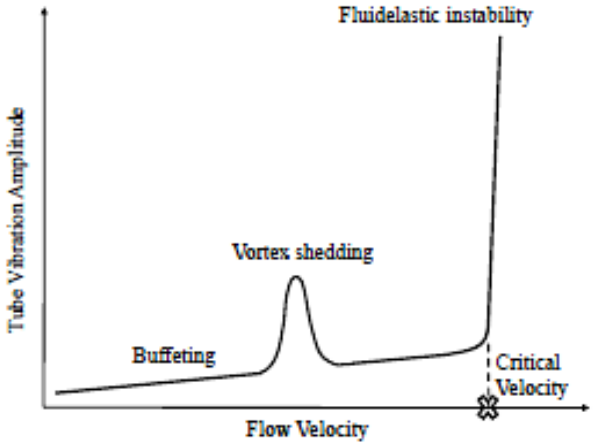


Figure 2-1 : Vibratory response of a tube in a bundle as a function of flow speed (Blevins, 1990).

### 2.1.1 Turbulent buffeting

Turbulent excitations result from the unsteady forces developed on a tube due to exposure to the random pressure perturbations in the flow field. Random velocity fluctuations from turbulent eddies spread over a wide range of frequencies producing random displacements of the tubes (Kuppan, 2000). While turbulent buffeting in steam generators is beneficial for heat transfer, the small vibration amplitudes caused by turbulence forces have to be estimated to determine the effective life of the equipment (Hassan et al., 2003). Turbulent buffeting in tube bundles is present at all flow velocities, but is only dominant before the critical velocity for fluidelastic

instability and vortex lock-in is reached. A detailed review of turbulent buffeting modeling techniques is introduced in Weaver *et al*. (2000)

### 2.1.2 Vortex shedding and general flow periodicities

Tube bundles subjected to cross-flow are generally excited by periodic fluid forces whose frequency vary linearly with flow velocity (Ziada & Oengoren, 1993). This phenomenon of periodic excitation is variously referred to in the literature as vortex shedding, periodic wake shedding or Strouhal excitation. There are many parameters that can affect the periodicity of vortex shedding. These include cylinder arrangement, cylinder pitch, upstream turbulence, vibration amplitude, surface roughness, two-dimensionality of the flow and the scale aspect ratio (Paidoussis, 1982). Vortex shedding on a single tube is markedly different from that in tube arrays where periodic forces have been noted in the upstream rows in single phase fluid flow. This periodicity is suppressed by turbulence deeper in the tube array (Weaver, 1993). Different array configurations experience different forms of periodicities. For instance, in staggered arrays, flow periodicity is caused by alternate vortex shedding from upstream rows whereas jet instability is the source of periodicity in normal square arrays (Weaver, 1993; Ziada & Oengoren, 1993). Ziada & Oengoren (1992) found that the flow structure, hence vortex shedding only occur in upstream rows for arrays with pitch-to-diameter, $(P/D)$, ratio less than 1.5 while it persists over the entire array for those with $P/D \geq 1.75$ in an in-line tube bundle configuration.

Vortex shedding causes fluctuations in the drag forces at a frequency twice that of the lift (Weaver et al., 2000) and is scaled using a non-dimensional frequency parameter, Strouhal number, $S_t$:

$$S_t = \frac{f_v D}{U} \tag{2-1}$$

where $f_v$ is the frequency of vortex shedding, D is the diameter of the cylinder and $U$ the fluid freestream velocity (Bearman, 1984). It is evident from Eq. (2-1) that the value of $S_t$ depends on the flow characteristics. For sub-critical flow $\left(40 \leq \mathrm{Re} \leq 2\times10^5\right)$, $S_t = 0.2$, while $S_t = 0.3$ for supercritical flow regime $\left(\mathrm{Re} \geq 3.5\times10^6\right)$ for circular cylinders. The transition between these two

regimes is not well defined (Paidoussis, 1982). Detailed discussion of vortex shedding in tube bundles may be found in Weaver et al. (1987) and Ziada (2006).

In a situation where the vibration amplitude is greater than $0.01D$ and the mass-damping parameter, $\frac{m\delta}{\rho D^2}$ is not too large, vortex shedding frequency may coincide with the cylinder natural frequency resulting in high amplitude oscillations, a phenomenon referred to as "lock-in". To avoid resonance and lock-in due to vortex shedding the natural frequency should be kept $\pm 40\%$ beyond $f_v$ (Paidoussis, 1982). Alternatively, one may reduce the vibration amplitude by increasing the structural damping.

### 2.1.3 Fluidelastic instability

The third excitation mechanism in tube bundles is the fluidelastic instability. This phenomenon can be described as a self-excited feedback mechanism between tube motion and fluid forces. If the feedback is positive, meaning that the fluid force has a component in the positive velocity direction, net damping will decrease as the fluid flow velocity increases. At a certain flow velocity, commonly referred to as critical velocity $(U_c)$, the net damping of the system vanishes, leading to high amplitude tube displacements potentially causing catastrophic failure. The spectrum of the response is characterized by a narrow peak revealing the absence of significant damping (Pettigrew & Taylor, 1991). To further illustrate what happens when the free stream flow reaches the critical velocity, consider a tube array subjected to cross flow as shown in Figure 2-2. The general equation of motion of the system may be expressed as:

$$[\mathbf{M}_s]\{\ddot{\mathbf{x}}\} + [\mathbf{C}_s]\{\dot{\mathbf{x}}\} + [\mathbf{K}_s]\{\mathbf{x}\} = \{\mathbf{F}_{\mathbf{ext}}\} \tag{2-2}$$

in which, $[\mathbf{M}_s]$ is the structural mass matrix, $[\mathbf{C}_s]$ is the structural damping matrix, $[\mathbf{K}_s]$ is the structural stiffness matrix, $\{\ddot{\mathbf{x}}\}$ is the tube acceleration vector, $\{\dot{\mathbf{x}}\}$ is the tube velocity vector, $\{\mathbf{x}\}$ is the tube displacement vector and $\{\mathbf{F}_{\mathbf{ext}}\}$ is the fluid force vector for tube array subjected to cross flow. $\{\mathbf{F}_{\mathbf{ext}}\}$ includes fluid added mass, fluid damping forces, and fluid stiffness forces which are all functions of the tube dynamics.

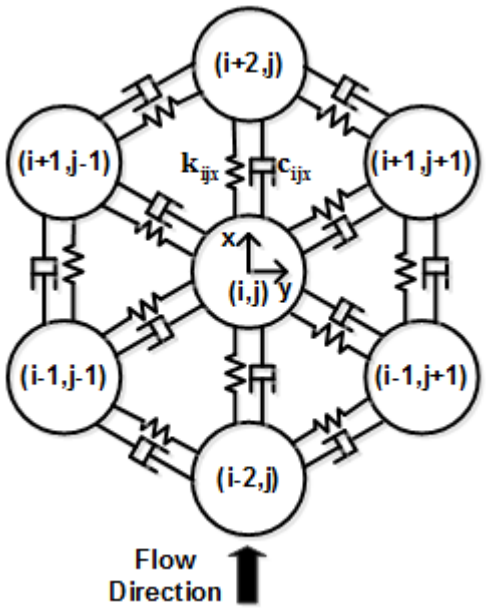


Figure 2-2 : Fluid coupling between adjacent tubes in an array

The system's equation of motion can therefore be written as:

$$\left([\mathbf{M}]_s + [\mathbf{M}]_f\right)\{\ddot{\mathbf{x}}\} + \left([\mathbf{C}]_s + [\mathbf{C}]_f\right)\{\dot{\mathbf{x}}\} + \left([\mathbf{K}]_s + [\mathbf{K}]_f\right)\{\mathbf{x}\} = \{\mathbf{0}\} \tag{2-3}$$

where $[\mathbf{M}]_f$ is the fluid added mass, $[\mathbf{C}]_f$ is the fluid damping and $[\mathbf{K}]_f$ is the fluid stiffness. The system is considered to be stable if the response motion diminishes with time, while it will be unstable if energy is fed into it through self-excitation with the response motion increasing with time (Rao, 2004). In order to guarantee system stability, both total damping and total stiffness terms in Eq. (2-3) should be positive.

Instability can be classified as either static or dynamic (Price, 1995). Static instability also known as divergence occurs when the negative fluid stiffness exceeds the structural stiffness leading to a negative total stiffness. As the total stiffness goes to zero the system's natural frequency, $\omega_n$, shown in Eq. (2-4), also tends to zero. Static instability is therefore characterized by a frequency of oscillation approaching zero at stability threshold. Static instability is rarely experienced in heat exchanger tube arrays as dynamic instability normally occurs before it.

$$\omega_n = \sqrt{\frac{K}{M}} \tag{2-4}$$

Dynamic instability on the other hand can be caused by two main mechanisms (Chen, 1983a, 1983b; Paidoussis & Price, 1988): damping controlled and stiffness controlled mechanisms. Damping-controlled mechanism is predominant for low mass-damping parameter, $\left(m\delta/\rho D^2\right)$ or high fluid density flows. This kind of instability occurs when the fluid force component in phase with the cylinder velocity overcomes the mechanical damping force leading to a negative total damping in the system. It only requires one-degree-of-freedom in which the destabilizing fluid force provides a negative damping effect. Stiffness-controlled instability which is predominant for low fluid density flows (high $m\delta/\rho D^2$ ), on the other hand, requires at least two-degrees-of-freedom (multiple-flexible tubes) such that the relative motion between tubes results in a net force that overcomes the structural damping.

### 2.1.4 Streamwise fluidelastic instability

A number of experimental studies (e.g. (Granger et al., 1993; Janzen et al., 2005; Mureithi et al., 2005; Nakamura et al., 2014; Roberts, 1962, 1966; Violette et al., 2006)) have reported observations of streamwise fluidelastic instability in both single- and two-phase flows. Roberts (1962), for instance, showed that instability was primarily in the streamwise direction (at least for tube rows) in liquid flow. Janzen et al. (2005) reported experimental evidence of streamwise two-phase flow induced fluidelastic instability in a rotated triangular U-tube array of pitch-to-diameter ratio, P/D=1.5. They observed streamwise fluidelastic instability in water flow and low-void fraction $\left(\leq 25\%\right)$ air-water two-phase flow. Mureithi et al. (2005) reported in-plane fluidelastic instability for a rotated triangular array with tubes preferentially flexible in the flow direction subjected to air flow. Their array $P/D=1.37$. Mureithi et al. (2005) determined streamwise fluidelastic instability for the case of fully flexible array and for a single flexible column in a rigid array. They, however, did not observe instability for a single flexible tube in a rigid array. Later, Violette et al. (2006) did a comprehensive experimental study of in-plane fluidelastic instability of a rotated triangular tube bundle of P/D=1.5 subjected to two-phase flow. They reported occurrence of fluidelastic instability for multiple tubes and not for a single tube only flexible in the flow direction. Recently, Nakamura et al. (2014) found that fluidelastic instability in the flow direction could occur at a lower critical flow velocity than that for the transverse flow direction in a fully flexible normal triangular array of small P/D (=1.2) subjected

to air flow. What is common in the above studies is the fact that streamwise fluidelastic instability was observed for multiple flexible tubes and not for a single flexible tube in a rigid array. This, therefore, suggests that streamwise fluidelastic instability is largely fluid stiffness controlled, requiring fluid coupling of different tubes in the array.

Details of the theoretical models for predicting fluidelastic instability in tube arrays subjected to cross-flow are discussed in section 2.3.

## 2.2 Two-phase flow induced vibrations

Even though numerous industrial components operate in two-phase flows, studies on vibration induced by this type of flow have grown only recently. The main excitation mechanisms in two-phase flows are turbulence and fluidelastic forces. Generally, forces due to the vortex shedding are absent for void fractions in excess of 15% (Taylor et al., 1989). The intensity and nature of the excitations induced by two-phase flows depend on several two-phase parameters which include void fraction, mass flow rate and flow regimes.

### 2.2.1 Two-phase flow models

The most important parameters in the study of vibrations induced by two-phase flows are void fraction, flow velocity and flow regime. Since measuring these parameters are complicated, several models have been developed for their estimation.

#### 2.2.1.1 Homogeneous model

The homogeneous model assumes a uniform flow through the cross section of the channel with the gas and liquid phases traveling at the same velocity. In this model, the void fraction is equal to the volumetric flow fraction and is given by:

$$\beta = \frac{Q_g}{Q_l + Q_g} \tag{2-5}$$

where Q is the volumetric flow rate, and the subscripts, $g$ and, $l$ denote the gaseous and liquid phases, respectively. The average homogeneous mass density and flow velocity of the two phase mixture are, respectively, expressed as:

$$\rho_h = \beta\rho_g + (1-\beta)\rho_l \tag{2-6}$$

and

$$U_\infty = \frac{\rho_g Q_g + \rho_l Q_l}{\rho_h A} \tag{2-7}$$

where $A$ is the cross-sectional area of the flow channel, $\rho$ is the mass density and the subscript, $h$ indicates homogeneous quantity. The pitch velocity, $U_p$, for tube bundles in cross-flow is defined as:

$$U_p = U_\infty \frac{P}{P-D} \tag{2-8}$$

where $U_\infty$ is the homogeneous velocity upstream of the tube bundles, $P$ the pitch spacing between tubes and $D$ the tube diameter.

The homogeneous model is widely used by researchers due to its simplicity, but under certain flow conditions, such as the case of vertical flow against gravity, the slip between the phases cannot be neglected. The homogeneous model gives best agreements in bubbly and dispersed or mist flow regimes where the entrained phase travels at nearly the same velocity as the uniform phase. The model is also the limiting case as the pressure tends towards the critical pressure, where the difference in phase densities disappears. Its use is also valid at very large mass velocities and at high vapor qualities (Thome, 2010).

#### 2.2.1.2 Feenstra model

In the Feenstra et al. (2000) model, void fraction is presented as a function of the velocity ratio, $S$, flow quality, $x$, and density ratio. A semi-empirical correlation is established between the velocity ratio and other flow parameters:

$$\beta = \left[1 + S\frac{\rho_g}{\rho_l}\left(\frac{1}{x} - 1\right)\right]^{-1} \tag{2-9}$$

The velocity ratio is given as:

$$S = \frac{U_g}{U_l} = 1 + 25.7\left(Ri \times Cap\right)^{0.5}\left(P/D\right)^{-1} \tag{2-10}$$

in which, $Ri$ is the Richardson number and $Cap$ the capillary number. The Richardson number represents the ratio between the buoyancy force and inertial force whereas the capillary number is the ratio between viscous force and the surface tension force, thus:

$$Ri = \Delta\rho^2 ga / G_p^2 \tag{2-11}$$

and

$$Cap = \eta_l U_g / \sigma \tag{2-12}$$

where, $U_g = \frac{xG_p}{\varepsilon\rho_g}$, $\Delta\rho^2$ denotes the square of the difference between the liquid and gas phase densities, $g$ is the gravitational acceleration, $a$ the gap between tubes, $G_p$ the pitch mass flux, $\eta_l$ the absolute viscosity of fluid phase, and $\sigma$, the surface tension. The Capillary number depends on the void fraction through the gas phase velocity. It therefore follows that calculation of the capillary number is an iterative process in which the velocity ratio is calculated using an iterative procedure. A better agreement with experimental results obtained using gamma ray densitometer has been realized with the Feenstra model compared to the homogeneous model (Feenstra et al., 2000).

### 2.2.2 Flow regimes

The nature of flow regimes inside tube bundles is an important factor in any study involving the prediction of two-phase flow-induced vibration phenomena, (Pettigrew & Taylor, 1994), therefore should not be neglected. The flow pattern may be influenced by several factors, such as surface tension, gravity, flow rates and density ratio of the gas to liquid phase.

The first flow regimes map in two-phase cross-flow was perhaps established by Grant & Murray (1972). Their study was conducted on a segmentally baffled transparent model heat exchanger of a rectangular cross section containing 39 tubes of 19 mm diameter and $P/D = 1.25$ arranged in a rotated triangular configuration. The bundle was subjected to a vertical two-phase cross-flow of air-water mixture. Based on visual observations, they distinguished three types of flow regimes: bubbly, intermittent and dispersed (spray) flow regimes.

Ulbrich & Mewes (1994) studied the flow regimes in a vertical air-water two-phase flow a cross a horizontal square inline tube bundle. They used visual observation with the aid of still and video photography over superficial liquid and gas velocities of 0.001-0.65 m/s and 0.047-9.3 m/s, respectively. Ulbrich & Mewes (1994) identified three distinct flow regimes: a bubbly flow regime characterized by a dispersion of roughly spherical gas bubbles, an intermittent flow regime characterized by irregular and chaotic distribution of gas in the liquid phase and a dispersed regime characterized by a distribution of liquid droplets in the gas phase. The flow regime map proposed by Ulbrich & Mewes (1994) and reproduced in Figure 2-3 is in good agreement with 85% of the data they considered, including those of Grant & Murray (1972).

Noghrehkar et al. (1999) studied the effect of bundle geometry on two-phase flow regimes. Their flow regime maps are reproduced in Figure 2-4. The results are similar to those of Grant & Murray (1972), Grant & Chishom (1979), and Ulbrich & Mewes (1994), except that the intermittent flow regime was not detected in the flow regime maps of Grant & Chishom (1979) and Ulbrich & Mewes (1994) for $J_L > 0.4\,\text{m/s}$ and $J_G \leq 9.3\,\text{m / s}$. This was attributed to the difference in methods used to define the flow regimes (Noghrehkar et al., 1999). According to Noghrehkar et al. (1999) the effect of bundle geometry on flow regimes is not significant at low values of superficial liquid velocities but the transition between bubbly and intermittent flow regimes is shifted to the right in the case of staggered tube arrays. Indeed, in staggered tube bundles, tubes break up the gas phase into smaller bubbles and pockets of gas and tend to mix the two phases, thereby delaying the occurrence of intermittent flow regime.

Whereas Ulbrich & Mewes (1994) determines the different flow regimes from the variation of pressure drop, Noghrehkar et al. (1999) uses probability density function profiles of the flow hence able to detect possible differences in the flow structure deep inside the array and at the proximity of the channel wall. These maps are used in the current study to identify approximate flow regimes for the different experimental conditions.

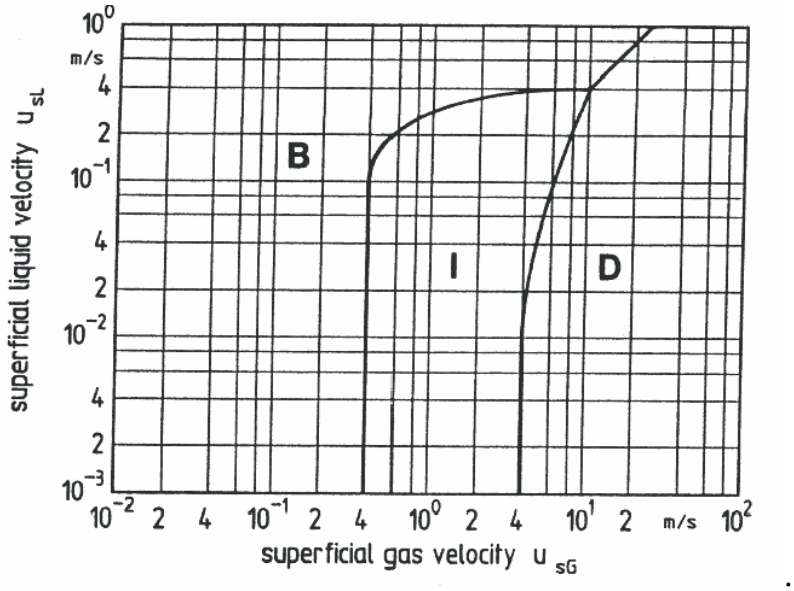


Figure 2-3 : Flow regime map proposed by Ulbrich & Mewes (1994). B-Bubbly, I-Intermittent and D-Dispersed

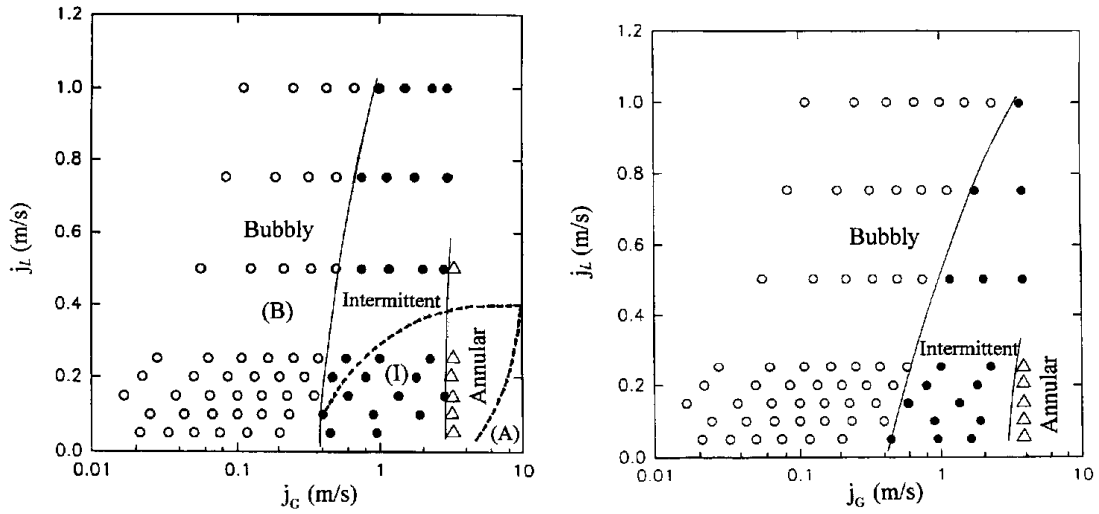


(a) In-line tube bundle (b) staggered tube bundle

Figure 2-4 : Flow regime maps proposed by Noghrehkar et al. (1999): Comparison with Ulbrich & Mewes (1994) map in dotted lines. (a) In-line tube bundle (b) staggered tube bundle

### 2.2.3 Added mass (hydrodynamic mass)

Hydrodynamic mass, $m_h$, is the equivalent external mass of the fluid vibrating with the tube (Pettigrew & Taylor, 2003). Hydrodynamic mass is related to the tube natural frequency and is expressed as (Carlucci & Brown, 1983):

$$m_h = m_s\left[\left(\omega_a/\omega\right)^2 - 1\right] \tag{2-13}$$

where $m_s$ is the structural mass per unit length, $\omega_a$ the tube angular natural frequency in air and $\omega$ the frequency of vibration. Hydrodynamic mass per unit length of a tube within a tube array may be expressed as (Pettigrew, Taylor, et al., 1989) :

$$m_h = \frac{\pi}{4}\rho_h D^2\left[\frac{\left(D_e/D\right)^2 + 1}{\left(D_e/D\right)^2 - 1}\right] \tag{2-14}$$

in which $\rho_h$ is the homogeneous two-phase density, $D$ the cylinder diameter, $D_e$ the hydraulic diameter and the ratio $D_e/D$ the array confinement parameter. $D_e/D = \left(0.96 + 0.5P/D\right)P/D$ for a tube inside triangular tube bundle (Rogers et al., 1984) and $D_e/D = \left(1.07 + 0.56P/D\right)P/D$ for a square tube bundle (Pettigrew & Taylor, 1994). The formulation of Pettigrew, Taylor, et al. (1989) yields results in good agreement with experimental data for in-line arrays. It, however, underestimates the hydrodynamic mass for staggered arrays, more so for high void fractions. Nevertheless, hydrodynamic mass is not a dominant factor in most practical applications since it is often only a small fraction of the overall mass, especially at high void fractions.

### 2.2.4 Damping

Damping is a measure of the structure's ability to dissipate vibratory energy. The total damping ratio, $\zeta_T$, in two-phase cross flow may be written in the following manner (Carlucci, 1980; Pettigrew et al., 1986; Pettigrew & Taylor, 2003):

$$\zeta_T = \zeta_V + \zeta_{SF} + \zeta_F + \zeta_{FD} + \zeta_{2\phi} \tag{2-15}$$

where $\zeta_V$ is the viscous damping ratio, $\zeta_{SF}$ the squeeze-film damping ratio, $\zeta_F$ the friction damping ratio, $\zeta_{FD}$ the flow-dependent damping ratio, and $\zeta_{2\phi}$ the two-phase damping ratio.

The friction damping ratio is estimated as:

$$\zeta_F = 5\left(\frac{N-1}{N}\right)\left(\frac{L}{l_m}\right)^{1/2} \tag{2-16}$$

in gases and

$$\zeta_F = 0.5\left(\frac{N-1}{N}\right)\left(\frac{L}{l_m}\right)^{1/2} \tag{2-17}$$

in liquids. In the above relations, $N$ is the number of tube spans, $L$ support thickness, and $l_m$, the span length. This type of damping, as the name suggests, emanate from friction between tubes and tube-supports.

Fluid viscous damping is given as (Pettigrew et al., 1986):

$$\zeta_V = \frac{100\pi}{\sqrt{8}}\left(\frac{\rho_h D^2}{m}\right)\left(\frac{2\nu_{TP}}{\pi f D^2}\right)^{1/2}\left\{\frac{\left[1+\left(D/D_e\right)^3\right]}{\left[1-\left(D/D_e\right)^2\right]^2}\right\} \tag{2-18}$$

where $\nu_{TP}$ is the equivalent two-phase kinematic viscosity given by (McAdams et al., 1942):

$$\nu_{TP} = \nu_l \Big/ \left[1+\beta_g\left(\nu_l/\nu_g - 1\right)\right] \tag{2-19}$$

Viscous damping is generally small for void fractions above 40% (Pettigrew & Taylor, 2003), but significant for lower void fractions.

Squeeze-film damping ratio can be estimated by (Pettigrew et al., 1986):

$$\zeta_{SF} = \left(\frac{N-1}{N}\right)\left[\frac{1460}{f}\left(\frac{\rho D^2}{m}\right)\left(\frac{L}{l_m}\right)^{1/2}\right] \tag{2-20}$$

Pettigrew & Taylor (1997) proposes a semi-empirical expression for the two-phase damping ratio as shown below:

$$\zeta_{TP} = 4.0\left(\frac{\rho_l D^2}{m}\right)\left[f\left(\beta_g\right)\right]\left\{\frac{\left[1+\left(D/D_e\right)^3\right]}{\left[1-\left(D/D_e\right)^2\right]^2}\right\} \tag{2-21}$$

where $f\left(\beta_g\right) = \beta_g/40$ for $\beta_g < 40\%$; $f\left(\beta_g\right) = 1$ for $40\% \le \beta_g \le 70\%$ and $f\left(\beta_g\right) = 1-\left(\beta_g - 70\right)/30$ for $\beta_g > 70\%$.

For the work reported in this thesis, only two categories of damping are considered: flow independent and flow dependent damping. Squeeze film and friction damping are not considered

since no tube supports are included in the test setup. In the experimental set up used for the current work, it is not possible to isolate the two-phase damping from the viscous damping, thus the two are measured together as flow independent damping.

Table 2-1 : Comparison of the physical properties of two-phase mixtures of air-water, steam-water, Freon R-11 and Freon R-22 (Feenstra et al., 1995; Feenstra et al., 2002)

| **Quantity** | **Air-water** | **Steam-water** | **R-11** | **R-22** |
|---|---|---|---|---|
| Temperature $\left(^{o}C\right)$ | 22 | 260 | 40 | 23.3 |
| Pressure $\left(kPa\right)$ | 101 | 4700 | 175 | 1000 |
| Liquid phase density $\left(kg/m^{3}\right)$ | 998 | 784 | 1440 | 1197 |
| Gas phase density $\left(kg/m^{3}\right)$ | 1.2 | 23.7 | 9.7 | 42.3 |
| Liquid phase dynamic viscosity $\left(\mu Pa*s\right)$ | 959 | 103 | 356 | 168 |
| Gas phase dynamic viscosity $\left(\mu Pa*s\right)$ | 18.2 | 17.8 | 11.5 | 12.4 |
| Liquid phase surface tension $\left(N/m\right)$ | 0.073 | 0.0238 | 0.0167 | 0.0074 |
| Density ratio $\left(\rho_{L}/\rho_{G}\right)$ | 832 | 33 | 148 | 28 |
| Viscosity ratio $\left(\mu_{L}/\mu_{G}\right)$ | 46 | 6 | 31 | 13 |

### 2.2.5 Types of two-phase mixtures

A majority of flow-induced vibration studies have been conducted in single phase flow; gas or liquid. Additionally, most of the reported experimental studies in two-phase flow are done in air-water mixture, yet more than one-half of all steam generators operate in steam-water flow

(Pettigrew & Taylor, 1994). As is seen in Table 2-1, the main two phase parameters vary from mixture to mixture thus, raising the question of the applicability of the laboratory experimental results to prototypical steam generator operating conditions. To overcome this challenge, some studies (e.g. (Pettigrew et al., 1995), (Pettigrew & Taylor, 2009), (Feenstra et al., 1995) ) have used Freon due to the close proximity of its liquid/vapor density ratio to that of water/steam as is evident in Table 2-1. However, in the study reported in this report, air-water mixture is used. Recently, Sawadogo (2016) demonstrated that there is no significant difference in the critical velocity for fluidelastic instability of a rotated triangular tube array of $P/D=1.5$ obtained with the array subjected to either two-phase Freon or air-water mixture.

## 2.3 Theoretical models for fluidelastic instability

As an aid to steam generator designers, ASME has recommended some design guidelines in the form of stability maps in which fluidelastic instability experimental data for different tube bundle geometrical configurations are plotted (Figure 2-5). A lower bound of this data is considered to be the stability threshold.

In as much as the design guideline has been an attempt to standardize steam generator production, it fails to provide information on the physics of the problem hence limits room for future improvements in steam generator design (Weaver, 2008). A number of models have been developed to predict the occurrence and improve understanding of the nature of the phenomenon of fluidelastic instability. These models are described in this section.

### 2.3.1 Jet-switch model

Roberts (1962, 1966) was the first to study self-excited oscillations of single and double row of cylinders subjected to cross-flow. His investigations showed that instability was primarily in the streamwise direction (at least for tube rows). Roberts (1962) considered the flow downstream of two adjacent cylinders to comprise two unequal wake regions supplied by a jet flow between them as illustrated in Figure 2-6.

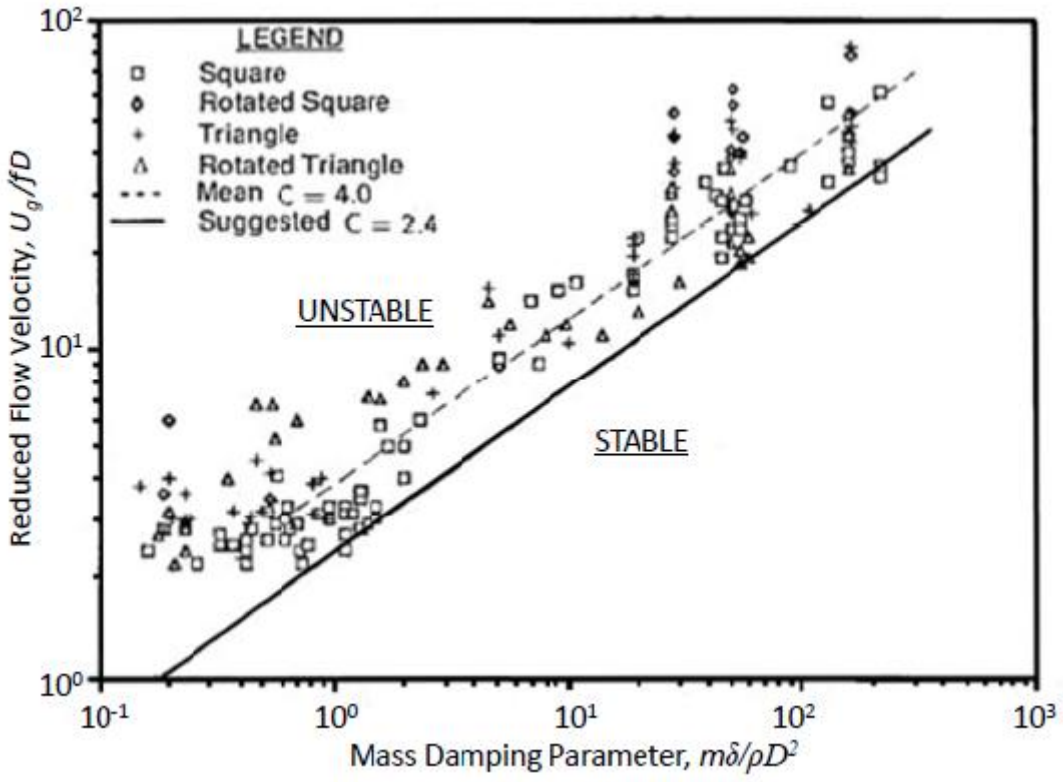


Figure 2-5 : ASME fluidelastic instability design guideline map for heat exchangers (Weaver, D.S. & Fitzpatrick, J. A., 1988)

He contended that instability would occur if the jet-switching mechanism synchronized with tube motion in such a way that net energy was absorbed by the cylinder. Roberts developed a semi-empirical model relating the critical velocity, $(U_c)$, for fluidelastic instability to the mass-damping parameter $\left(m\delta/\rho D^2\right)$ in the following manner:

$$\frac{U_c}{\omega_n \varepsilon D} = K\left(\frac{\delta m}{\rho D^2}\right)^{1/2} \tag{2-22}$$

where $\omega_n, D, \delta, m$ , $\varepsilon$ , $\rho$ and $K$ are the tube natural frequency, the outer diameter of the cylinder, the logarithmic decrement of damping, the mass per unit length , the ratio of fluidelastic frequency to structural frequency , the fluid density and a constant obtained from experiments, respectively.

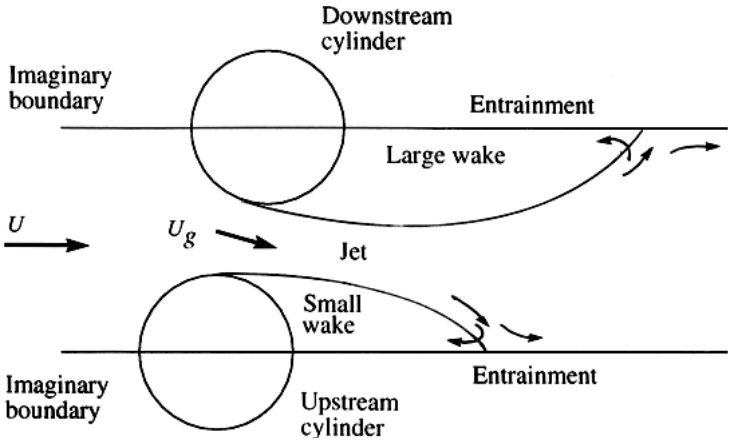


Figure 2-6 : Idealized model of jet-flow between two cylinders in a staggered row of cylinders (Roberts, 1962)

The key assumptions of Roberts (1962) model are as follows. First, single or double rows of cylinders can be used to model fluidelastic instability in tube arrays. Second, the pressure in the wake regions behind the cylinders is constant resulting in a constant pressure difference across the jet. Third, the flow separates at the minimum gap between cylinder centers, and fourth, the fluid flow is inviscid in the jet region and upstream of the separation points. As shown in Figure 2-7, Roberts' stability boundary is in good agreement with empirical data for higher mass damping parameter values while it overestimates the reduced critical velocity, $\left(U_c / f_n D\right)$ for lower values of mass damping parameter (Price, 1995). It is therefore evident that the jet-switching model proposed by Roberts (1962, 1966) does not accurately describe the nature of fluidelastic instability for the entire range. To clarify Roberts' analysis, Seitanis et al. (2005) performed experiments in which they varied the mean location of the in-flow flexible tubes. In their case, they found negative fluid stiffness to be the excitation mechanism and not jet-switching as earlier reported by Roberts (1966). Roberts is, however, credited with identifying, for the first time, self-excited vibration as a source of failure in heat exchanger tube arrays. He also performed dimensional analysis and presented the reduced velocity and damping parameter relations which are still being employed in defining stability boundaries to date.

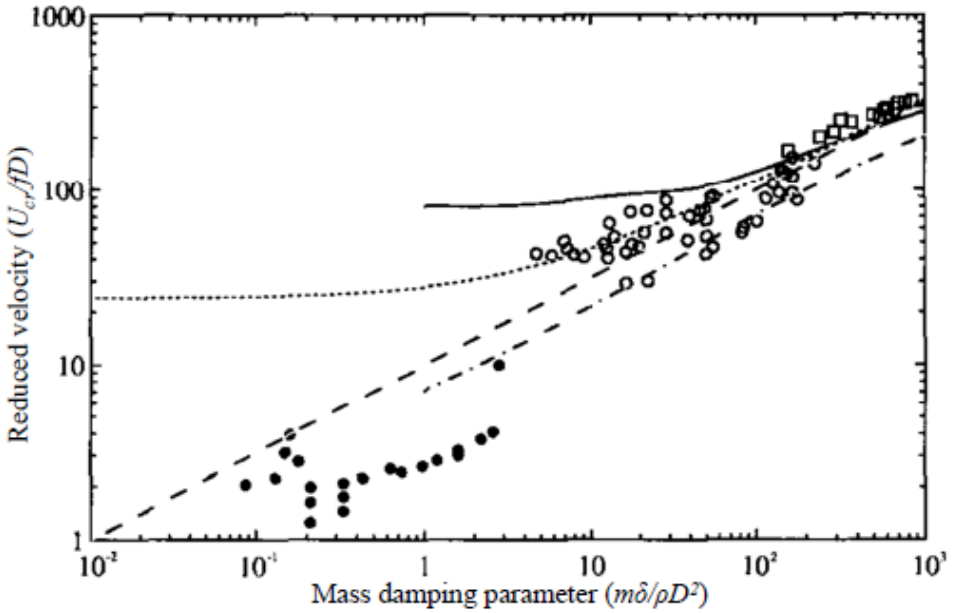


Figure 2-7 : Comparison between theoretical and experimental fluidelastic instability boundaries; ○, multiple flexible tubes in liquid flow; ●, multiple flexible tubes in gas flow; □, single flexible tube in gas flow; (─), Roberts(1966); (---), Connors (1970); (…), Blevins (1974). Adapted from (Price, 1995)

### 2.3.2 Quasi-static model

This model, developed by Connors (1970), was based on experiments involving a single row of cylinders. Connors (1970) observed whirling of alternate cylinders predominantly in either in-flow or transverse directions. He simulated his observations by moving the two nearby cylinders in either a symmetric or antisymmetric patterns and measuring the resulting fluid forces on the central cylinder (see Figure 2-8). By performing energy balance for the two directions, Connors (1970) managed to derive a relationship between the critical flow velocity for fluidelastic instability and the mass damping parameter as shown in Eq. (2-23):

$$\frac{U_c}{f_n D} = K\left(\frac{m\delta}{\rho D^2}\right)^{1/2} \tag{2-23}$$

where $f_n$ the cylinder natural frequency and $K$, the Connors constant, $m$ cylinder mass per unit length including the fluid added mass. Connors (1970) found the value of K to be 9.9 for his specific case. Blevins (1974) later found the value of K to be dependent on the array geometry

and fluid characteristics. Even though Connors equation emanated from data based on a single row of cylinders and the assumption that oscillation of neighboring cylinders at the same frequency is necessary for fluidelastic instability, the model has been the most widely used in the design of various tube bundles with different geometric patterns. Weaver & Elkashlan (1981a) studied the influence of mass ratio and damping on fluidelastic instability. They noted, contrary to the Connors equation (Eq. (2-23)), that the fluid damping $\delta$ and mass ratio $m/\rho D^2$ terms are not linearly related and re-wrote Eq. (2-23) as follows:

$$\frac{U_c}{fD} = K\left(\frac{m}{\rho D^2}\right)^{n_1} \delta^{n_2} \tag{2-24}$$

in which $n_1$ and $n_2$ are additional constants. Weaver & Elkashlan (1981b) established that the fluidelastic instability threshold in tube bundles is influenced by the number of rows thereby discounting the previous hypothesis by Robbers (1962) and Connors (1970) that a single row of tubes could be representative of the whole bundle. They recommended usage of not less than six tube rows to obtain typical stability behavior of a tube array. Weaver & Koroyannakis (1982) conducted experiments to study tube array response in both air and water flows. They noted that the variation of tube response frequency in water was more pronounced than in air flow, an effect they attributed to the effect of surrounding tube vibration mode on the added mass term which is more significant in water than air flows.

Blevins (1974, 1977, 1979a) re-derived Eq. (2-23) by considering the fluid forces to be single valued functions of the relative displacements of the neighboring tubes. This assumption was later disproved by Price & Paidoussis (1986a) who contended that it is the absolute motion of the individual cylinders and not the relative motion between them which is important. Price (1995) compared the stability boundaries obtained from available experimental data with that obtained by Connors model (Figure 2-7) showing that the quasi-static model underestimates the critical velocity for fluidelastic instability.

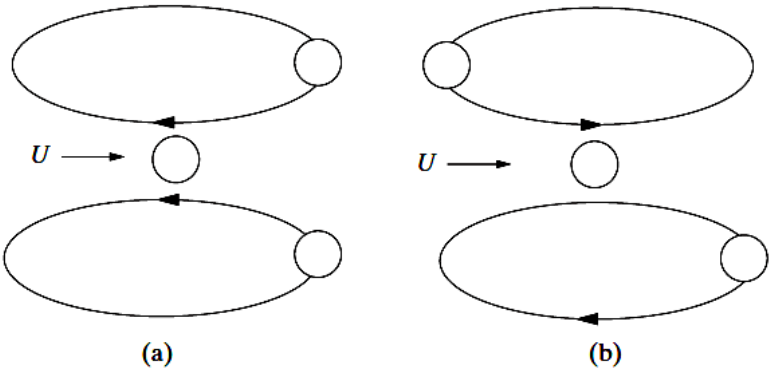


Figure 2-8 : Idealized cylinder motion of neighboring cylinders used by Connors (1970) during force measurements on the central cylinder: (a) symmetric motion (b) antisymmetric motion (Païdoussis et al., 2011)

### 2.3.3 General unsteady models

The unsteady models rely on directly measured dynamic fluid forces on the oscillating cylinder. Tanaka & Takahara (1980, 1981) measured the fluid dynamic forces generated on neighboring tubes by harmonically exciting a central tube in an in-line tube array. Their assumption was that fluid forces on a cylinder, $C$, in the array are affected only by its own motion and that of the immediate neighboring tubes as illustrated in Figure 2-9.

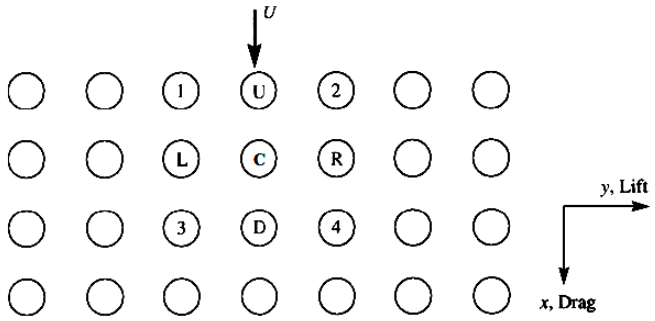


Figure 2-9 : Representation of cylinder numbering system used by Tanaka & Takahara (1980).

In their stability analysis, Tanaka & Takahara (1980, 1981) obtained a discontinuity in the stability boundary curves for mass ratio in the range of $50 \le m/\rho D^2 \le 500$. This discontinuity varied with the value of the logarithmic decrement of damping, $\delta$. They concluded that the instability mechanisms above and below this range are two different phenomena.

Later, Tanaka et al. (1982) conducted unsteady fluid force measurements on a single flexible cylinder free to oscillate only in the lift direction in an otherwise rigid array. Discontinuity was again observed in the stability curves leading the authors to conclude that it could not be as a result of a fundamental change in the instability mechanisms (instability of a single flexible cylinder is always due to negative damping (Chen, 1983a)).

Even though Tanaka & Takahara's unsteady model display's good agreement with experimental results, the experimental effort involved can be prohibitive for practical heat exchanger design.

Chen (1983a, 1983b) showed that fluidelastic instability is caused by two distinct mechanisms: damping and stiffness mechanisms. The fluid damping controlled instability is the dynamic instability caused by fluid damping forces which, at certain flow velocities, may act as excitation mechanism for the structural oscillations leading to a reduction in system damping. When the flow velocity exceeds a certain critical value, the total damping becomes negative and the system loses stability.

The stiffness mechanism results from position dependent fluid forces. The coupling between tube vibrations in the array and the fluid flow generate fluidelastic forces which necessarily augment the overall system stiffness. With increasing flow velocity, the fluidelastic forces increase leading to a decrease in system modal damping. At some critical flow velocity the modal damping becomes negative making the system unstable. The existence of the two mechanisms was later confirmed by Paidoussis & Price (1988), and Yetisir & Weaver (1993a, 1993b).

Little (2003) measured the total damping in a fully flexible parallel triangular tube bundle subjected to air cross flow and found that the sign of total system damping changes from positive to negative at instability.

Chen (1983a, 1983b) developed a mathematical model using force measurements obtained by Tanaka & Takahara (1980) in which he coupled the fluid forces with the tube equations of motion. His stability boundary maps were in good agreement with Tanaka & Takahara (1981) experimental results. Chen's model predicted existence of multiple stability regions and explained the discontinuity in the experimental results of Tanaka & Takahara (1981) indicating the boundary between damping and stiffness controlled instabilities for velocities less and greater than the discontinuity, respectively. However, the existence of practical multiple stability boundaries are "doubtful" (Paidoussis et al., 1996).

### 2.3.4 Semi-analytical models

Lever & Weaver (1982) presented a semi-analytical approach for the determination of the fluidelastic instability threshold. They experimentally determined that a single flexible cylinder in an otherwise rigid array essentially had the same stability threshold as that of a fully flexible array. Lever & Weaver (1982) divided the flow through the cylinder array into wake regions and flow channel which they called stream tubes as illustrated in Figure 2-10. From flow visualization, they observed that the fluid flowed through the channels with approximately the same channel width. The flow through the stream tubes was assumed to be incompressible, one dimensional and friction losses accounted for by a pressure drop term. Fluidelastic excitation was assumed to be independent of the wake phenomena thus only perturbations in the stream tubes on either side of the flexible tube were considered. In this model, the stream tube disturbance over the flow attachment length is considered to be in phase with the tube motion, while a finite time delay is required for the disturbance caused by the tube vibration to propagate downstream.

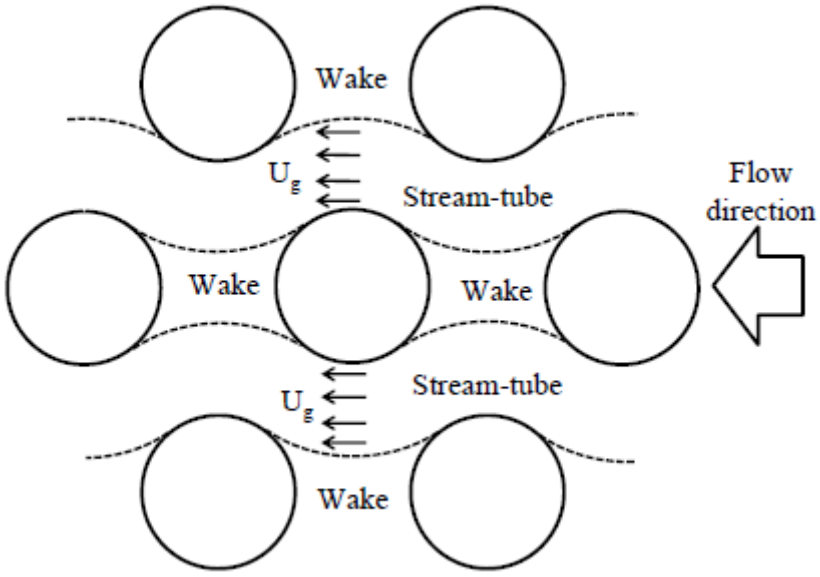


Figure 2-10 : Typical flow pattern through a staggered tube array

The authors assumed the time delay to originate from the fluid inertia and be equal to the time required by the flow to reorganize its pattern when the tube vibrates. Lever & Weaver (1982) modeled the time delay in the form of a phase lag function $\phi(s)$, as shown in Eq. (2-25), where

, $\phi$, is a phase representing the time delay, $U_g$, mean gap velocity, $f_n$, tube vibration frequency and $s$, the distance from the vibrating tube.

$$\phi(s) = \frac{4\pi f_n s}{U_g} \tag{2-25}$$

Since the flow in the stream tubes is dependent on the array geometry and with the knowledge of the cross-sectional area in space and time, Lever & Weaver (1982) applied one dimensional unsteady Bernoulli's equation to solve the flow field in the channels. To predict the tube response, they integrated the pressures over the flow attachment length on both sides of the tube and obtained the fluid forces which are coupled with the tube motion. The stability boundaries are then obtained by setting the damping term in the tube equation of motion to zero. Stability boundaries obtained by the Lever and Weaver model showed similar trends as experimental data in spite of its simplicity as shown in Figure 2-11. The theoretical model of Leaver and Weaver (1982) predicted multiple stability boundaries in the lower mass damping parameter regions similar to what Chen (1983a) found.

The manner in which the time delay is presented in the Lever & Weaver model (Eq. (2-25)) was challenged by Price (1995) who stated that this semi-analytical model required inclusion of some empirical quantities, for example, the pressure drop term used to present the friction losses in the array, the attachment and separation points in the channel and the length of the stream tube. Leaver & Weaver (1986a, 1986b) studied the effect of these parameters on the model, and showed that they had minor effects on the stability boundaries. Varying the time delay parameter was, however, found to significantly affect the stability boundary of the Lever & Weaver model (Weaver, 2008).

To further refine the model, Yetisir & Weaver (1993a, 1993b) accounted for in-flow tube motion, considered a fully flexible array and introduced a generic function to model the decay of perturbations caused by the tube vibrations upstream. They also unconstrained the tube response frequency which was constrained by Lever & Weaver (1982) to be equal to the tube natural frequency. These modifications by Yetisir & Weaver (1993a, 1993b) showed that fluidelastic instability at low mass damping parameters is attributed mainly to the damping mechanism and to the stiffness mechanism at high mass damping parameters. No significant differences were

reported between the stability boundaries of Yetisir & Weaver (1993b) and those of Lever & Weaver (1982).

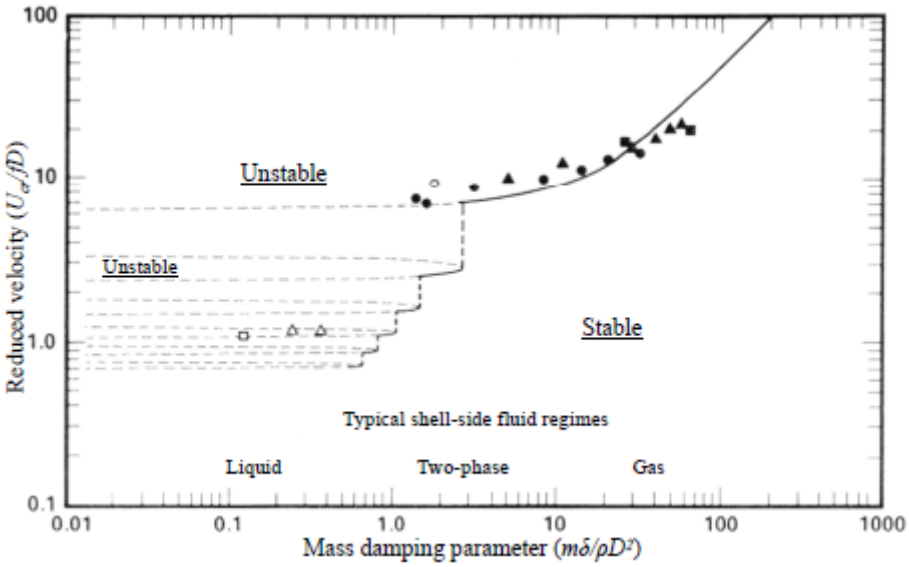


Figure 2-11 : Theoretical stability boundaries for fluidelastic instability obtained by Lever & Weaver (1986b) for a single flexible tube in a parallel triangular tube array $P=1.375$; $(-)$, practical stability boundary, $(---)$, theoretical stability boundary.

Initially, the model by Lever & Weaver could only be applied to fluidelastic vibrations of a single tube in the lift direction, however, it has since been extended to multiple flexible tubes and has recently been used to analyze streamwise fluidelastic instability (Hassan & Weaver, 2016) of a tube array in single phase flow.

### 2.3.5 Computational fluid dynamic models

Due to the complexity and relatively large computational resources required to handle fluid-structure interaction problems, use of computational fluid dynamics (CFD) simulations in the study of fluidelastic instability phenomenon in tube arrays started gaining prominence in the early 1990s. Marn & Catton (1990) presented a code based on one-dimensional unsteady integral approach to investigate flow-induced vibrations in tube bundles. Later, Marn & Catton (1991) considered a column of cylinders in an array of rigid cylinders and assumed the flow to be two-dimensional. Fluid variables such as pressure and velocity were divided into two parts: one

constant part representing the mean and the other fluctuating and solely due to the tube motion. The fluid forces obtained by integrating the pressure around the tube were then applied to the vibrational equation of motion. Marn & Catton (1992) extended their numerical model to two-phase flow, however, the analysis was considered too simplistic to be of any practical application (Price, 1995).

Eisinger et al. (1995) developed a finite element model of an in-line tube array using ABAQUS, a commercial finite element software and incorporated the same fluid forces used in Chen's (1983a, 1983b) unsteady model. The numerical results were in good agreement with the experimental data of Chen & Jendrzejczyk (1983). Schroder & Gelbe (1999b) in an attempt to improve their design guidelines for fluidelastic instability (Schroder & Gelbe, 1999a) came up with two- and three- dimensional models for a row of flexible tubes. They implemented different turbulence models and found that the $k-\omega$ model gave the most satisfactory results. Their results for the pressure coefficients obtained from numerical simulation was in good agreement with experimental results, nevertheless, the same agreement was not achieved for fluidelastic instability patterns. Hassan et al. (2010) developed a numerical estimation for the fluidelastic instability threshold in tube arrays. They solved the flow using Reynolds averaged Navier-Stokes equations to obtain the fluid force coefficients and used the unsteady model of Chen (1983a) to predict fluidelastic instability. The stability boundaries from Hassan et al. (2010) simulations were in relatively good agreement with experimental data in the literature.

The current computational fluid dynamics capabilities still rely on the other theoretical models to estimate the critical velocity for fluidelastic instability and are confined to low Reynolds numbers. Solving fully coupled Navier-Stokes equations with the tubes equations of motion for practical Reynolds numbers will still remain a challenge for CFD techniques in the foreseeable future.

### 2.3.6 Quasi-steady model

The quasi-steady model proposed by Price & Paidoussis (1983) assumes that the effect of the motion of an oscillating cylinder subjected to cross-flow on the resulting fluid forces is exclusively to modify the velocity vector relative to the body, with the resultant drag and lift forces being parallel and normal, respectively, to the relative velocity (Figure 2-12). The force coefficients in the drag and lift directions are also assumed to be unchanged by the oscillation and

can be obtained from measurements or calculations on a stationary body. The quasi-steady assumption is only valid when the motion of the cylinder is much slower than the fluid flow velocity. According to Blevins (1977) quasi-steady fluid dynamics is only accurate for $U_{pc}/f_nD \geq 10$.

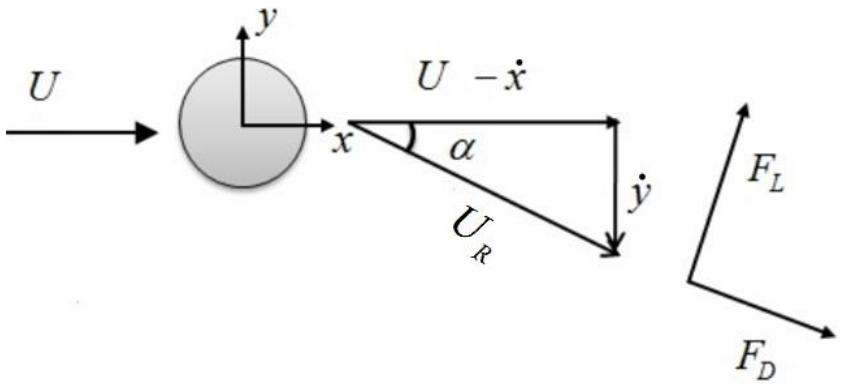


Figure 2-12 : Fluid forces on a typical tube in a tube bundle

Stability analysis of cylinder arrays in fluid cross-flow through quasi-steady approach was first attempted by Gross (1975). Gross proposed a criterion for the determination of instability in the lift direction, relating the reduced critical velocity, $U_{pc}/f_nD$, mass damping parameter, $m\delta/\rho D^2$, and derivative of the lift coefficient with respect to the angle of incidence, $\partial C_y/\partial\alpha$, in the following manner:

$$\frac{U_{pc}}{f_nD} = \frac{m\delta}{\rho D^2\left(-\partial C_y/\partial\alpha\right)} \tag{2-26}$$

Price & Paidoussis (1982, 1983) considered a double row of cylinders in which they assumed that the force coefficients were linear functions of the displacement of the oscillating cylinder itself and that of its two adjacent cylinders; as well as the apparent incidence of the resultant velocity vector vis-à-vis the streamwise direction. Instead of measuring the coefficients, $\partial C_L/\partial\alpha$, and, $\partial C_D/\partial\alpha$, the authors related them to the coefficients $\partial C_L/\partial y$ and $\partial C_D/\partial y$, a relationship they later discovered to be incorrect.

In order to refine this model, Price & Paidoussis (1984, 1985, 1986a, 1986b) and Price et al. (1990) suggested that the fluid forces on any cylinder in an array are directly influenced only by

the cylinder's own motion and its immediate neighbors. They further incorporated a time delay between the tube motion and the fluid response based on the time required for the mean flow to travel one tube row downstream and the inclination of the wake shed from a cylinder due to the latter's transverse motion. Following the work of Simpson & Flower (1977), Price & Paidoussis (1984) accounted for the retardation of the flow approaching a cylinder by multiplying the cylinder displacements by a factor $\exp(-\lambda\mu D/U)$, where, $\mu$ is the flow retardation parameter taken to be of order 1, $\lambda$ is the eigenvalue and, $U$ is the gap velocity . To simplify the model and reduce the computational effort required for stability analysis of multiple flexible cylinders, Price & Paidoussis (1986a) and Price et al. (1990) proposed a constrained mode reduction representing the full array with a small kernel of cylinders decoupled from the rest of the array. They then determined the specific inter-cylinder modal pattern (the constrained mode) leading to the minimum instability critical velocity.

Price & Paidoussis (1984) later used the model to analyze the stability of a single flexible cylinder in a rigid array and obtained, for values of $U_p/f_nD \geq 10$, the following expression for the critical flow velocity at the onset of instability in the lift direction:

$$\frac{U_{pc}}{f_nD} = \frac{4m\delta/\rho D^2}{\left(-C_D - \mu D\,\partial C_L/\partial y\right)} \tag{2-27}$$

and for the drag direction:

$$\frac{U_{pc}}{f_nD} = \frac{4m\delta/\rho D^2}{\left(-2C_D - \mu D\,\partial C_D/\partial x\right)} \tag{2-28}$$

In a later work, Paidoussis & Price (1988) demonstrated the effects of the damping and stiffness controlled mechanisms by comparing the stability boundaries for a single flexible tube in a rigid array and those of a fully flexible array. They concluded that the damping mechanism dominates for, $m\delta/\rho D^2 \leq 300$, while stiffness mechanism reigns for, $m\delta/\rho D^2 \geq 300$.

Granger & Paidoussis (1996) modified the quasi-steady model leading to quasi-unsteady analysis. They introduced a memory effect and represented the unsteady fluid dynamic forces as a combination of decaying exponentials whose constants are obtained by matching the response to experimental data. In as much as the quasi-unsteady model gives better agreement with

experimental data for the critical velocity for fluidelastic instability for known constants, it is limited to single-flexible cylinder analysis.

Recently, attempts have been made to apply the quasi-steady model to two-phase flows. Shahriary et al. (2007) measured the quasi-static forces in air-water two-phase cross-flow in a rotated triangular cylinder array and conducted a stability analysis for single and multiple flexible tubes in the framework of quasi-steady model. Their results were in good agreement with experimental data. More recently, Sawadogo & Mureithi (2014b) measured both the unsteady and quasi-static fluid forces in two-phase air-water cross-flow in a rotated triangular array and estimated the time delay. Their quasi-steady stability analysis results using the measured time delay showed fairly good agreement with experimental dynamic stability tests in the lift direction.

It should be noted that these fluidelastic instability models were developed and validated for single phase flow, hence, the need to investigate their applicability to two-phase flow. Compared to the semi-analytical model of Lever & Weaver (1986a, 1986b), the quasi-steady model requires more experimental data as input. However, the complexity of the two-phase flow makes Lever & Weaver (1986a, 1986b) model difficult to apply for two-phase flow. The unsteady models of Tanaka & Takahara (1981) and Chen (1983a, 1983b) rely heavily on experimental data thus require considerable experimental effort. Besides, Inada et al. (2002) and Mureithi et al. (2002) found the unsteady fluid force coefficient to be a multi-valued function of the reduced velocity in air-water and steam-water two-phase flows, respectively. Additionally, Mureithi et al. (2002) reported weak correlation between the tube displacement and the generated unsteady fluid forces in two-phase steam-water flow. Due to the stated challenges, the quasi-steady model (Price & Paidoussis, 1982, 1983, 1984) is used to analyze instability in two-phase air-water flow in the current work.

#### 2.3.6.1 Quasi-steady model: theory and key assumptions

Since this study is based on the quasi-steady approach, it is important to outline some of its key features. Quasi-steady model has been selected since previous works in single-phase flow (Paidoussis & Price, 1988; Price & Paidoussis, 1984, 1985, 1986a, 1986b; Price et al., 1990) and two-phase cross-flow (Sawadogo & Mureithi, 2014a; Shahriary et al., 2007) suggest that it is more practical in terms of the experimental effort and agreement with experimental data.

### 2.3.6.2 Fluid forces

Referring to Figure 2-12, the velocity of the fluid relative to the cylinder motion may be expressed as:

$$U_r = \left[ \left( U - \dot{x} \right)^2 + \dot{y}^2 \right]^{0.5} \tag{2-29}$$

By first order approximation,

$$\frac{U_r}{U - \dot{x}} = \left[ 1 + \left( \frac{\dot{y}}{U - \dot{x}} \right)^2 \right]^{0.5} \approx 1 \tag{2-30}$$

Thus

$$U_r \approx \left( U - \dot{x} \right) = U \left( 1 - \frac{\dot{x}}{U} \right) \tag{2-31}$$

where $x$ and $y$ are displacements in the streamwise and crosswise directions, respectively, and $U$ is the pitch velocity.

For small displacements,

$$cos\left( \alpha \right) = \frac{U - \dot{x}}{U_r} \approx 1; \;\; \sin\left( \alpha \right) \approx \frac{\dot{y}}{U_r} \tag{2-32}$$

The steady fluid forces in the streamwise and crosswise directions then become:

$$\begin{aligned} F_x &= F_D \cos(\alpha) + F_L \sin(\alpha) \\ F_y &= F_L \cos(\alpha) - F_D \sin(\alpha) \end{aligned} \tag{2-33}$$

where

$$\begin{aligned} F_D &= \frac{1}{2} \rho U_r{}^2 D C_D \\ F_L &= \frac{1}{2} \rho U_r{}^2 D C_L \end{aligned} \tag{2-34}$$

with , $F_D$ being the drag force, $F_L$ the fluid lift force on the tube, respectively, $\rho$, the fluid density, $D$, the tube diameter, $C_D$, the drag coefficient and $C_L$, the lift coefficient. The fluid forces can further be expressed in terms of the drag and lift coefficients by:

$$F_x = \frac{1}{2}\rho D U^2 \left( C_D - 2\frac{\dot{x}}{U} C_D + \frac{\dot{y}}{U} C_L \right)$$
$$F_y = \frac{1}{2}\rho D U^2 \left( C_L - 2\frac{\dot{x}}{U} C_L + \frac{\dot{y}}{U} C_D \right) \quad (2\text{-}35)$$

#### 2.3.6.3 Flow retardation

As already been mentioned, a time lag exists between tube displacement and the resulting fluid-dynamic forces. Different authors have interpreted this feature in various ways. Simpson & Flower (1977) consider the time lag to be a result of the retardation experienced by the fluid as it approaches the vicinity of the cylinder stagnation point. Lever & Weaver (1982, 1986a) see the time delay as the time taken by the flow to readjust itself to the changing flow pattern as the tube oscillates. Paidoussis et al. (1984) conceive it as a delay in the viscous wake adjusting itself to the fluctuating flow configurations resulting from cylinder vibrations while Granger & Paidoussis (1996) associate the time lag to the necessary reorganization of the flow, arising from the diffusion-convection of the vorticity generated by the cylinder motion.

Price & Paidoussis (1984), using potential theory, demonstrated that time lag may be expressed as:

$$\tau = \mu \frac{D}{U} \quad (2\text{-}36)$$

where, $U$, is the flow velocity, $D$, the tube diameter and, $\mu$, the time retardation parameter taken to be of order 1. A few researchers have attempted to experimentally determine this time lag. Mahon & Meskell (2010) considered a single flexible tube in a normal triangular tube array of $P/D = 1.32$ subjected to air flow and measured the time delay between the cylinder motion and the resulting fluid forces by integrating the pressure distribution around the cylinder. They found the time delay to correspond to Eq. (2-36), with $\mu \simeq 2.9$. Khalifa et al. (2011) measured the time delay between tube vibration and induced flow perturbations at several points around the oscillating tube in a rotated triangular tube array of $P/D = 1.54$ subjected to air cross-flow. However, this is quite different from the time delay between the tube motion and the generated fluid forces as the relation between the flow perturbation and the fluid forces acting on the tube is not clear. Similarly, Sawadogo & Mureithi (2014b) considered a single flexible tube in a rotated triangular array of $P/D = 1.50$ subjected to air-water two-phase cross-flow and estimated the

time lag in the lift direction by equating experimentally measured unsteady and quasi-steady fluid forces. The time lag was found to behave in a similar manner to Eq. (2-36) , but with, $\mu$ , varying between 1.7 and 2.7 for void fractions between 60% and 90%.

#### 2.3.6.4 Effect of time delay on tube motion

For multiple flexible tube arrays, there exists a time delay, $\tau_i$ , between the displacements of a tube and the resulting change in fluid forces on the tubes adjacent to it. This delay may be seen as the time taken by the fluid to traverse the distance between adjacent tubes. For example, the time delay results in an apparent displacement of a tube, $i$ , in the $x$ direction of $x_i(t-\tau_i)+\tau_i\dot{x}_i(t-\tau_i)$ and $y_i(t-\tau_i)$ in the, $y$ , direction (as viewed from an adjacent upstream tube) with $\tau_i = S_i/U$ where $S_i$ is the distance between tubes and $U$ , the interstitial velocity (Price & Paidoussis, 1984, 1986b) .

#### 2.3.6.5 Linearization of the fluid forces

In the expression for fluid force (Eq. (2-35)) $C_{DC}$ and $C_{LC}$ are generally nonlinear functions of the fluid forces on a tube, C, and the derivatives of the fluid forces with respect to displacement of the immediate neighboring tubes. However, for stability analysis, it is sufficient to consider the linearized form of the forces, thus:

$$\begin{aligned} C_{DC} &= C_{D0} + g\sum_{C,i=1}^{N}(\chi_i\frac{\partial C_{DC}}{\partial \chi_i}+\eta_i\frac{\partial C_{DC}}{\partial \eta_i}) \\ C_{LC} &= C_{L0} + g\sum_{C,i=1}^{N}(\chi_i\frac{\partial C_{LC}}{\partial \chi_i}+\eta_i\frac{\partial C_{LC}}{\partial \eta_i}) \end{aligned} \tag{2-37}$$

where $g$ is a time delay term, N is the number of neighboring tubes, $\chi_i = x/D$ is the dimensionless displacement of tube $i$ in the flow direction and $\eta_i = y/D$ is the dimensionless displacement of tube $i$ in the transverse direction.

The fluid forces can then be expressed as (Price & Paidoussis, 1984):

$$\{\mathbf{F}\} = Q\{\mathbf{F_0}\} + Q[\mathbf{C}]\{\dot{\mathbf{z}}\} + Qg[\mathbf{K}]\{\mathbf{z}\} \tag{2-38}$$

where $Q = \frac{1}{2}\rho U^2$. The first term on the right hand side of Eq. (2-38) is the vector of steady state forces at equilibrium position, the second term is the fluid damping matrix, and the third term is the fluid stiffness matrix. **z** is the displacement vector.

The steady/quasi-steady forces and consequently the unsteady forces are experimentally determined in the present work and the time delay extracted for a kernel of tubes in a rotated triangular array subjected to air-water two-phase flow. The quasi-steady force coefficients and their derivatives (Eq. (2-35) in addition to the time delay are important inputs for the quasi-steady model.

# CHAPTER 3 ARTICLE 1: PREDICTION OF STREAMWISE FLUIDELASTIC INSTABILITY OF TUBE ARRAYS IN TWO-PHASE FLOWS AND EFFECT OF FREQUENCY DETUNING

Olala, S. and Mureithi, N. W. (2016)

Accepted for publication in "Journal of Pressure Vessel Technology (Transactions of the ASME)". DOI: 10.1115/1.4034467

**Abstract**

Experimental measurements of the steady forces on a central cluster of tubes in a rotated triangular array $(P/D = 1.5)$ subjected to two-phase air-water cross-flow have been conducted. The tests were done for a series of void fractions and a Reynolds number (based on the pitch velocity), $\mathrm{Re} = 7.2 \times 10^4$. The forces obtained and their derivatives with respect to the static streamwise displacements of the central tube in the cluster were then used to perform a quasi-steady fluidelastic instability analysis. The predicted instability velocities were found to be in good agreement with dynamic stability tests. Since the effect of the time delay was ignored, the analysis confirmed the predominance of the stiffness-controlled mechanism in causing streamwise fluidelastic instability.

The effect of frequency detuning on the streamwise fluidelastic instability threshold was also explored. It was found that frequency detuning has, in general, a stabilizing effect. However, for a large initial variance in a population of frequencies (e.g. $\sigma^2 = 7.84$) , a smaller sample drawn from the larger population may have lower or higher variance resulting in a large scatter in possible values of the stability constant, $K$, some even lower than the average (tuned) case. Frequency detuning clearly has important implications for streamwise fluidelastic instability in the steam generator U-bend region where in-plane boundary conditions, due to preload and contact friction variance, are poorly defined. The present analysis has, in particular, demonstrated the potential of the quasi-steady model in predicting streamwise fluidelastic instability threshold in tube arrays subjected to two-phase cross-flows.

*Keywords*: Streamwise fluidelastic instability, Tube arrays, Two-phase cross-flows, frequency detuning

## 3.1 Introduction

Many components especially in the nuclear and chemical engineering industries operate in two-phase flows; for instance two phase cross-flow occurs in many tube-and-shell type heat exchangers such as nuclear steam generators, condensers, boilers, and evaporators. The high velocity two-phase cross-flows normally encountered in these heat exchangers, especially the U-bend region of nuclear steam generators and most shell-and-tube heat exchangers generate dynamic fluid forces that may induce structural vibrations. Excessive vibrations often lead to tube failures due to fatigue and fretting wear at the supports. A review of the different mechanisms that excite tube vibrations is given in Weaver, D. S. & Fitzpatrick, J. A. (1988). Of these vibration mechanisms, fluidelastic instability has the greatest destructive potential in the short-term due to the resulting large amplitude oscillations. In practice, the onset of this phenomenon is estimated by the flow velocity at which the tubes begin to undergo large oscillation. This threshold flow velocity, also referred to as the critical velocity, is therefore the most important parameter in steam generator design and operation (Chen & Srikantiah, 2001). Due to its detrimental nature, fluidelastic instability has attracted extensive research efforts and many theories and semi-empirical models have been developed to predict its onset. These include the jet-switch model (Roberts, 1962, 1966), the quasi-static model (Connors, 1970), the quasi-steady model (Price & Paidoussis, 1982, 1983, 1984), the unsteady model (Tanaka & Takahara, 1980, 1981) and the semi-analytical flow channel model (Lever & Weaver, 1982, 1986b). It should, however, be noted that these formulations were developed for single phase flow even though many heat exchangers operate in two-phase flow (Pettigrew & Taylor, 1994).

Fluidelastic instability is governed by two mechanisms: the velocity mechanism and displacement mechanism (Chen, 1983a, 1983b). In the case of the velocity mechanism, the component of the fluid force proportional to the tube velocity may act as a source of excitation leading to fluid-damping-controlled instability (galloping) and generally results in tube vibrations in the cross-flow direction. For the displacement mechanism (also known as the stiffness-controlled-mechanism), the instability results from fluid coupling effects between several tubes in an array. Of importance here are the fluid force components that depend on the displacement of a

tube and its neighbors. Which of these two mechanisms is dominant depends on the configuration of the tube array as well as on the fluid density. Besides, a combination of both effects may occur (Austermann & Popp, 1995).

A number of experimental studies (e.g. (Granger et al., 1993; Janzen et al., 2005; Mureithi et al., 2005; Nakamura et al., 2014; Roberts, 1962, 1966; Violette et al., 2006)) have reported observations of streamwise fluidelastic instability in both single- and two-phase flows. However, until recently, streamwise instability of tube arrays has not been a major concern to steam generator designers. This is not surprising since most experimental data and analysis results show that, fluidelastic instability occurs predominantly in the direction transverse to the flow (Mureithi et al., 2005; Weaver & Koroyannakis, 1983). Consequently, the apparent lack of (pure) streamwise fluidelastic instability in most of the experimental data used to develop design guidelines may have given the impression that streamwise instability was not expected hence could not occur. In the past, steam generators were fabricated with large clearances, to deal with thermal expansion of the tube/support materials and manufacturing tolerances resulting in both large gaps as well as preloads at the tube supports. This partly led to the addition of improved tube supports or anti-vibration bars (AVBs) in modern steam generators to constrain tube vibration in the cross-flow direction. However, in the U-bend region, these supports may not effectively prevent in-plane (streamwise) oscillations leading to the possibility of streamwise fluidelastic instability.

Weaver & Schneider (1983) experimentally investigated, in a wind-tunnel, the effectiveness of flat bar supports in stabilizing tubes in the U-bend region. The authors found that flat bar supports with small clearances prevented both transverse and streamwise fluidelastic instabilities. Tests with scallop bar supports in the same study, however, displayed considerable streamwise tube vibrations. Similarly, Weaver & Koroyannakis (1983), simulated the effect of asymmetric stiffness on a rotated triangular array subjected to water flow. In this case, straight tubes were fixed on beams of different geometries to enable independent variation of stiffness levels in both the transverse and streamwise directions. Fluidelastic instability was found to always occur in the direction of least stiffness (lowest frequency). Since transverse oscillations are constrained by AVBs in the U-bend region of a steam generator, the direction of lower frequency then would be streamwise.

To give further insight into the tube-support interaction problem, Feenstra et al. (2014) considered the damping effect of dry and wet flat bar supports. They found that, in the absence of contact between the tube and wet supports during streamwise tube vibration, less energy than expected was dissipated suggesting the possibility of streamwise fluidelastic instability. More recently, Hassan & Weaver (2014) performed numerical simulation of the tube-support interaction during streamwise tube motion. The researchers found that, in the absence of preload and for low frictional force, minimizing the gap between tubes and the flat AVBs had significant destabilizing effects.

There is now no doubt about the possibility of occurrence of in-plane fluidelastic instability in steam generators and heat exchangers following tube failures in a steam generator at San Onofre Nuclear Generating Station (SONGS) in California, U.S.A. in 2012 attributed to streamwise fluidelastic instability (S.C.E., 2013). Clearly what remains is to develop predictive tools that would enable design against its occurrence.

As has been shown both experimentally (Violette et al., 2006) and from theoretical analysis (Lever & Weaver, 1982; Olala et al., 2014; Sawadogo & Mureithi, 2014a), a single flexible tube in an otherwise rigid rotated triangular array can become unstable in the transverse and not in the flow direction. This kind of instability is associated with the negative fluid damping arising from fluid dynamic forces acting on the tube due to its own motion hence does not require any coupling between tubes. The foregoing therefore suggests that streamwise fluidelastic instability in rotated triangular tube bundles depends on fluid coupling between tubes hence is fluidelastic stiffness controlled. Even though there are a number of studies on streamwise fluidelastic instability reported in the literature, very few are dedicated to two-phase flows (Granger et al., 1993; Janzen et al., 2005; Mureithi et al., 2005; Nakamura et al., 2014; Roberts, 1962, 1966; Violette et al., 2006). Besides, the existing theoretical models for the prediction of fluidelastic instability were developed for single phase flow; therefore there is a need for their validation or extension to two-phase flows.

The present study presents steady cross-coupling forces for a kernel of tubes in a rotated triangular tube array of pitch-to-diameter ratio of 1.5 subjected to air-water two-phase flow. The measured fluid drag force coefficients and their derivatives are then used in the quasi-steady model to perform streamwise fluidelastic instability analysis for different flexible tube

configurations. The results are compared to those previously obtained from dynamic stability tests in the same test loop (Violette et al., 2006).

### 3.1.1 Definition of two-phase flow parameters

In the homogeneous model, the void fraction $\beta$, is equivalent to the volumetric fraction and given by:

$$\beta = \frac{Q_g}{Q_l + Q_g} \tag{3-1}$$

The homogeneous mixture density, $\rho_h$, and the freestream velocity $U_\infty$, are defined as:

$$\rho_h = (1-\beta)\rho_l + \beta\rho_g \tag{3-2}$$

and

$$U_\infty = \frac{\rho_l Q_l + \rho_g Q_g}{\rho_h A} \tag{3-3}$$

The pitch velocity $U_p$, then becomes:

$$U_p = U_\infty \frac{P}{P-D} \tag{3-4}$$

## 3.2 Theoretical formulation

The streamwise fluidelastic force per unit length (excluding the hydrodynamic mass) acting on a given tube in an array such as the one shown in Figure 3-1 may be expressed as (Price & Paidoussis, 1986b):

$$F_x = \frac{1}{2}\rho_h D U_p^2 \left( C_D - 2\frac{\dot{x}}{U_p} C_D + \frac{\dot{y}}{U_p} C_L \right) \tag{3-5}$$

where $\rho_h$ is the fluid density, $D$ the tube diameter, $U_p$ the pitch velocity, $C_D$ the drag coefficient, $C_L$ the lift coefficient and, $\dot{x}$ and $\dot{y}$ velocity of the tube parallel and transverse to the flow, respectively. A first order Taylor's approximation of $C_D$ and $C_L$ yields:

$$C_D = C_{D0} + \frac{\partial C_D}{\partial x} x + \frac{\partial C_D}{\partial y} y$$
$$C_L = C_{L0} + \frac{\partial C_L}{\partial y} x + \frac{\partial C_L}{\partial y} y \tag{3-6}$$

Here $C_{D0}$ and $C_{L0}$ are the drag and lift coefficients at the tube equilibrium position; and $x$ and $y$ are small displacements of the tube in the streamwise and transverse directions, respectively. Due to the geometrical symmetry of the array under consideration,

$$C_{L0} = \partial C_L / \partial x = \partial C_D / \partial y = 0 \tag{3-7}$$

For multiple tubes the linearized drag force coefficient may therefore be expressed as:

$$C_{D_k} = C_{D0k} + \sum_{n=1}^{N} \frac{\partial C_{Dk}}{\partial x_n} x_n + \sum_{n=1}^{N} \frac{\partial C_{Dk}}{\partial y_n} y_n \tag{3-8}$$

where $C_{Dk}$ is the drag coefficient of tube $k$ and, $x_n$ and $y_n$ the displacement of tube $n$ in the drag and lift directions, respectively.

Consider an array having $N$ tubes flexible only in the flow ($x$) direction. Taking into consideration the fluid added mass, the time lag relative to tube motion (Price & Paidoussis, 1984) and the linearized drag force coefficient, the $x-$ direction fluid force for tube $k$ becomes:

$$F_{x_k} = \frac{1}{2} \rho_h D U_p^2 \left\{ -\frac{m_a}{1/2 \rho_h D U_p^2} \ddot{x}_k - 2 \frac{C_{D0_k}}{U_p} \dot{x}_k + e^{-i\omega\tau} \sum_{n=1}^{N} \frac{\partial C_{D_k}}{\partial x_n} x_n + C_{D0_k} \right\} \tag{3-9}$$

where $m_a$ is the added mass, $\omega$ the circular frequency of the tube and $\tau$ is the time lag (which is considered in this expression to include time delays emanating from both apparent adjacent tube displacements and flow retardation effects (Price & Paidoussis, 1984)). The added mass may be estimated using the formulation of Pettigrew, Taylor, et al. (1989):

$$m_a = \frac{\pi}{4} \rho_h D^2 \left[ \frac{\left(D_e/D\right)^2 + 1}{\left(D_e/D\right)^2 - 1} \right] \tag{3-10}$$

where $\rho_h$ is the fluid homogeneous density and $D_e/D$ the confinement parameter given by $D_e/D = \left(0.96 + 0.5 P/D\right) P/D.$

In-plane fluidelastic instability of a rotated triangular tube array in cross-flow is predominantly stiffness controlled (displacement dependent) (Olala et al., 2014; Olala & Mureithi, 2014; Paidoussis & Price, 1988; Violette et al., 2006), requiring the presence of multiple flexible tubes. Therefore, as a first order approximation, the negative fluid damping instability generating mechanism term ($e^{-i\omega\tau}$) may be neglected. The governing equation of motion for the full array free to vibrate purely parallel to the flow direction thus takes the form:

$$\left(\left[\mathbf{M}\right]_s+\left[\mathbf{M}\right]_f\right)\left\{\ddot{\bar{\mathbf{x}}}\right\}+\left(\left[\mathbf{C}\right]_s+\left[\mathbf{C}\right]_f\right)\left\{\dot{\bar{\mathbf{x}}}\right\}+\left(\left[\mathbf{K}\right]_s+\left[\mathbf{K}\right]_f\right)\left\{\bar{\mathbf{x}}\right\}=\left\{\mathbf{0}\right\} \tag{3-11}$$

where

$$\left[\mathbf{M}\right]_s=m_s\left[I\right]_{n\times n};\quad \left[\mathbf{M}\right]_f=m_a\left[I\right]_{n\times n};\quad \left[\mathbf{C}\right]_s=2\omega\zeta m_s\left[I\right]_{n\times n};$$

$$\left[\mathbf{C}\right]_f=\rho_h DUC_{D0}\left[I\right]_{n\times n};\quad \left[\mathbf{K}\right]_s=m_s\omega^2\left[I\right]_{n\times n}$$

Subscripts '$s$' and '$f$', respectively, indicate 'structural' and 'fluid' quantities. The fluid stiffness term takes the form:

$$\left[\mathbf{K}\right]_{f_{kn}}=-\frac{1}{2}\rho_h U^2\left[\frac{\partial C_{Dk}}{\partial \bar{x}_n}\right] \tag{3-12}$$

with $\bar{x}=x/D$ and $\left\{\bar{\mathbf{x}}\right\}$ the reduced displacement vector. The damping factor, $\zeta$ in Eq. (3-11) includes both the structural and flow-independent damping components.

In the foregoing formulation, the most important fluid dynamic parameters in fluidelastic vibration analysis of multiple flexible arrays are the derivatives of the drag coefficients which indicate cross-coupling between the tubes due to fluid flow and the equilibrium drag coefficients. In the present study, only the effects of the immediate neighboring tubes are considered.

## 3.3 Experimental apparatus

### 3.3.1 Two-phase test loop

The two-phase test loop shown in Figure 3-1 consists of a 1.5 $m^3$ capacity water tank, 1.56 $m^3$/min centrifugal water pump, a magnetic water flow meter (MAG500), a 15 $m^3$/min compressed air supply system and connecting piping. The compressed air is injected into the loop

below the test section and the two fluids are homogenized by a mixer. The air flow rate is measured using two distinct orifice plates, for low and high flow rates, respectively, located away from the test section and connected to a differential pressure transducer and an electronic readout system. Pressure at the test section is measured to correct the air flow rate.

### 3.3.2 Test Section

The test section shown in Figure 3-2 has a rectangular cross sectional area of 0.0380 $m^2$ (0.2 m × 0.19 m). A total of nineteen full tubes and fourteen half tubes are arranged in a rotated triangular configuration with pitch-to-diameter ratio, $P/D = 1.5$, each tube having a diameter, $D = 38$ mm. The length of each tube is 190 mm. The half tubes are attached to the test section wall to minimize wall effect. The number of tube rows in a streamwise column is six or seven. Except for the central tube, all the other tubes are rigid and made of Plexiglas. The central tube which is made of aluminum, is mounted on an ATI Nano 25 transducer attached to a displacement mechanism consisting of a linear motor (Parker Trilogy Ironless Positioner). An Aries smart servo-drive AR-04CE is used to control the motor. Four tubes (1, 2, 3 & 4 in) adjacent to the central tube are strain gage instrumented. The strain gages are glued to the inner diameter of the tubes with epoxy and located as close as possible to the fixed end. Two pairs of diametrically opposite strain gages installed at 90° from one another in each tube are used to measure forces in the in-flow and cross-flow directions, respectively. The strain gage pairs are connected to a Wheatstone bridge in half-bridge configuration. The instrumented tubes are located in the middle of the array such that there are four rows upstream and downstream of the instrumented cluster, respectively.

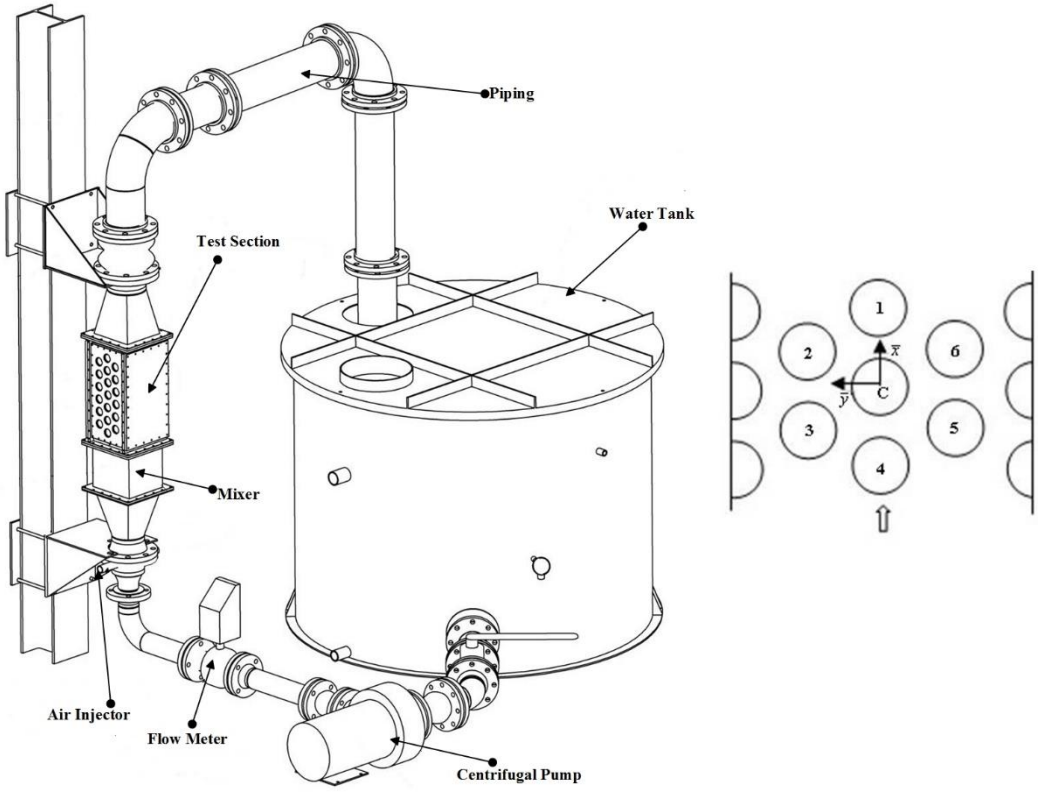


Figure 3-1 : Two-phase test loop and array configuration

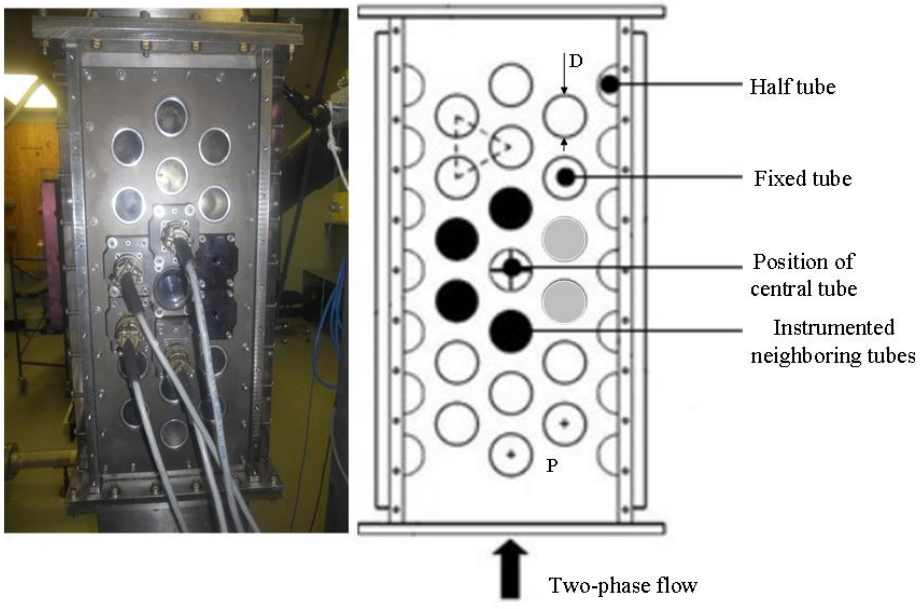


Figure 3-2 : Test section

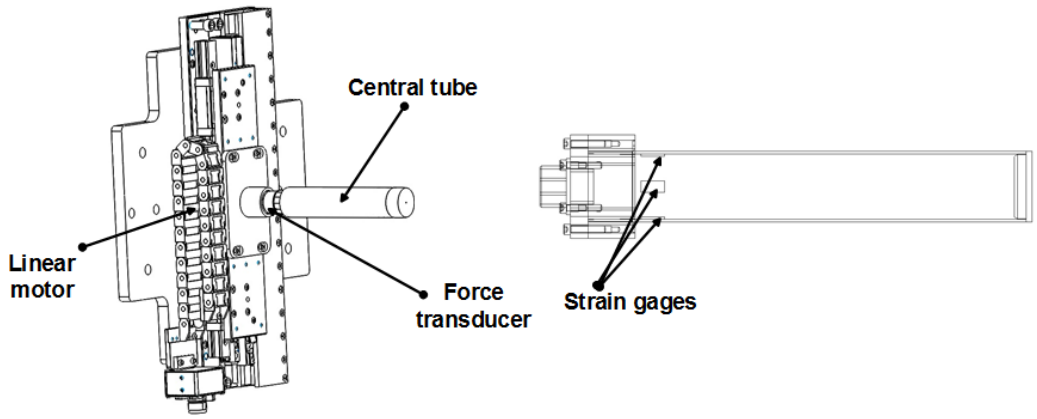


(a) (b)

Figure 3-3 : Instrumented tubes (a) central tube mounted on linear motor and (b) instrumented neighboring tube

## 3.3.3 Test procedure

### 3.3.3.1 Drag and Lift forces measurements

Due to the symmetry of the test section, only the tubes labelled C, 1, 2, 3 and 4 in Figure 3-1 were instrumented. To calculate the force coefficients and their derivatives, which are necessary in the quasi-static/steady fluidelastic instability models, measurement of the steady forces was performed. The static strain-force relation was obtained through careful calibration using known calibrated weights. Force measurement was achieved by statically displacing the central tube in the streamwise direction in increments of 0.026D in the range ±0.13D using the displacement mechanism shown in Figure 3-3(a). For each incremental step, the fluid flow was allowed to attain steady state before initiating data acquisition. The present study employs an improved traverse system (shown in Figure 3-3(a)) as compared to that of Shahriary et al. (2007). Due to the unsteadiness of the flow and strain signals, the generated signals were acquired with a Labview® program via a National Instruments data acquisition module, NIPXIe-1073 and recorded every 0.5 ms over a period of sixty seconds. The mean drag and lift forces were then extracted for each tube as a function of the central tube position. All measurements were conducted at atmospheric conditions (22°C) and a Reynolds number (based on pitch velocity), $\mathrm{Re} = 7.2 \times 10^4$.

In upward flow, the streamwise (drag) fluid force measured is coupled to a buoyancy force. The buoyancy effect is estimated here by letting the water rise above the instrumented tubes in the test section and measuring the force in the drag direction, $F_B$. The corrected drag force in two phase flow is therefore given by:

$$F_D = F_{DM} - F_B \frac{\rho_h}{\rho_l} \tag{3-13}$$

where $F_{DM}$ is the measured drag force, $\rho_h$ the homogeneous density of the two-phase mixture and $\rho_l$ the liquid density. The buoyancy force acts purely in the drag direction; hence any measured lift force in a stagnant fluid is cross-coupling induced, that is, coupling of the force sensors' different measuring axes emanating either from misalignment in sensor/test section orientation or inherent in the sensor. The ratio of the lift to drag forces in static fluid may thus be used as a cross coupling correction factor for every tube, therefore:

$$F_L = F_{LM} - F_{DM}\left(\frac{F_{LS}}{F_B}\right) \tag{3-14}$$

where $F_L$ is the corrected lift force, $F_{LM}$ measured lift force and $F_{LS}$ the measured lift force in stagnant fluid. The force coefficients can then be obtained as:

$$C_D = \frac{2F_D}{\rho_h A U_p^2} \tag{3-15}$$

and

$$C_L = \frac{2F_L}{\rho_h A U_p^2} \tag{3-16}$$

## 3.4 Experimental results

### 3.4.1 Steady fluid force coefficients

The fluid force coefficients are calculated according to Eqs. (3-15) and (3-16). All the force coefficients presented in this section are based on the pitch velocity and are functions of the

streamwise displacement of the central tube, C. The fluid forces were measured in water flow and two-phase flows with superficial void fractions up to 90%.

The effect of streamwise displacement of the central tube on both drag and lift force coefficients for the instrumented tubes C, 1, 2, 3 and 4 for different void fractions are presented in Figure 3-4 to Figure 3-8. Figure 3-4 shows the variation of force coefficients for tube C due to its own static displacement in the flow direction. The drag coefficient, $C_{DC}$, basically increases as the static displacement increases downstream. This is attributed to higher resistance experienced by the flow due to increased blockage as tube C approaches the downstream tube 1. The lift coefficient, $C_{LC}$, on the other hand remains invariant at zero with the streamwise displacement of the central tube C. This should be the case due to the symmetry of the tube array under consideration. A similar situation holds for tubes 1 and 4 which are located downstream and upstream of tube C, respectively. From Figure 3-1, as tube C approaches tube 1 due to the displacement of tube C downstream, tube 1 gets into its wake leading to less and less fluid impinging on tube 1 as the central tube gets closer. The foregoing explains the decreasing trend of tube 1 drag coefficient, $C_{D1}$, with increasing displacement of tube C in the flow direction as shown in Figure 3-5. Upstream of tube C is tube 4. Downstream displacement of the central tube C leads to decreased blockage behind tube 4 leading to increasing drag force hence drag coefficient, $C_{D4}$ as presented in Figure 3-6(a). The trend of the lift coefficient for both tubes 1 and 4 ($C_{L1}$ and $C_{L4}$) is similar to that of the central tube C, again, due to geometrical symmetry of the array.

Figure 3-7 and Figure 3-8 show the influence of the streamwise displacement of tube C on the drag and lift coefficients for tubes 2 and 3, respectively. The drag coefficient increases for tube 2 while it decreases for tube 3 when the central tube is displaced in the flow direction. This is again due to the varying blockage in the central column as tube C is displaced downstream. A look at the lift coefficients for both tubes (2 and 3) in Figure 3-7(b) and Figure 3-8(b) show that there is slight variation for the coefficients. $C_{L2}$ is negative for negative displacements and positive for positive displacements of tube C. On the other hand, $C_{L3}$ is slightly positive for negative displacement of tube C while negative for positive displacement of the same tube C. The above observation is attributed to the positions of the tubes 2 and 3 in relation to tube C while being displaced. The position of tube C slightly modifies the flow direction around these tubes hence

the effective fluid forces in the transverse and flow directions. The trend of the drag coefficient for each particular tube can therefore be said to depend on whether the central tube moves closer or away from it, thereby modifying the flow distribution between them. Additionally, the drag coefficient was found to increase with void fraction till $\beta = 40\%$ then start decreasing for all the tubes. This tendency may be attributed to changing flow mixture composition hence flow pattern. It should be noted that the tests were conducted at the same Reynolds number, meaning that tests at higher void fractions were done at more elevated superficial flow velocities than for the lower void fractions. The effect on the lift coefficient is very small hence it can be argued that the variation of the central tube's position in the flow direction only significantly affects the drag coefficient for the tube array used in the present tests.

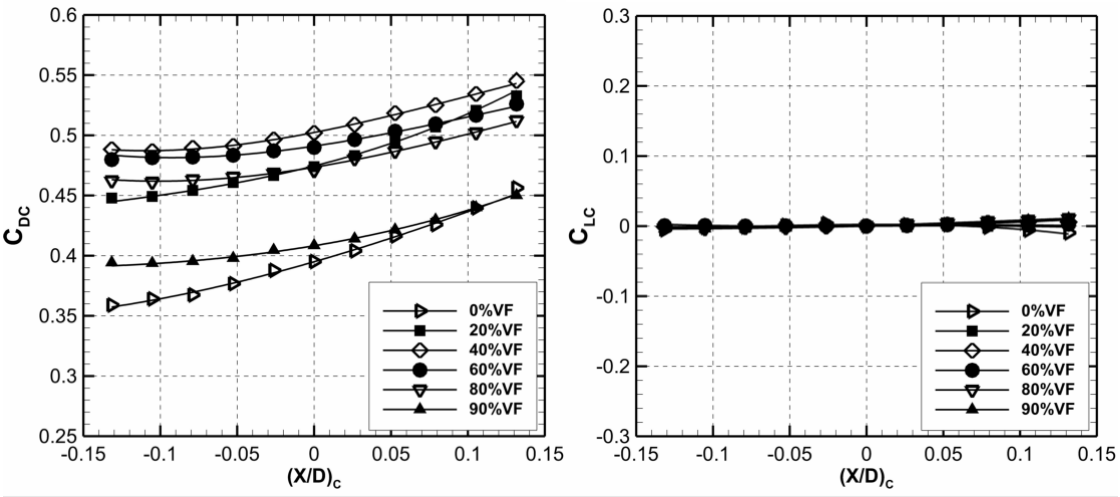


(a) (b)

Figure 3-4 : Variation of tube C drag and lift coefficients with streamwise dimensionless displacement of tube C

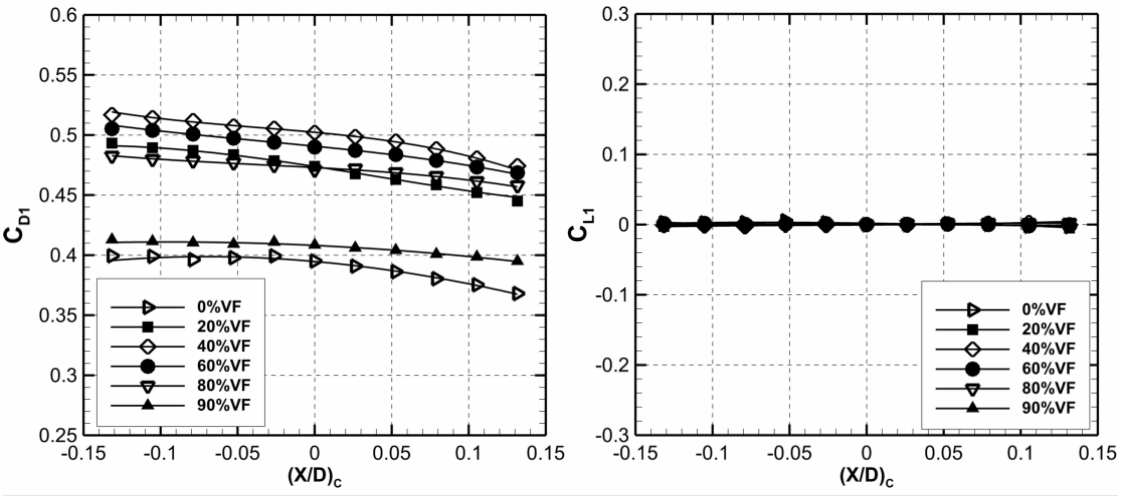


(a) (b)

Figure 3-5 : Variation of tube 1 drag and lift coefficients with streamwise dimensionless displacement of tube C

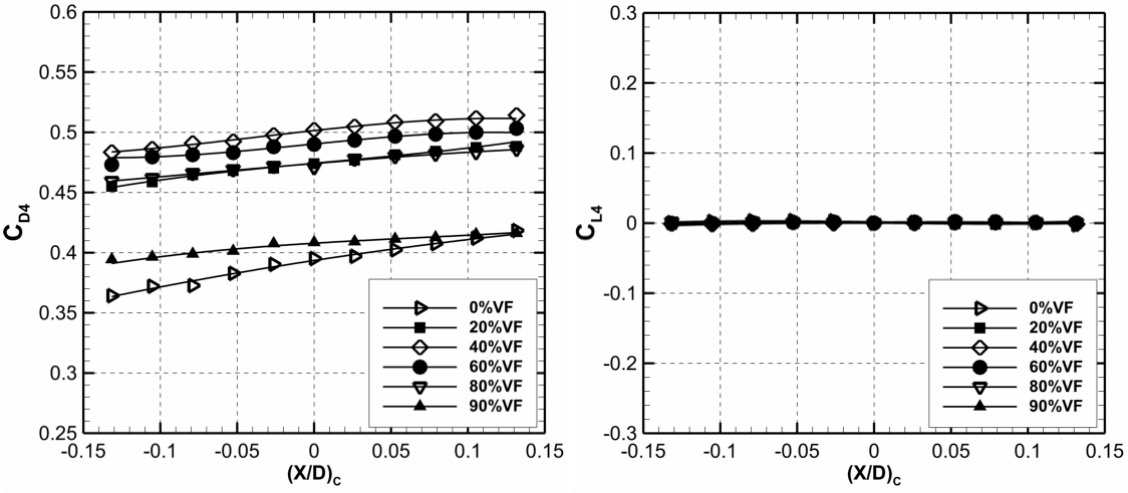


(a) (b)

Figure 3-6 : Variation of tube 4 drag and lift coefficients with streamwise dimensionless displacement of tube C

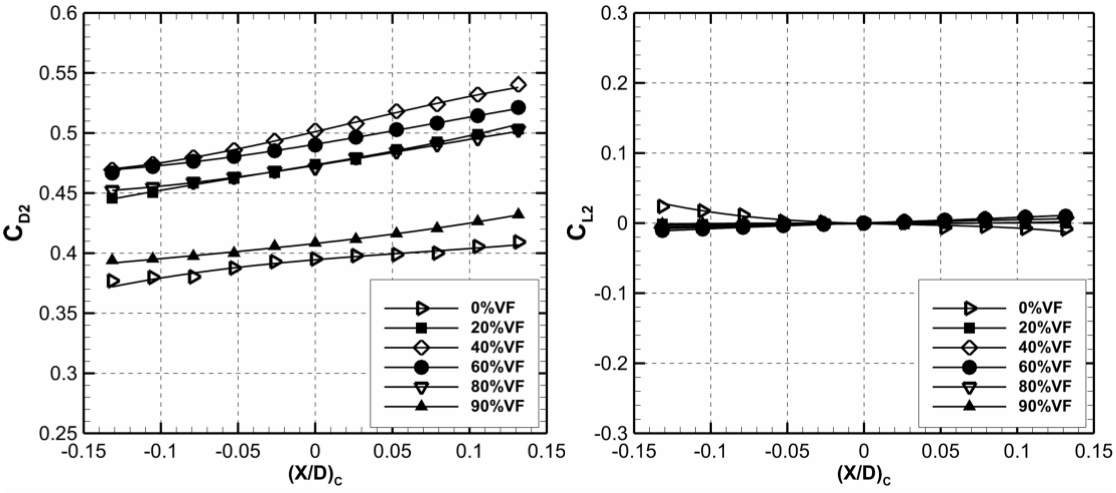


(a) (b)

Figure 3-7 : Variation of tube 2 drag and lift coefficients with streamwise dimensionless displacement of tube C

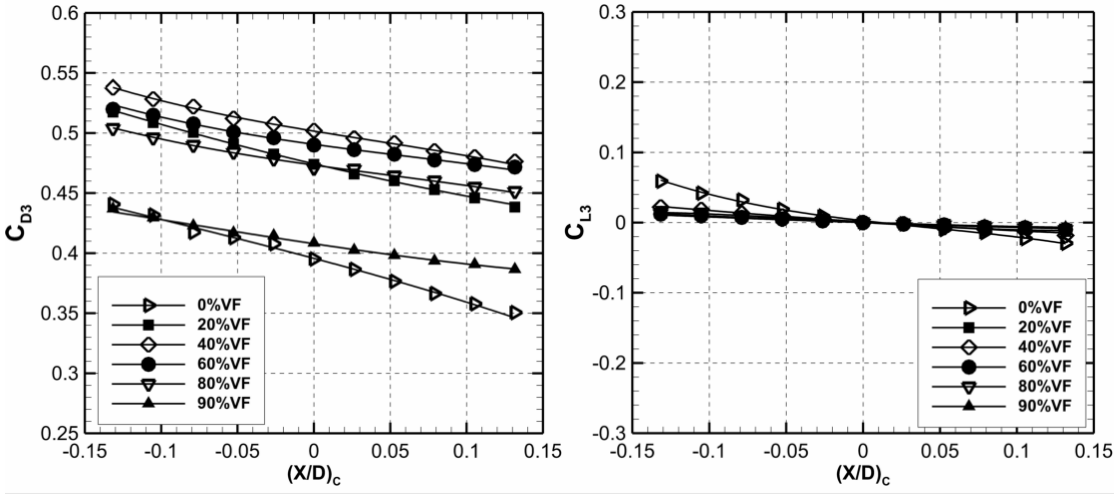


(a) (b)

Figure 3-8 : Variation of tube 3 drag and lift coefficients with streamwise dimensionless displacement of tube C

### 3.4.2 Drag coefficients derivatives

As mentioned earlier in this paper, only the central tube, 'C', was displaced during the tests. Therefore, the derivatives with respect to other tube displacements are inferred to complete the fluid-stiffness matrix in Eq. (3-11) and Eq. (3-12). Due to symmetry in the array (Fig. 2-1), they can be expressed as shown in Table 3-1.

Table 3-1 : Equivalent force coefficients derivatives

| **Experimental data** | **Equivalent quantities** |
|---|---|
| $\partial C_{Dc}/\partial \overline{x}_c$ | $\partial C_{D4}/\partial \overline{x}_4, \partial C_{D3}/\partial \overline{x}_3, \partial C_{D2}/\partial \overline{x}_2, \partial C_{D1}/\partial \overline{x}_1$ |
| $\partial C_{D1}/\partial \overline{x}_c$ | $\partial C_{Dc}/\partial \overline{x}_4$ |
| $\partial C_{D2}/\partial \overline{x}_c$ | $\partial C_{Dc}/\partial \overline{x}_5$ |
| $\partial C_{D3}/\partial \overline{x}_c$ | $\partial C_{Dc}/\partial \overline{x}_6$ |
| $\partial C_{D4}/\partial \overline{x}_c$ | $\partial C_{Dc}/\partial \overline{x}_1$ |

The variation of the derivatives of the drag coefficients as functions of the streamwise displacement of the central tube with respect to void fraction is presented in Figure 3-9. The continuous lines represent third order polynomial curve fitting to the data. Also shown in the figure are average error bars for the drag coefficient derivatives of each tube. Derivatives for tubes 'C', 2 and 4 are positive while those for tubes 1 and 3 are negative. For the central tube, this derivative $(\partial C_{DC}/\partial \overline{x}_C)$ decreases approximately linearly from 0% to 60% void fraction then increases between 60% and 90% void fractions. Tube 4 drag coefficient derivative $(\partial C_{D4}/\partial \overline{x}_C)$ on the other hand shows a continually decreasing trend with void fraction.

The derivative of the drag coefficient for tube 2, $(\partial C_{D2}/\partial \overline{x}_C)$ initially increases between 0% and 40% void fractions then decreases between 40% and 90% void fractions. In the case of tube 3, this derivative $(\partial C_{D3}/\partial \overline{x}_C)$ showed an increasing trend with void fraction between 0% and 90%

but with a gentler slope from 40% to 90% void fraction. For tube 1, $\partial C_{D1}/\partial \overline{x}_C$ , initially decreases between 0% and 20% void fractions, then increases nearly linearly with void fraction till 90%.

These derivatives represent the fluid induced stiffness on a tube as a result of the motion of the adjacent tube hence the tube-tube stiffness coupling. The signs of the derivatives are of importance. For the two-degree-of-freedom case, it has been shown (Paidoussis & Price, 1988) that, the cross-coupling terms in the $[\mathbf{K}]_{f_{kn}}$ matrix (Eq. (3-12)) must have opposite signs for stiffness-controlled fluidelastic instability to occur. For a larger number of tubes, this relationship would, of course, be more complex.

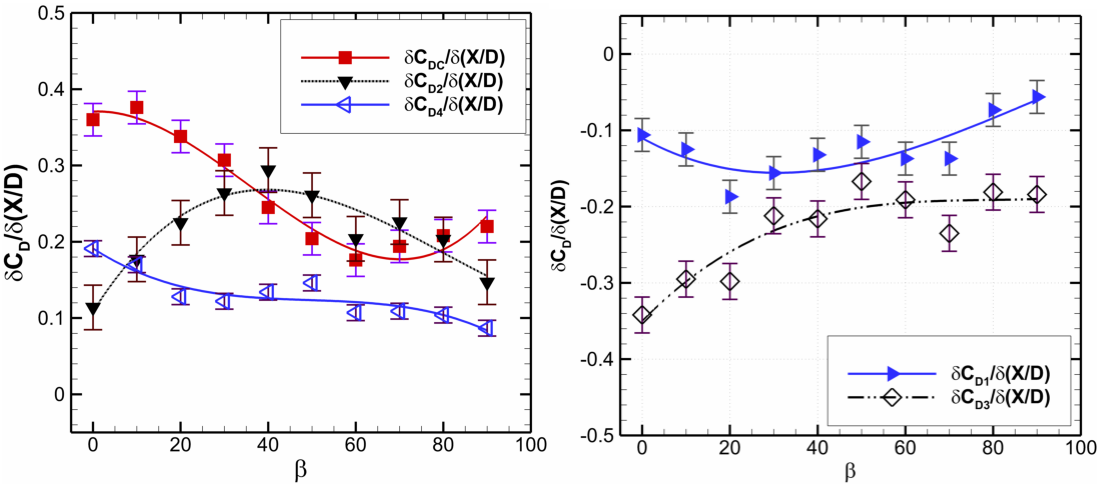


(a) (b)

Figure 3-9 : Variation of the derivative of the drag coefficients with void fraction for (a) tubes C, 2 and 4 (b) tubes 1 and 3

## 3.5 Fluidelastic stability analysis

Equation (3-11) may be expressed in the generalized coordinate system in the form:

$$\mathbf{M}\ddot{\mathbf{q}}(t)+\mathbf{C}\dot{\mathbf{q}}(t)+\mathbf{K}\mathbf{q}(t)=\mathbf{0} \tag{3-17}$$

where $\mathbf{M}, \mathbf{C}$ and $\mathbf{K}$ are the $(n\times n)$ total mass, total damping and total stiffness matrices respectively, and $\mathbf{q}(t)$ is the $(n\times 1)$ vector of generalized coordinates, whose length, $n$, in this case corresponds to the number of flexible tubes. By defining a state vector $\mathbf{x}(t)$ as the $(2n\times 1)$ vector comprising the generalized coordinates vector, $\mathbf{q}$ and generalized velocity vector $\dot{\mathbf{q}}$:

$$\mathbf{x}(t) = \begin{bmatrix} \mathbf{q} \\ \mathbf{...} \\ \dot{\mathbf{q}} \end{bmatrix} \tag{3-18}$$

Eq. (3-17) can then be reduced to a first-order state-space differential equation of the form:

$$\dot{\mathbf{x}}(t) = \mathbf{B}\mathbf{x}(t) \tag{3-19}$$

where $\mathbf{B}$ is a $(2n \times 2n)$ matrix defined as:

$$\mathbf{B} = \begin{bmatrix} \mathbf{0} & \mathbf{I} \\ \mathbf{-M^{-1}K} & \mathbf{-M^{-1}C} \end{bmatrix} \tag{3-20}$$

in which $\mathbf{0}$ and $\mathbf{I}$ are the zero and unit matrices, respectively. By further assuming that Eq. (3-19) admits solutions of the form $\mathbf{x} = e^{\lambda t}\tilde{\mathbf{x}}$ , where $\lambda$ represents an eigenvalue and $\tilde{\mathbf{x}}$ the corresponding eigenvector, Eq. (3-19) may be reduced to the standard eigenvalue problem:

$$\mathbf{B}\tilde{\mathbf{x}} = \lambda\tilde{\mathbf{x}} \tag{3-21}$$

By solving Eq. (3-21), the lowest velocity at which the real part of any eigenvalue becomes null defines the critical velocity for fluidelastic instability. The eigenvector $\tilde{\mathbf{x}}$ of Eq. (3-21) assumes the following structure:

$$\tilde{\mathbf{x}} = \begin{bmatrix} \tilde{\mathbf{q}} \\ ... \\ \lambda\tilde{\mathbf{q}} \end{bmatrix} \tag{3-22}$$

in which $\tilde{\mathbf{q}}$ is the $(n \times 1)$ eigenvector of the eigenvalue problem in the physical space. Here, again, $n$ is the number of degrees-of-freedom or as stated earlier, the number of flexible tubes in the present case. The vector $\tilde{\mathbf{q}}$ generally appears in complex conjugate pairs and defines the system mode shapes. The eigenvalues, which also appear in complex conjugate pairs, take the form (Inman, 2001):

$$\begin{aligned} \lambda_i &= -\zeta_i\omega_{ni} - \omega_{ni}\sqrt{1-\zeta_i^2}\, j \\ \lambda_{i+1} &= -\zeta_i\omega_{ni} + \omega_{ni}\sqrt{1-\zeta_i^2}\, j \end{aligned} \tag{3-23}$$

where $j=\sqrt{-1}$ , $\omega_{ni}$ and $\zeta_i$ are the undamped natural frequency and the damping ratio, respectively of the $i^{th}$ mode. Writing the complex eigenvalue as:

$$\lambda_i = \alpha_i + j\sigma_i \tag{3-24}$$

where $\alpha_i = \mathrm{Re}(\lambda_i)$ and $\sigma_i = \mathrm{Im}(\lambda_i)$, and comparing Eqs. (3-23) and (3-24) yields,

$$\omega_{ni} = \sqrt{\alpha_i^2 + \sigma_i^2} \tag{3-25}$$

$$\zeta_i = \frac{-\alpha_i}{\sqrt{\alpha_i^2 + \sigma_i^2}} = \frac{-\alpha_i}{\omega_{ni}} \tag{3-26}$$

and

$$\sigma_i = \omega_{ni}\sqrt{|\zeta_i^2 - 1|} = \omega_{di} \tag{3-27}$$

in which $\omega_{di}$ is the $i^{th}$ mode damped natural frequency. Thus the real part of the eigenvalue is related to the tube modal damping (Eq. (3-26)) while the imaginary part relates to the modal frequency (Eq. (3-27)).

For tubes each of mass 3.062 kg/m with the damping values presented in Table 3-2 (Olala et al., 2014) and a natural frequency (in air) of 14 Hz, the stability analysis results follow. No assumptions are made regarding the expected tube vibration frequency or vibration modes. Figure 3-10 shows the tube configuration for a single flexible column while multi-column cases are presented in Figure 3-11.

Table 3-2 : Total damping factor (structural + flow independent) for various void fractions (Olala et al., 2014)

| Void fraction (%) | 0 | 10 | 20 | 30 | 40 | 50 | 60 | 70 | 80 | 90 |
|---|---|---|---|---|---|---|---|---|---|---|
| $\zeta$ (%) | 1.0 | 2.4 | 2.5 | 3.6 | 4.0 | 3.9 | 4.0 | 4.1 | 3.5 | 3.0 |

As presented in Figure 3-12 the critical reduced velocity for instability, $U_c / f_n D$ , was found to decrease with increase in number of flexible tubes for a single flexible column for all the void fractions considered. On the contrary, however, the critical reduced velocity increased with void fraction, primarily due to the decrease in mixture density with void fraction. For flexible tubes located in neighboring columns of the array, Figure 3-13, a similar trend as that for flexible tubes located in a single column is observed. However, the values of the critical reduced velocity are lower for the latter case. For example, two adjacent flexible tubes in a single column are more stable than two flexible tubes in neighboring columns. It can therefore be argued that (for a particular void fraction or mass damping parameter) the instability threshold for multiple flexible tubes depends on the number and relative location of the flexible tubes. This variation can be explained in terms of the instability mechanism and flow distribution in the array. Rewriting Eq. (3-11) for a two degree-of-freedom system,

$$\begin{bmatrix} m & 0 \\ 0 & m \end{bmatrix} \ddot{\vec{X}} + \begin{bmatrix} c & 0 \\ 0 & c \end{bmatrix} \dot{\vec{X}} + \begin{bmatrix} k & 0 \\ 0 & k \end{bmatrix} \vec{X} = -\begin{bmatrix} m_a & 0 \\ 0 & m_a \end{bmatrix} \ddot{\vec{X}} - \rho_h DU \begin{bmatrix} C_{D01} & 0 \\ 0 & C_{D02} \end{bmatrix} \dot{\vec{X}} + \frac{1}{2} \rho_h U^2 \begin{bmatrix} C_{D1,1} & C_{D1,2} \\ C_{D2,1} & C_{D2,2} \end{bmatrix} \vec{X} \tag{3-28}$$

where the left-hand side represents structural quantities and the right-hand side the fluid quantities. For stiffness controlled instability, it is the cross coupling between tubes due to the fluid flow that causes instability, in this case the off-diagonal terms in the last matrix of Eq. (3-28). These off-diagonal terms, as stated earlier,, must be of opposite signs for stiffness-controlled instability to occur (Paidoussis & Price, 1988). From Figure 3-12 and Figure 3-13 there is no significant difference in the predicted critical velocity using more than four flexible tubes. Since the mechanism causing instability here, is dependent on the fluid coupling between tubes, the more the number of the flexible tubes, the stronger the coupling strength. However, the present analysis suggests that there is no much benefit in using more than five flexible tubes for reliable prediction of the fluidelastic instability threshold for a rotated triangular array.

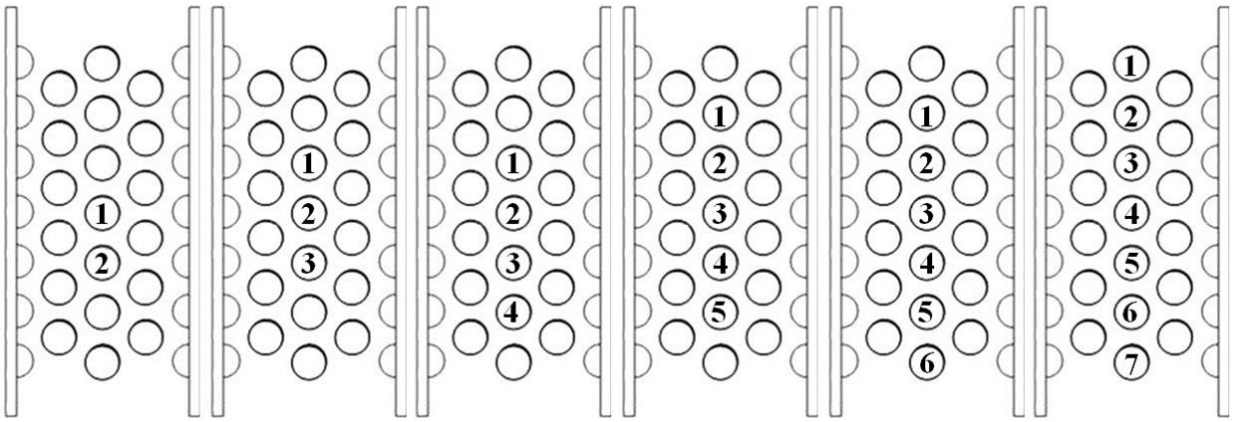

(a) (b) (c) (d) (e) (f)

Figure 3-10 : Flexible tubes configuration for stability analysis - single column

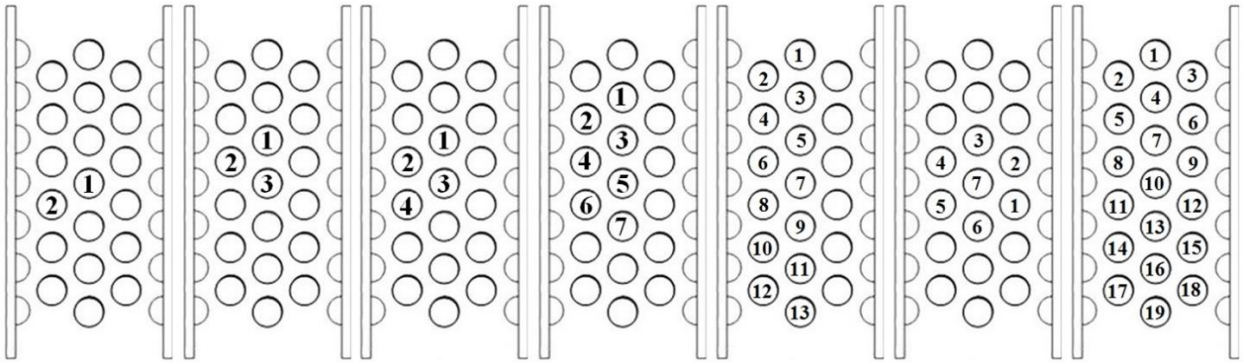

(a) (b) (c) (d) (e) (f) (g)

Figure 3-11 : Flexible tubes configuration for stability analysis - multiple columns

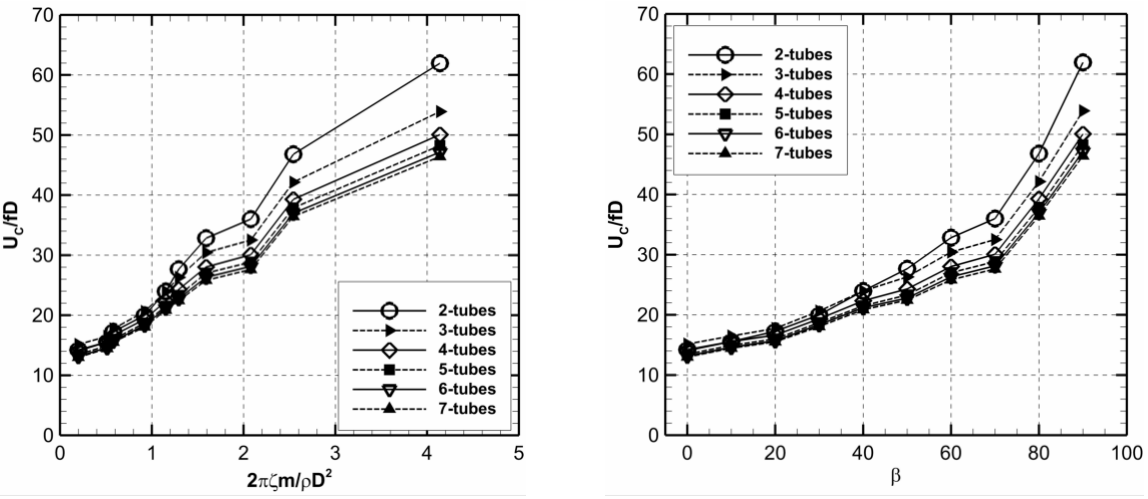


(a) (b)

Figure 3-12 : Effect of the number of flexible tubes on the critical velocity for a column of tubes (Refer to Figure 3-10)

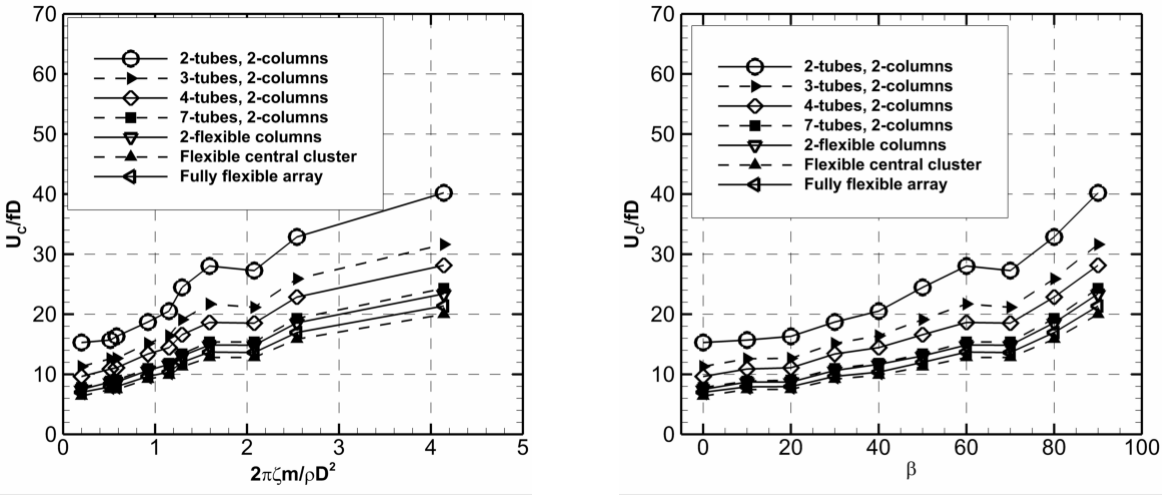


(a) (b)

Figure 3-13 : Effect of the number of flexible tubes on the critical velocity for multiple columns of tubes (Refer to Figure 3-11)

### 3.5.1 Fluidelastic instability results comparison

Figure 3-14 shows results comparison between the present analysis with the dynamic tests of Violette et al. (2006) that were conducted on the same tube array as the one used in the present study. The critical reduced velocities predicted by the model are slightly higher, by up to 19%,

for the central cluster and 22% for the partially flexible column than those from the dynamic tests. The difference may be attributed to assumptions and simplifications made in the present analysis. Firstly the quasi-static model itself. The underlying quasi-static assumptions ignore unsteady flow effects. Beyond the model limitation, it is also assumed that the flow is homogeneous and uniform in the entire bundle enabling replication of the measured fluid forces and derivatives to any number and arrangement of flexible tubes. However, this may not necessarily be true. In their dynamic instability tests, Violette et al. (2006) found that tube instability depended on the location of the tube in the array and the void fraction; instability being well developed throughout the flexible array for void fractions lower than 60% while in the case of void fractions greater than 80%, the downstream tubes experienced much more developed instability than the rest of the array tubes. This phenomenon may partially explain the observation in Figure 3-14 (a) where data points from the two methods (experiments and theory) converge for lower void fractions and seem to diverge for higher void fractions. Overall, the trends of the critical velocities relative to the void fraction are similar for both cases. Even though Violette et al. (2006) did not observe instability for the case of a single central column (Figure 3-10 (f)) flexible only in the flow direction, the current study did obtain instability for this configuration, though at relatively high critical velocity. In a wind tunnel dynamic instability test for the same tube configuration, Mureithi et al. (2005) obtained, similarly to the present analysis, instability for a single flexible column. It is therefore possible that the limit of the test loop was reached before instability could be realized in the work of Violette et al. (2006).

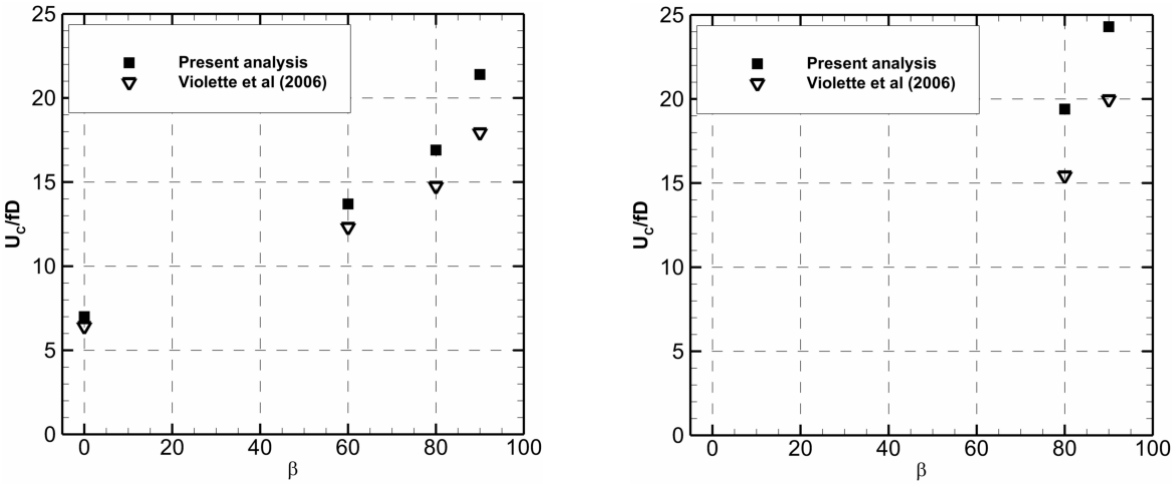


(a) (b)

Figure 3-14 : Comparison between present analysis and dynamic stability test (a) Flexible central cluster (Figure 3-11(f)) (b) Two-partially flexible columns (Figure 3-11(d))

Figure 3-15 presents a comparison between the fluidelastic instability results of the present analysis and existing data for the rotated triangular array pattern. The critical reduced velocity is plotted against the mass damping parameter. The continuous lines correspond to fixed values of the factor $K$, the Connors proportionality constant which is defined in the following relation:

$$\frac{U_c}{f_n D} = K\left(\frac{2\pi\zeta m}{\rho_h D^2}\right)^{0.5} \tag{3-29}$$

The data from the present analysis tend to follow the same trend as those of Violette et al. (2006) and Mureithi et al. (2005) but collapse well on the $K \simeq 10$ as opposed to $K \simeq 8$ in the latter two studies. This difference has been explained at the beginning of this sub-section. Data from Pettigrew, Tromp, et al. (1989) which are for tubes flexible in the direction transverse to the flow collapse on $K \simeq 3.7$ reinforcing the fact that instability threshold of tubes preferentially flexible in the flow direction is higher than for those flexible in the transverse direction. The results of Figure 3-14 and Figure 3-15 confirm the potential of the present analysis method to predict fluidelastic instability for rotated triangular tube bundles of similar pitch ratio with tubes flexible purely in the flow direction.

The reader could be rightly wondering why bother then with streamwise fluidelastic instability when it has been documented that transverse instability occurs way earlier than the in-plane

instability. Recent work by Nakamura et al. (2014) suggests that for closely spaced tube arrays, in their case, a triangular tube array with pitch-to-diameter ratio, $P/D=1.2$, in-plane instability occurs at a velocity lower than that found for out-of-plane instability. Additionally, improved alignment of tubes and the anti-vibration bars (AVBs) resulting in tube-AVB gap uniformity may lead to reduced friction damping forces at the tube-AVB contacts hence increasing susceptibility to in-plane instability. For tubes with support non-uniformity, the varying boundary conditions of the neighboring tubes will generally render the tubes to have different frequencies and mode shapes. This variation in frequency, simply called frequency detuning, is more prevalent for non-uniformly supported tubes. Since streamwise instability is fundamentally a coupled-mode instability involving multiple tubes, coupling forces are strongly dependent on the frequency differences between tubes. As is shown in subsection 3.5.2, smaller frequency differences enhance the cross-coupling and the resulting fluidelastic forces.

### 3.5.2 Streamwise fluidelastic instability and effect of frequency detuning

Due to varying boundary conditions at the tubes supports and manufacturing imperfections, variations of the natural frequencies of steam generator tubes are an unavoidable occurrence. In this sub-section the effect of varying tube cross-coupling, via frequency detuning is investigated for a central cluster of tubes (Figure 3-11 (f)). The effect of frequency detuning is expressed here in terms of statistical variance of tube frequencies from a given mean frequency, here 14 Hz. Firstly, statistical populations of 1000 tube natural frequencies with a mean of 14Hz and variances 5%, 10% and 20% about the mean are created. From each population, random samples of 7 frequencies (for the 7 tubes in Figure 3-11 (f))) are selected and a stability analysis performed according to Eq. (3-21). The critical velocity is defined here as the velocity at which the real part of the eigenvalue of one of the roots changes sign to positive. The tube structural damping is maintained constant at 0.2%. This is repeated for 1000 samples. Using the obtained reduced critical velocity, a corresponding stability constant, $K$ is calculated for each sample using Eq. (3-29).

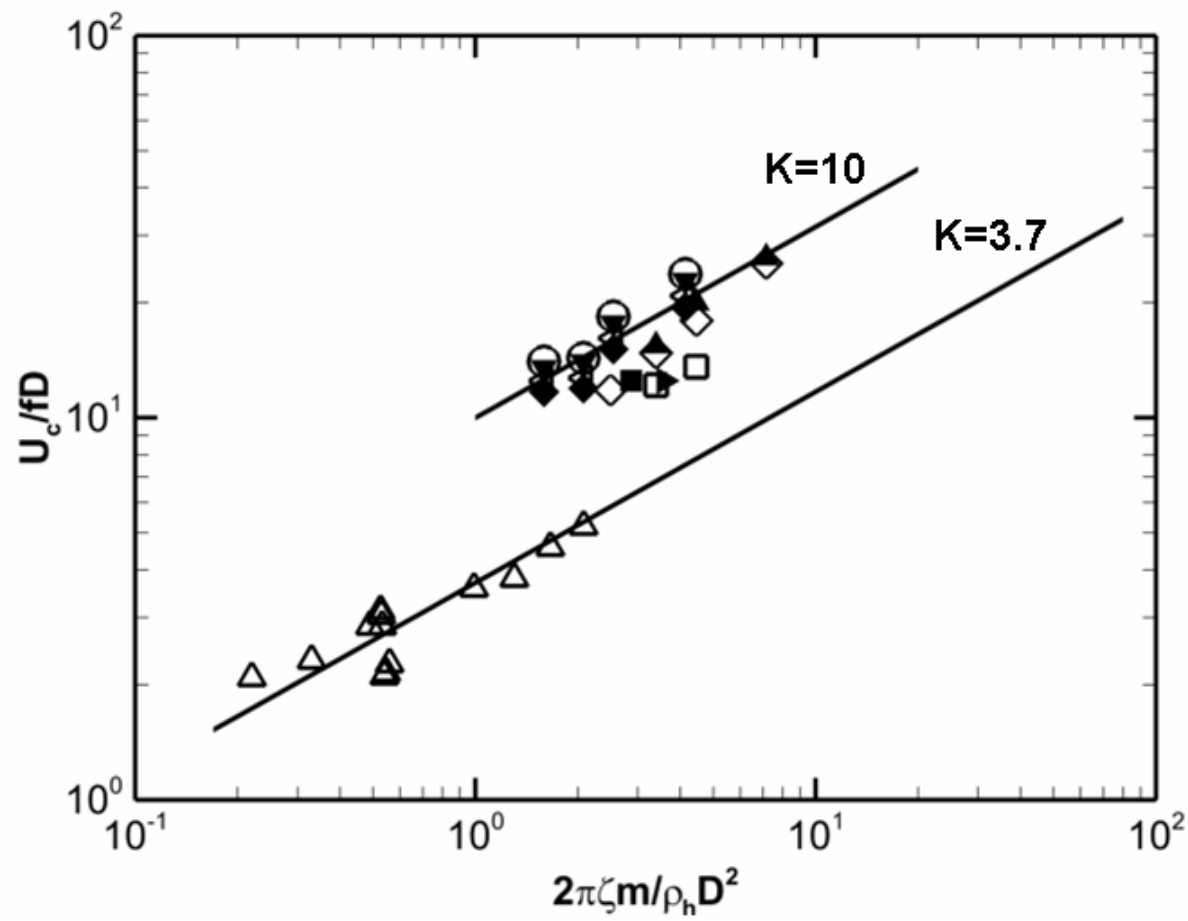


Figure 3-15 : Instability map: comparison of present analysis with published data, ▼ two flexible columns in air-water two-phase flow with tubes flexible in flow (present analysis), ○ two partially flexible columns in air-water two-phase flow (present analysis), ◁ flexible central cluster in air-water two-phase flow (present analysis), ◆ a fully flexible array in air-water two-phase flow (present analysis), △ axisymetrically flexible tube bundles in air-water two-phase flow (Pettigrew, Tromp, et al., 1989), ■ a single flexible column in air flow with tubes flexible in flow (Mureithi et al., 2005), ► a central flexible cluster in air flow with tubes flexible in flow (Mureithi et al., 2005), □ a central flexible cluster in air-water two-phase flow with tubes flexible in flow, $f_n = 28$ Hz (Violette et al., 2006), ◇ a central flexible cluster in air-water two-phase flow with tubes flexible in flow, $f_n = 14$ Hz (Violette et al., 2006), ▲ two partially flexible columns in air-water two-phase flow with tubes flexible in flow (Violette et al., 2006).

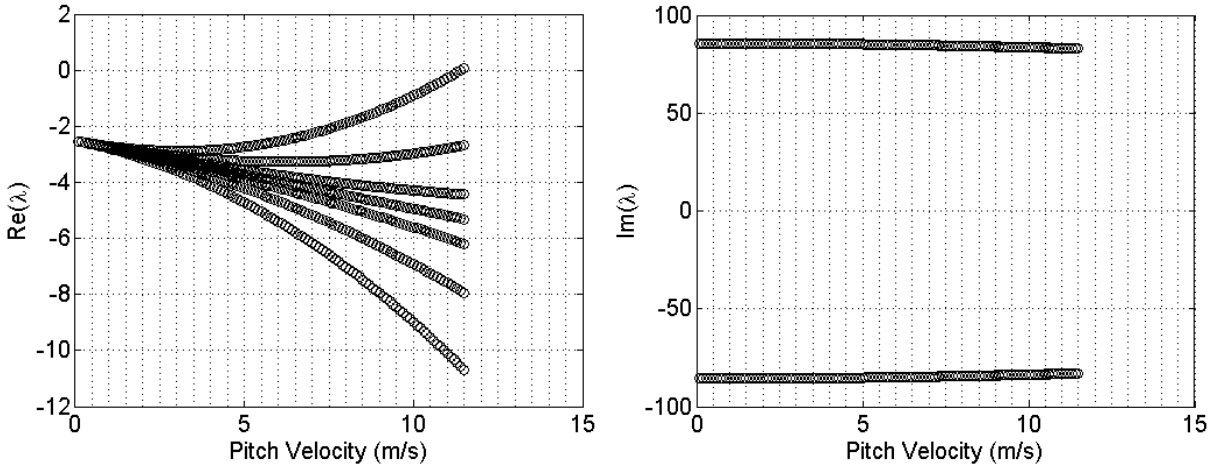


(a) (b)

Figure 3-16 : Evolution of eigenvalue with flow velocity for 90% void fraction, $\sigma^2$=0 (0% detuning) (a) real part (b) imaginary part

Figure 3-16 shows the evolution of the eigenvalue real and imaginary parts as functions of pitch flow velocity for the case of a cluster of 7 tubes each having a frequency of 14 Hz (zero detuning). The two-phase flow homogeneous void fraction is 90%. It is seen in Figure 3-16 (a) that the flow has a stabilizing effect at low velocities (positive damping (Eq. (3-26))). However, above a velocity of about 4 m/s, one of the modes separates and eventually loses stability at about $U = 11.5\,\text{m/s}$ when the damping for this particular mode becomes negative. The tube frequencies (Eq. (3-27) show no discernible change with flow velocity as shown in Figure 3-16 (b).

The first two vibration modes of the bundle (Figure 3-11 (f)) corresponding to the eigenvalues of Figure 3-16 are shown in Figure 3-17. It should be recalled, from Eq.(3-22), that the mode shapes are determined from the eigenvectors. On this figure, the open big circle indicate the tube position at an arbitrary time, the open small circle the tubes' equilibrium positions, the plus signs are the tube movement limits and the dot (filled small circle) the tube center. Indicated by the arrow is the tube movement direction. The phase angle of each of the tubes is with respect to the central tube, Tube 7. The sign of the phase angle indicates whether the specific tube lags or leads Tube 7; where a positive phase would mean that the tube being considered leads Tube 7 and vice-versa. Figure 3-17 (a) shows the vibration pattern for the first mode (unstable mode) while the second mode is presented in Figure 3-17 (b). A well defined pattern is observed for the relative movement of the flexible tubes. It is seen in Figure 3-17 (a) (the unstable mode) that for two

neighboring tubes of the same column, the downstream tube leads the upstream tube by a phase angle of about $144^{\circ}$. However, for two neighboring tubes in adjacent columns, the downstream tube lags the upstream tube by a phase angle of about $69^{\circ}$. An exact opposite scenario is observed for the second mode of vibration. Here (Figure 3-17 (b)), the upstream tube leads the downstream tube for tubes in the same column by a phase angle of $144^{\circ}$. Similarly, the upstream tubes lag the downstream tubes by a phase of $69^{\circ}$ for adjacent tubes in neighboring columns.

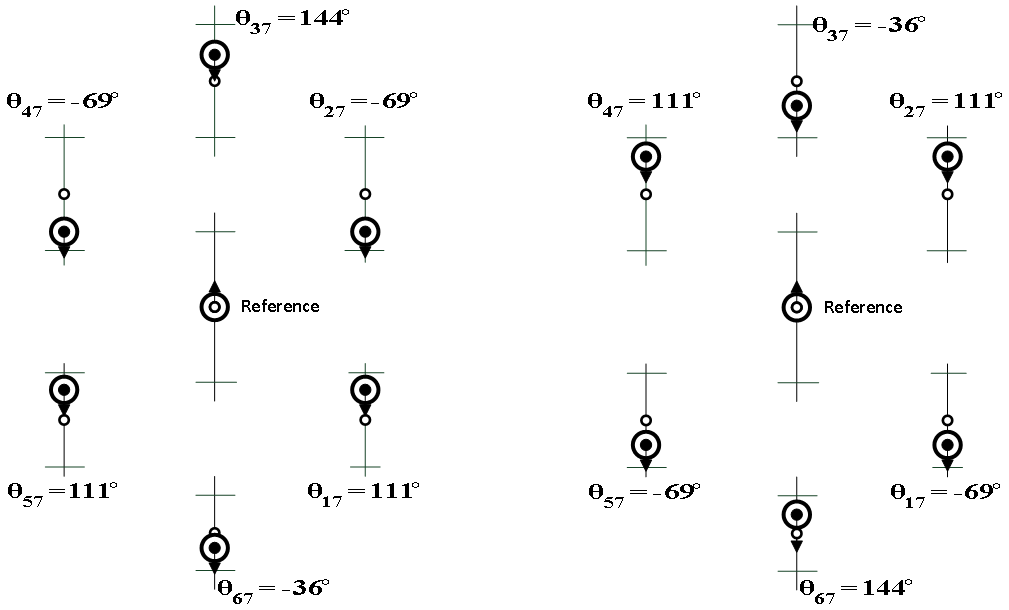


(a) (b)

Figure 3-17 : Modes of Vibration for 90% void fraction, $\sigma^2$=0 (0% detuning) (a) Unstable mode (mode 1) and (b) Mode 2

The same analysis is next repeated for samples of tube frequencies taken from populations with 5% (variance $\sigma^2 = 0.49$), 10% (variance $\sigma^2 = 1.96$) and 20% (variance $\sigma^2 = 7.84$) frequency detuning. In Figure 3-18 the evolution of the eigenvalues for seven different sets of seven frequencies (hence seven different clusters of seven tubes) randomly selected from an original population with 5% detuning (representing seven different arrays of the same configuration) is displayed. The eigenvalue evolutions for 10% and 20% detuning, are shown in Figure 3-19 and Figure 3-20, respectively. It is seen that random detuning has no significant effect on the minimum critical velocity 11.6 m/s for 5% detuning (Figure 3-18 (a)), 11.6 m/s for 10%

detuning (Figure 3-19 (a)) and 11.2 m/s for 20% detuning (Figure 3-20 (a)), respectively. The critical velocity for the tuned case is 11.5 m/s (Figure 3-16).

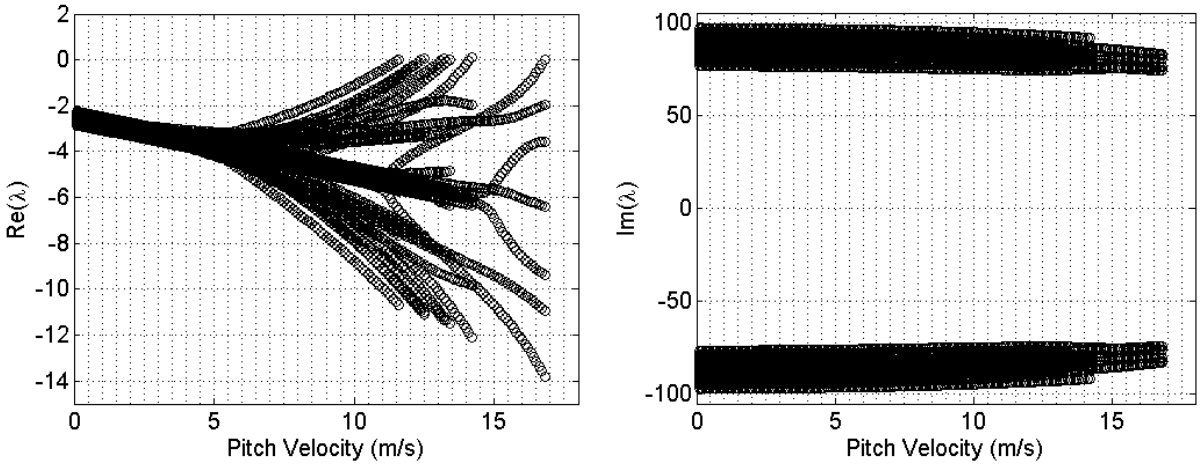


(a) (b)

Figure 3-18 : Evolution of eigenvalue for seven arrays, original population $\sigma^2$=0.49 (5% detuning) (a) real part and (b) imaginary part

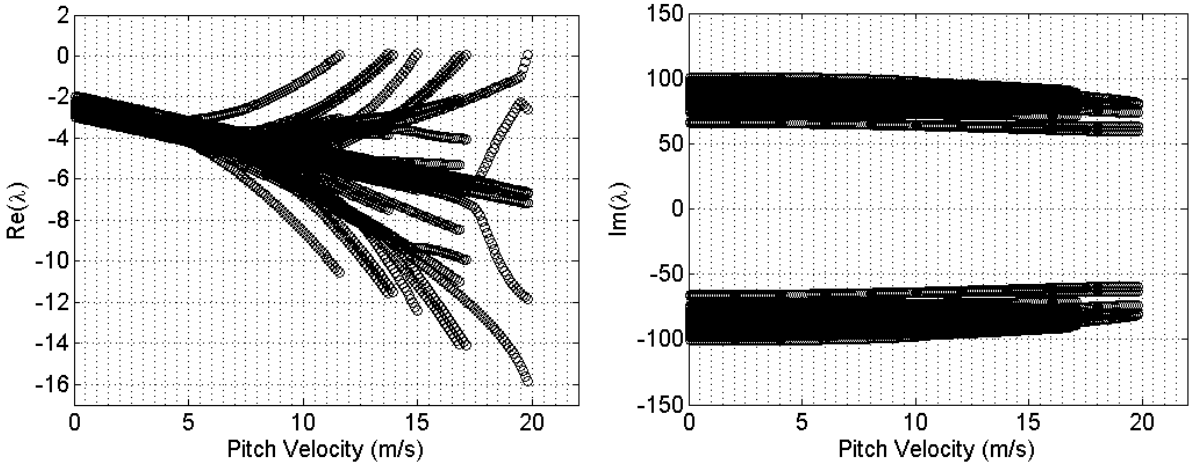


(a) (b)

Figure 3-19 : Evolution of eigenvalue for seven arrays, original population $\sigma^2$=1.96 (10% detuning): (a) real part and (b) imaginary part

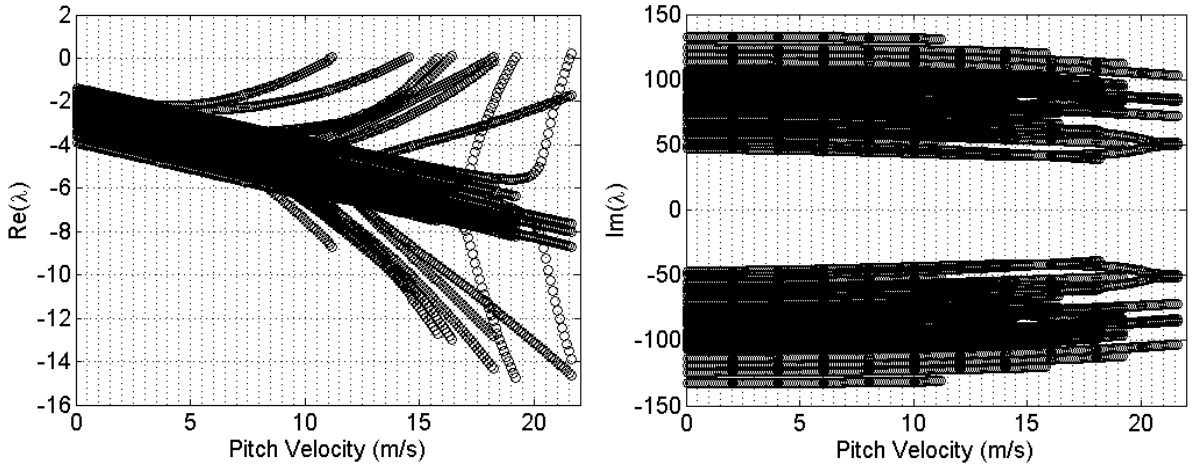


(a) (b)

Figure 3-20 : Evolution of eigenvalue for seven arrays, original population $\sigma^2$=7.84 (20% detuning) (a) real part and (b) imaginary part

It should, however, be noted that the frequency variance for individual samples of seven tubes can be lower or higher than the original population variance. The cross-coupling strength between neighboring tubes is strongly dependent on relative tube frequencies. The smaller the variance the higher the cross-coupling strength between the tubes, resulting in a lower critical velocity. Additionally, the value of the individual frequencies also plays a critical role on the critical velocity. For large initial population variance, it is possible to get a set of lower frequencies than the tuned case resulting in much lower mean frequencies and lower critical velocities. This is exemplified by the minimum critical velocity obtained for the 20% detuning which was found to be 11.2 m/s, with a mean frequency of 12.9 Hz, as compared to 11. 5 m/s for the tuned case (mean frequency of 14 Hz).

The results of the stability analysis for a large number of samples are summarized in Figure 3-21 for tube populations with initial frequency variances, $\sigma^2 = 0.49$ (5% detuning) and $\sigma^2 = 7.84$ (20% detuning), respectively. In both cases the population frequency is normally distributed about the mean value of 14 Hz. In Figure 3-21(a) the initial population variance is $\sigma^2 = 0.49$. However, the variance (and mean) of a given sample of 7 frequencies can be higher or lower as already indicated. In Figure 3-21, the stability constant, $K$, is plotted versus sample frequency variance. The value of $K$ is calculated by Eq. (3-29) and $f_n$ is the average of the seven frequencies in this case. Generally the stability constant increases with frequency variance –

reflecting the stabilizing effect of frequency detuning. Note also that for a given variance, $K$ takes a range of values depending on the frequency combinations and the sample mean frequency. While for the tuned array $K \simeq 10.5$, the effect of detuning increases $K$ to as high as 16 for $\sigma^2 = 0.49$ .

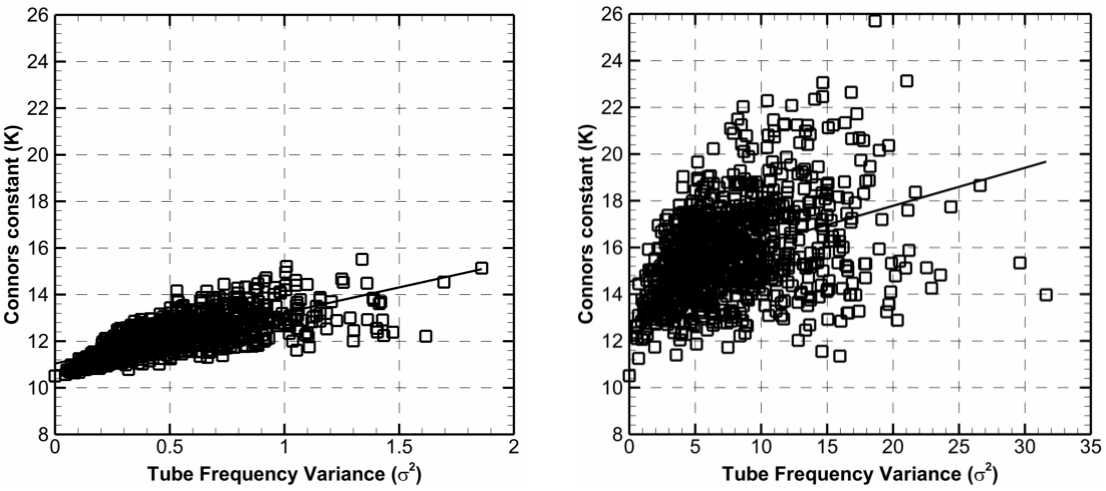


(a) (b)

Figure 3-21 : Effect of frequency detuning on streamwise stability constant (a) $\sigma^2$=0.49 (5% detuning) and (b) $\sigma^2$=7.84 (20% detuning)

The stability results for a frequency detuning of 20% in the original population are shown in Figure 3-21(b). The average stability of the tube cluster is much higher than the tuned cluster. More importantly, however, is the large scatter in possible $K$ values. Stability constants as high as three times the tuned cluster case are possible. The high $K$ values make the tube array very stable. However, the scatter in the value of $K$ suggests that the average $K$ value (shown by the solid line in Figure 3-21) is not a reliable indicator of the array stability.

Figure 3-22 presents analysis done with random frequencies between 14Hz and 2Hz. Here, the objective is to investigate the effect of increasing the unsupported span length due to tube supports becoming inactive. The tube is approximated by a multispan beam whose modal natural frequency is given by (Blevins, 1979b):

$$f_i = \frac{\lambda_i^2}{2\pi l_s^2}\left(\frac{EI}{m}\right)^{0.5} \tag{3-30}$$

where $\lambda_i$ is a dimensionless frequency factor that depends on the mode number, the boundary conditions and the number of spans; $E$ is the modulus of elasticity of the beam material, $I$ is the moment of inertia and $l_s$ the unsupported span length. It can be seen from Eq. (3-30) that the natural frequency varies roughly as the reciprocal of the unsupported span length squared, $l_s^2$. Therefore, taking a hypothetical case of three consecutive supports being inactive, the presence of the longer span lowers the beam frequency by roughly 0.1. It is also instructive to note that, as the length of the span increases (due to several supports being inactive), the frequency of the beam increasingly becomes independent of the number of spans as the longer section dominates the vibration. Similarly to the case of 20% frequency detuning (Figure 3-21 (b)) a large scatter is also observed in the case of span length variation (Figure 3-22). Note, however, that in Figure 3-22, the frequency range is limited to between 14Hz and 2Hz while in the former case the frequencies could be higher or lower than 14Hz, respecting a variance of 7.84 about the mean (14Hz). In the latter case (Figure 3-22) the mean of a sample of seven frequencies can get very low, hence presence of much lower $K$ values. From a frequency variance of about 7 (Figure 3-22), instances of $K$ values lower than the tuned case start becoming manifest. Values of $K$ as low as 50% of the tuned case are possible. The variability in the $K$ values makes it a challenge to accurately estimate the stability boundary for in-plane instability for a detuned group of tubes (the case in practice).

This complex stability behavior associated with frequency detuning is tied to the governing instability mechanism for streamwise vibrations. For out-of-plane instability, where the damping controlled mechanism is dominant, frequency detuning has minimal effect on the critical velocity (Cheng, 1994). In all cases, the tube with the lowest frequency would become unstable (assuming identical tube damping) at a lower velocity than the others. From a vibration design point of view, the choice of stability constant, $K$, is vitally important. The results above suggest that this must be done with care for streamwise instability due to possible significant variance in the stability constant with frequency detuning. Physically, this leads to the challenge of defining the correct in-plane boundary conditions, hence in-plane frequencies for fluidelastic instability analysis. In view of the difficulty in controlling tube support/AVB contact conditions, a possible remedy is to introduce in-plane AVBs. In-plane AVBs would result in well-defined support conditions, similar to the out-of-plane situation. The well-defined support conditions would yield

acceptable stability constant, $K$, variance allowing for the possibility of performing in-plane fluidelastic instability analysis with the same confidence as that for the out-of-plane direction.

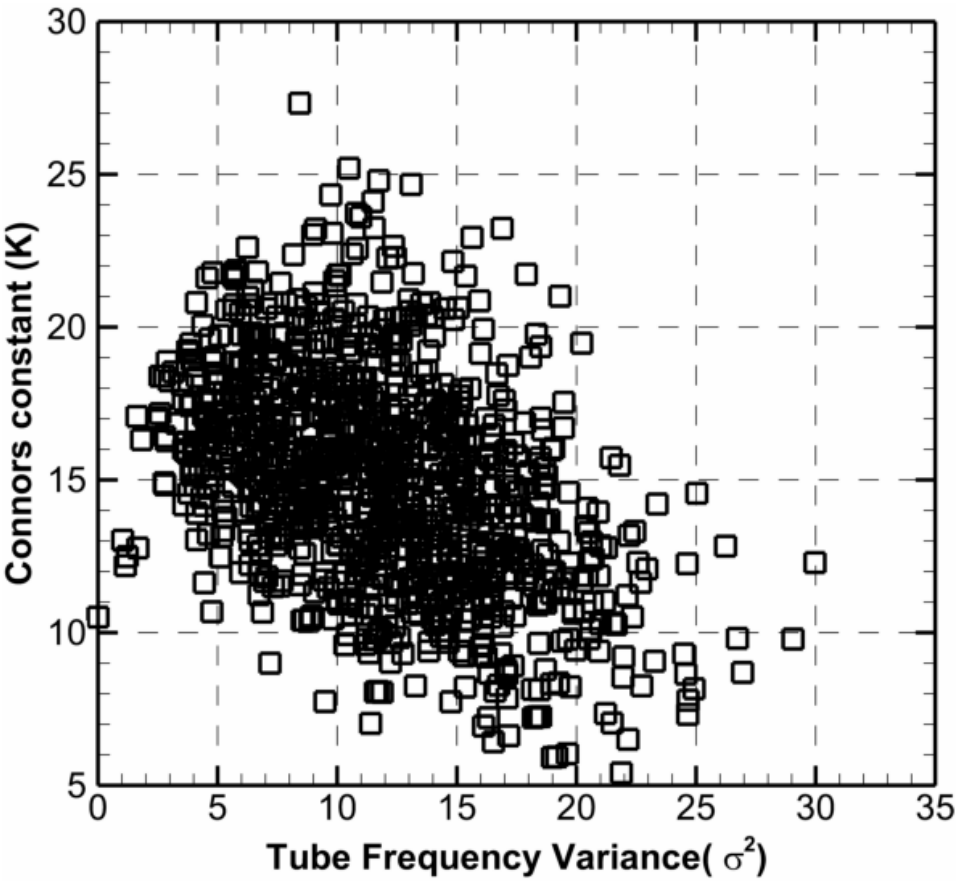


Figure 3-22 : Effect of random frequency detuning on streamwise stability constant, $2Hz \le f \le 14Hz$

## 3.6 Conclusion

Steady fluid forces were measured for a kernel of tubes in a rotated triangular tube array of pitch-to-diameter ratio, $P/D = 1.5$ subjected to air-water two-phase cross-flow. The derivatives of the forces were used in the quasi-steady model to estimate streamwise fluidelastic instability of multiple flexible tubes in a rotated triangular array. The results were found to be in good agreement with dynamic stability tests data of Violette et al. (2006). It was found that the critical velocity decreases with increasing number of flexible tubes in a single column. Additionally, a single flexible column was found to be more stable than multiple flexible adjacent columns.

Since the time delay term was neglected in the present analysis, the results indicate that cross-coupling forces are more important than the time delay effects in generating streamwise instability for the case of multiple flexible tubes in a rotated triangular array.

Frequency detuning has been shown to strongly affect the stability boundary of a cluster of tubes purely flexible in the flow direction, much more than would be the case for out-of-plane fluidelastic instability where the damping controlled mechanism dominates. This means that estimating conservative values for the stability constant will be a challenge due to this strong sensitivity to frequency detuning. In particular, typical stability constants from experimental tests may not be conservative if frequency detuning is not carefully controlled.

Finally, the present analysis demonstrates the potential of the quasi-steady model in predicting streamwise fluidelastic instability threshold in tube arrays of the type studied here subjected to two-phase cross-flow, with the benefit of reduced experimental effort.

# CHAPTER 4 ARTICLE 2: STREAMWISE FLUIDELASTIC VIBRATION OF A TRIANGULAR TUBE ARRAY IN TWO-PHASE FLOW. PART I: UNSTEADY FLUID FORCES AND TIME DELAY ESTIMATION

Olala, S. and Mureithi, N. W. (2016)

Submitted to "Journal of Fluids and Structures" on 20th July 2016

## Abstract

Experimental tests were conducted to measure unsteady fluid forces acting on a kernel of tubes in a rotated triangular tube array of P/D =1.5 subjected to air-water two-phase flow when the central tube was oscillated in the flow direction. The measurements were done for a series of void fractions, excitation frequencies and flow velocities with the excitation amplitude maintained at 5 mm (0.13D). The measured unsteady streamwise fluid force magnitude was found to be a single valued function of the reduced velocity, and showing no dependence on the reduced velocity for high values of the reduced velocity. The cross-coupling fluid force phase, however, showed scatter possibly due to weak coherence between the central tube motion and the induced unsteady forces.

The unsteady fluid forces together with previously measured quasi-steady forces were then used to estimate, firstly, the time delay between the central tube motion and fluid forces on itself and secondly, the time delay between the central tube motion and the fluid forces generated on the adjacent tubes. The time lag was extracted for each of the instrumented tubes and the time delay parameter obtained for void fractions between 60%-90%. The time delay showed significant dependence on tube position and void fraction.

*Key words***:** Two-phase flow, tube array, streamwise fluidelastic instability, quasi-steady model, Time delay, cross-flow

## 4.1 Introduction

Nuclear steam generator tubes especially those in the U-bend region are subjected to two-phase cross-flows that ordinarily lead to tube vibrations emanating from a number of excitation sources,

notably: turbulent buffeting, flow periodicities and fluidelastic instability (Pettigrew & Taylor, 1991). Being the most prevalent source of tube failures in the short term, fluidelastic instability has attracted considerable study efforts and several theories have been formulated for its modeling. The first study of fluidelastic instability was conducted by Roberts (1962) in the early 1960s. Roberts studied the stability behavior of both single and double tube rows subjected to cross flow. The streamwise instability of the tube was attributed to a jet-switch mechanism, which resulted in motion-dependent changes in pressure distribution around the tubes. The jet-switch model could not be easily extended to tube arrays in part due to lack of clearly identifiable jet switching in closely packed tube arrays. The next significant contribution was by Connors (1970) and Blevins (1974) who proposed what was effectively an aero-elastic model in which tube displacement dependent forces created a destabilizing effect via the cross-coupling between different degrees-of-freedom. The main assumption of the quasi-static model of Connors (1970) is that the vibration characteristics of an oscillating tube may be approximated by the tube's successive static states.

Following the work of Connors (1970), other models have been developed. These include the quasi-steady model (Price & Paidoussis, 1982, 1983, 1984, 1986b), the quasi-unsteady model (Granger & Paidoussis, 1996), the unsteady model (Chen, 1983a, 1983b; Tanaka & Takahara, 1980, 1981) and the semi-analytical model (Lever & Weaver, 1982, 1986a, 1986b). These theories were developed primarily for single phase flows hence a need for their extension to two-phase flows.

Fluidelastic instability is generally governed by two distinct mechanisms: the damping controlled and fluidelastic stiffness controlled mechanisms. The damping controlled instability requires only one degree-of-freedom and occurs when the net system damping becomes negative. It generally results in tube oscillations in the cross-flow direction. The stiffness controlled instability on the other hand results from the cross-coupling between tubes due to the flowing fluid, thus requires at least two-degrees-of-freedom.

A number of studies (Lever & Weaver, 1982; Olala et al., 2014; Sawadogo & Mureithi, 2014a; Violette et al., 2006) have shown that a single flexible tube in a rigid tube array becomes unstable in the cross-flow direction and not in the streamwise direction. This implies that streamwise

fluidelastic instability is predominantly stiffness controlled thus dependent on the fluid coupling between tubes.

Among the aforementioned fluidelastic instability models, the quasi-steady model was used in the current study. As observed by Sawadogo & Mureithi (2014b) the quasi-steady model is able to overcome the challenges posed by the other models namely: complexity of the two-phase flow making implementation of the semi-analytical model (Lever & Weaver, 1982, 1986a, 1986b) cumbersome, enhanced experimental effort required by the unsteady model (Chen, 1983a, 1983b; Tanaka & Takahara, 1980, 1981), the apparent multi-valued functional relation between the unsteady fluid force coefficient and the reduced flow velocity, $(U/fD)$ (Inada et al., 2002; Mureithi et al., 2002) and weak correlation between the tube displacement and the resulting unsteady fluidelastic forces (Mureithi et al., 2002) in two-phase flow.

The most important parameters for the quasi-steady model are the quasi-steady fluid forces and the time delay between tube displacement and the fluid forces. Shahriary et al. (2007) measured the quasi-steady forces on a central kernel of tubes in a rotated triangular array subjected to air-water two-phase flow and employed the quasi-steady model to perform stability analysis. The analysis in this study was restricted to the cross-flow direction. Recently, Sawadogo & Mureithi (2014a) used the quasi-steady model to perform stability analysis for a single tube constrained to vibrate in the transverse direction to the flow in a rotated triangular tube array. Sawadogo & Mureithi (2014a) measured both the quasi-steady and the unsteady forces which were used to extract the time lag between the tube motion and the resulting fluid forces. More recently, Olala & Mureithi (2016a) conducted streamwise quasi-steady force measurements for a central cluster of tubes in the same rotated triangular array used by Sawadogo & Mureithi (2014b). The authors performed streamwise stability analysis of multiple flexible tubes using the quasi-steady model (with the effect of the time delay ignored) and found the results to be in fairly good agreement with the dynamic stability tests of Violette et al. (2006). The current study is thus a continuation of the work reported in Olala & Mureithi (2016a).

In the present study, detailed unsteady cross-coupling force and phase measurement results for a central cluster of tubes in a rotated triangular tube array of P/D=1.5 subjected to air-water two-phase cross-flow are presented. The unsteady fluid forces are then used, together with previously measured quasi-steady forces (Olala & Mureithi, 2016a) to estimate the time delays between the

motion of the central tube and the forces on the neighboring tubes by the same approach used in Sawadogo & Mureithi (2014b). The obtained time delays are later used to determine fluidelastic stability threshold in the second part of the paper (Olala & Mureithi, 2016c).

### 4.1.1 Definition of two-phase flow parameters

The homogeneous model was used to estimate the two-phase flow parameters in the current work. The model assumes a uniform flow through the cross section of the channel with the gas and liquid phases traveling at the same velocity. The void fraction $\beta$, is equal to the volumetric flow fraction and is given by:

$$\beta = \frac{Q_g}{Q_l + Q_g} \tag{4-1}$$

while mixture density, $\rho_h$, and the free stream flow velocity $U_\infty$ are expressed as:

$$\rho_h = (1-\beta)\rho_l + \beta\rho_g; \quad U_\infty = \frac{\rho_g Q_g + \rho_l Q_l}{\rho A} \tag{4-2}$$

The pitch velocity, $U$, defined in terms of the free stream velocity is given by:

$$U = U_\infty \frac{P}{P-D} \tag{4-3}$$

The Reynolds number, $\mathrm{Re}$, based on the pitch flow velocity is then expressed as:

$$\mathrm{Re} = \frac{\rho_h U D}{\mu_{tp}} \tag{4-4}$$

where the homogeneous mixture viscosity, $\mu_{tp}$, is obtained by McAdams relation (McAdams et al., 1942):

$$\frac{1}{\mu_{tp}} = \frac{x}{\mu_g} + \frac{(1-x)}{\mu_l} \tag{4-5}$$

and the gas mass quality $x$, is given by:

$$x = \frac{\rho_g Q_g}{\rho_g Q_g + \rho_l Q_l} = \frac{\beta}{\beta + (1-\beta)\rho_l/\rho_g} \tag{4-6}$$

## 4.2 Experimental apparatus

### 4.2.1 Experimental Setup

#### 4.2.1.1 Two-Phase Test Loop

The two-phase test loop used for the experiments is shown in Figure 4-1. The test loop consists of a 1500 l capacity water tank, a 26 l/s centrifugal pump, a water flow meter (MAG500), a 250 l/s compressed air supply system and connecting piping. The compressed air is supplied to the loop below the test section and the two fluids are homogenized by a mixer. The air flow rate is measured using two distinct orifice plates, for low and high flow rates respectively, located away from the test section and connected to a differential pressure transducer. Pressure at the test section is measured to correct the air flow rate. All measurements were conducted at atmospheric conditions ($22^{\circ}$ C).

#### 4.2.1.2 Test section

The measurement test section shown in Figure 4-2 comprises 19 full tubes and 14 half tubes arranged in a rotated triangular configuration. The half tubes are attached to the wall to minimize wall effect. Except for the central tube, all the other tubes are fixed, rigid and made of Plexiglas. The central tube, made of aluminum, is mounted on a force transducer attached to a displacement mechanism consisting of a linear motor (Figure 4-3 (a)). The test section has a flow area of 0.038 $m^2$ (0.2 m x 0.19 m) and the diameter of each of the tubes is 38 mm with the pitch-to-diameter ratio $P/D = 1.5$. Four tubes (1, 2, 3 & 4 in Figure 4-2) neighboring the central tube are strain-gauge instrumented (Figure 4-3 (b)). Two pairs of diametrically opposite strain gauges installed at 90° from one another in each tube are used to measure forces in the drag and lift directions, respectively. The instrumented tubes are located in the middle of the array such that there are four rows upstream and downstream of the instrumented cluster, respectively. A more detailed description of the test section can be found in Olala & Mureithi (2016a).

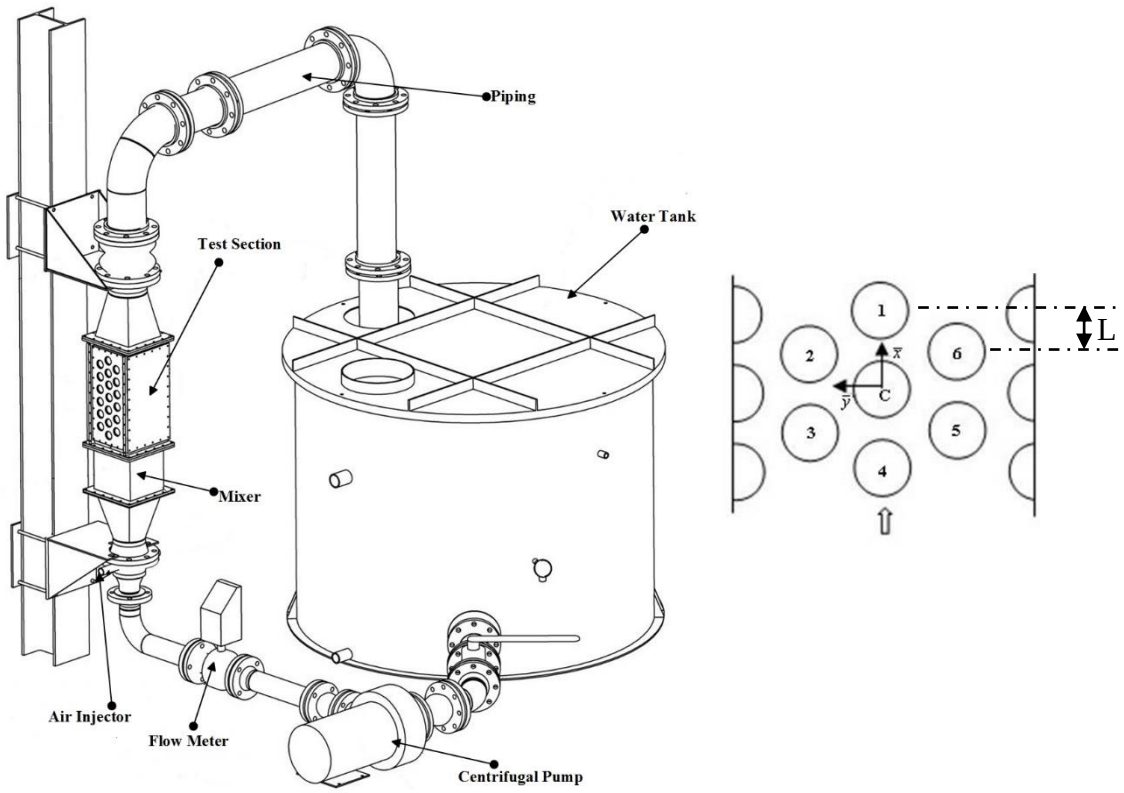


Figure 4-1 : Two-phase flow test loop and array configuration

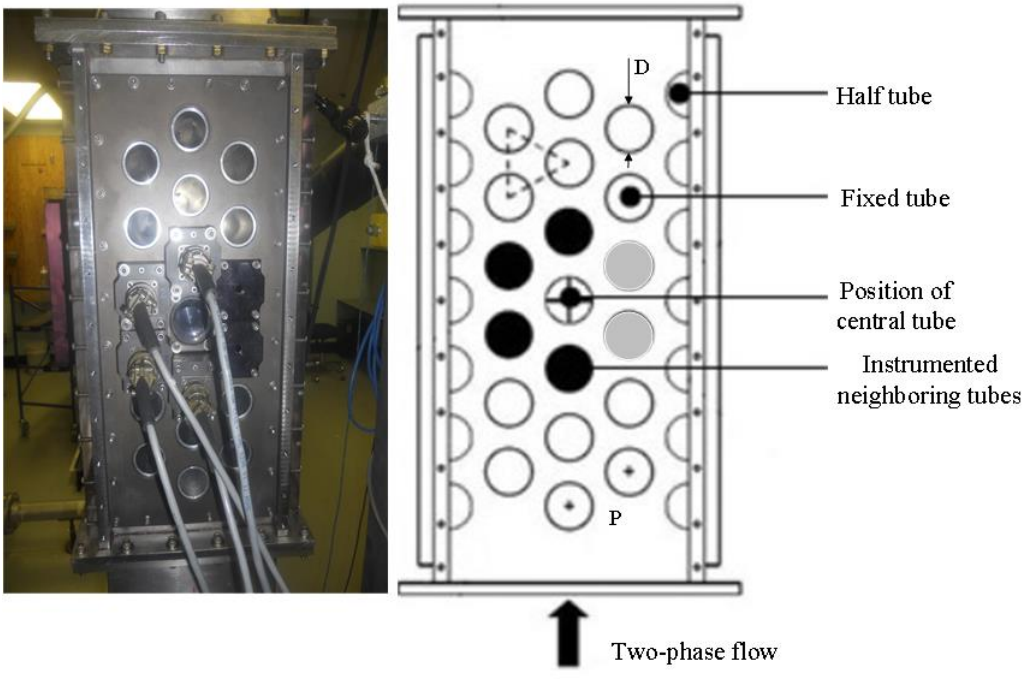


Figure 4-2 : Test section for unsteady fluid forces cross-coupling measurements

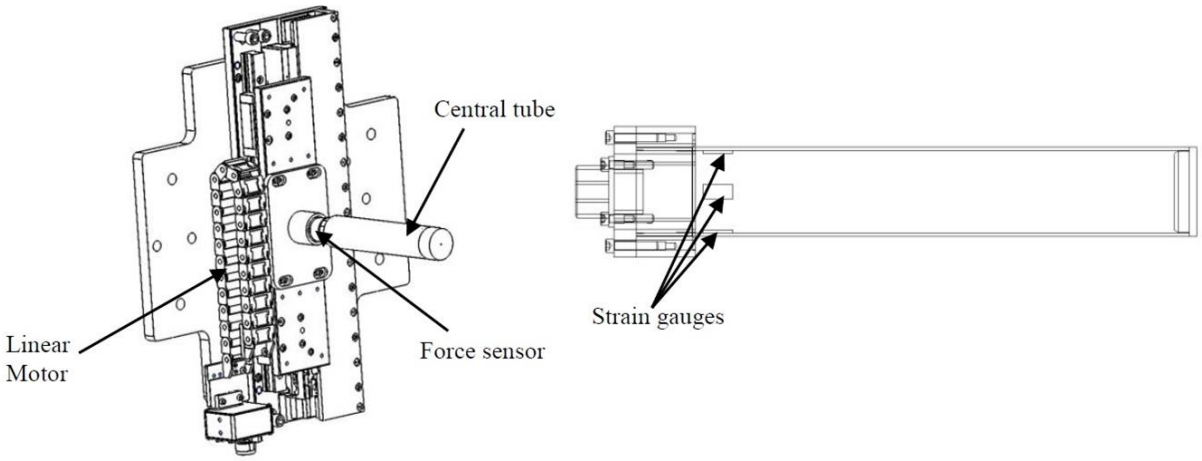


(a) (b)

Figure 4-3 : Instrumented tubes (a) central tube mounted on linear motor (b) instrumented neighboring tube

### 4.2.2 Test procedure

The instrumented tubes used in this study (labeled C, 1, 2, 3, 4) are shown in Figure 4-1 and Figure 4-2. Due to the symmetry of the test section, only force measurements of the tubes marked C, 1, 2, 3 and 4 are reported in this paper. Measurements of the unsteady forces were conducted for five void fractions: 0% (liquid flow), 60%, 70%, 80% and 90%. The central tube was excited at seven different frequencies, using the linear motor, up to 16 Hz. For each void fraction, measurements were done for up to twelve different flow velocities and the excitation amplitude of the central tube set at 5mm (0.13D) for all the frequencies. This amplitude is equivalent to 26% of the inter-tube spacing. The choice of the excitation amplitude is informed by the necessity to induce measurable cross-coupling effect on the neighboring tubes while at the same time minimizing non-linearity that may appear in the unsteady fluid force due to large vibration amplitudes. Inada et al. (2002) found the non-linearity in the unsteady fluid force coefficient to be negligible for vibration amplitudes $\leq$0.14D in a square tube array of P/D=1.42. The forcing amplitude in Inada et al. (2002) was 33% of the inter-tube spacing. The effect of amplitude on the fluid force coefficient was also tested in this study by varying the vibration amplitude from 2mm (0.05D) to 5mm (0.13D). For $U_\infty = 0.3\,\text{m/s}$, the change in the force coefficient magnitude and phase for tube C was found to be 1.4%-1.8% and 0.1%-3.6%, respectively for 60% void fraction.

In the current study, the fluid force and displacement data were acquired at a sampling rate of 2000 Hz and averaged over 240 seconds.

## 4.3 Unsteady fluid force measurements

The measured force per unit length on the central tube when it is harmonically excited in the streamwise direction may be expressed as:

$$F_{\_measured} = \left[ \omega^2 \left( m_s + m_h \right) + i\omega \frac{\rho_h UD}{2} C_{dh} + \frac{\rho_h U^2}{2} C_{sh} \right] x_c \tag{4-7}$$

where $C_{dh}$ and $C_{sh}$ are, respectively, the fluid damping and stiffness coefficients. $m_s$ is the tube mass per unit length, $m_h$ the hydrodynamic mass per unit length, $D$ the tube diameter while $U$, $\rho_h$ and $\omega$ are the pitch velocity, the fluid homogeneous density and the angular excitation frequency, respectively. $x_c = x_0 e^{i\omega t}$ is the central tube displacement amplitude.

The unsteady fluid force, $F_{Uns}$, may then be obtained from Eq. (4-7) by removing the tube inertia term. Thus

$$F_{Uns} = \left[ \omega^2 m_h + i\omega \frac{\rho_h UD}{2} C_{dh} + \frac{\rho_h U^2}{2} C_{sh} \right] x_c = \left[ \frac{1}{2} \rho_h U^2 C_F e^{i\phi_F} \right] x_c \tag{4-8}$$

The dimensionless damping coefficient, $C_{dh}$, and stiffness coefficient, $C_{sh}$, in Eq. (4-8) can then be written in terms of the magnitude and phase of the dynamic fluid force coefficient as

$$C_{dh} = \frac{U}{D\omega} C_F \sin\phi_F \tag{4-9}$$

and

$$C_{sh} = C_F \cos\phi_F - \frac{\omega^2 m_h}{\rho_h U^2 / 2} \tag{4-10}$$

However, for the fixed instrumented neighboring tubes (labeled 1, 2, 3 and 4), the total measured unsteady force represents a coupling force induced by the vibration of the central tube. The tube mass, $m_s$, in Eq. (4-7) is therefore absent in the expression of this cross-coupling force. The $C_{dh}$,

$C_{sh}$ and $m_h$ consequently represent cross-coupling damping, stiffness and hydrodynamic mass components, respectively. Equation (4-8) then becomes, for the fixed tubes:

$$F_{Uns-CC} = \left[ \omega^2 m_{h_{cc}} + i\omega \frac{\rho_h U_p^2 D}{2} C_{dh_{cc}} + \frac{\rho_h U_p^2}{2} C_{sh_{cc}} \right] x_c \qquad (4\text{-}11)$$

A more elaborate data reduction procedure may be found in Mureithi et al. (2002).

The measured force for tube C is subject to a phase shift induced by the flow independent damping and the electronic measuring devices. This is accounted for by subtracting the phase difference obtained at the lowest possible velocity for each void fraction (typically $U_\infty = 0.4$ m/s) and each frequency from the rest of the measured phases. A similar procedure is performed for the fixed surrounding tubes to eliminate the phase induced by the electronic measuring devices. Therefore the fluid force phases presented in Figure 4-4 to Figure 4-12 are all corrected as outlined above. Only the streamwise unsteady force coefficients are presented in this paper.

The results of the dynamic fluid force measurements are presented in Figure 4-4 to Figure 4-12. The continuous solid line represents a trend line obtained by polynomial "least-square" curve fitting to the experimental data. It is noted that for all the void fractions considered, all the data points for the unsteady fluid force coefficient magnitude collapse onto a single curve denoting the fluid force coefficient magnitude to be approximately a single valued function of the reduced flow velocity, $(U/fD)$. The magnitude of the fluid force coefficient also appears to be relatively independent of the reduced velocity for high $U/fD$. This, as previously noted by Chen (1987), is due to the velocity of the tube being much smaller than the fluid flow velocity at high $U/fD$ resulting in the transient motion of the tube having no significant influence on the fluid force coefficients.

Figure 4-4 to Figure 4-6 show the magnitude and phase of the fluid force coefficient for liquid water flow. It is observed that in water flow, the induced dynamic fluid force magnitudes for tubes 1 and 4 which are, respectively, downstream and upstream of the central vibrating tube C are equal while the phases are opposite in sign but of similar order of magnitude in general. The phase for tube 1 show an increasing trend with an inflection point at $U/fD \simeq 2$. The phase reaches a maximum at $U/fD \simeq 5$. The phase difference for tube 4, however, displays almost a

linear trend for the range of the reduced velocity tested. Similarly, tubes 2 and 3, tube 2 being downstream of tube 3, but both on the same side of the central vibrating tube C (as shown in Figure 4-1) have effectively equal fluid force coefficient magnitude but opposite phase differences. The phases are negative for tubes upstream (tubes 3 and 4) and positive for the ones downstream (tubes 1 and 2) of the central vibrating tube, respectively.

The unsteady fluid force on the central tube C is much higher than for the rest of the tubes since it is the only vibrating tube. Its phase is, however, negative, similarly to the cases of tubes 3 and 4. The phases represent the time lag/lead between the displacement of the central tube and the motion-dependent unsteady fluid forces on the specific tube. It follows therefore, that the dynamic fluid force on tubes 1 and 2 leads the central tube displacement while it lags in the case of tubes C, 3 and 4.

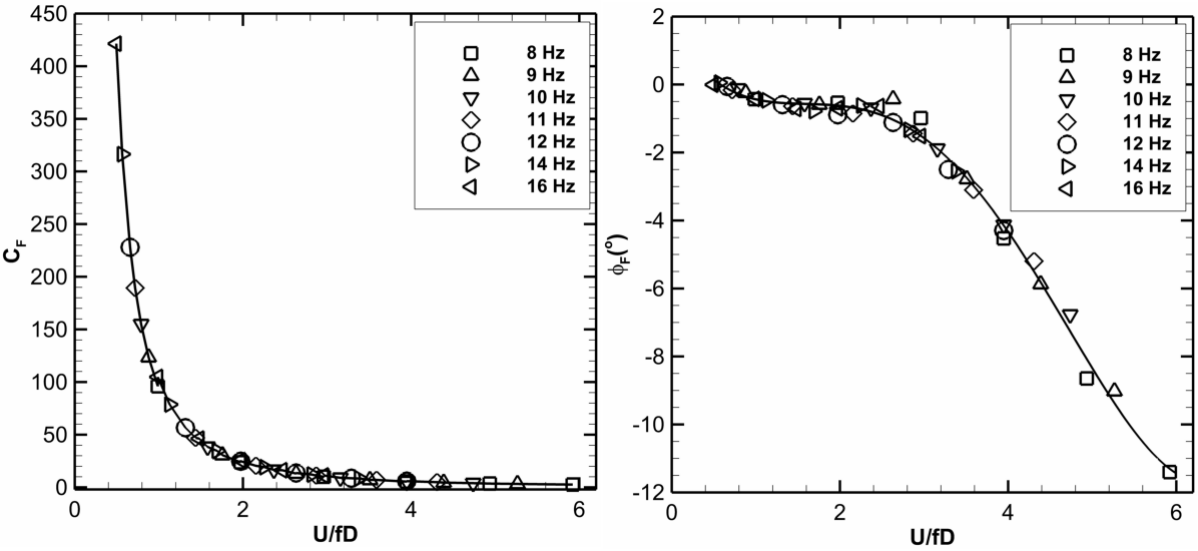


(a) (b)

Figure 4-4 : Variation of the unsteady streamwise fluid force coefficient with $U/fD$ for tube C, $\beta = 0\%$

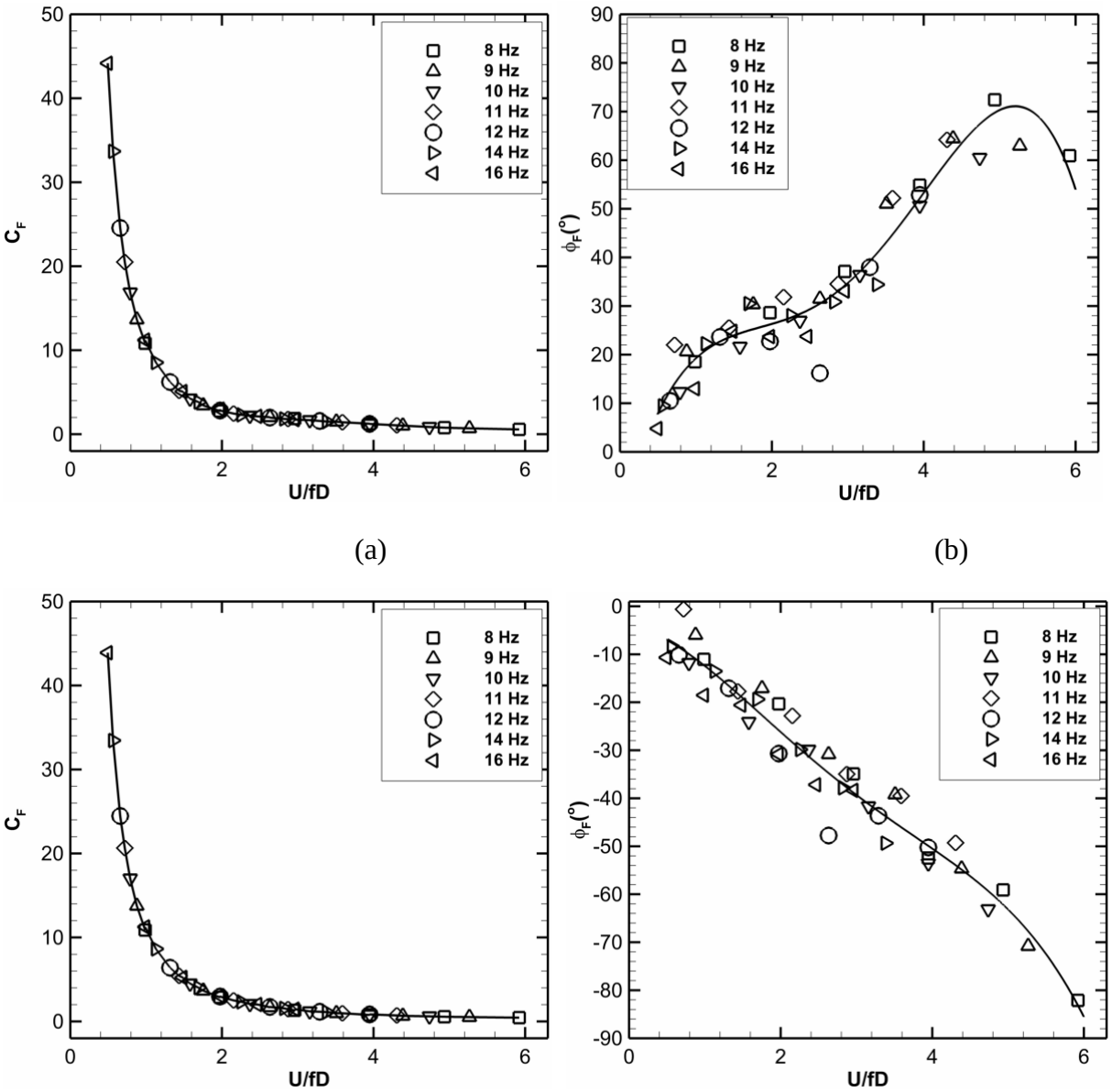


Figure 4-5 : Variation of the unsteady streamwise fluid force coefficient with $U/fD$ for $\beta = 0\%$ (a-b) Tube 1, (c-d) Tube 4

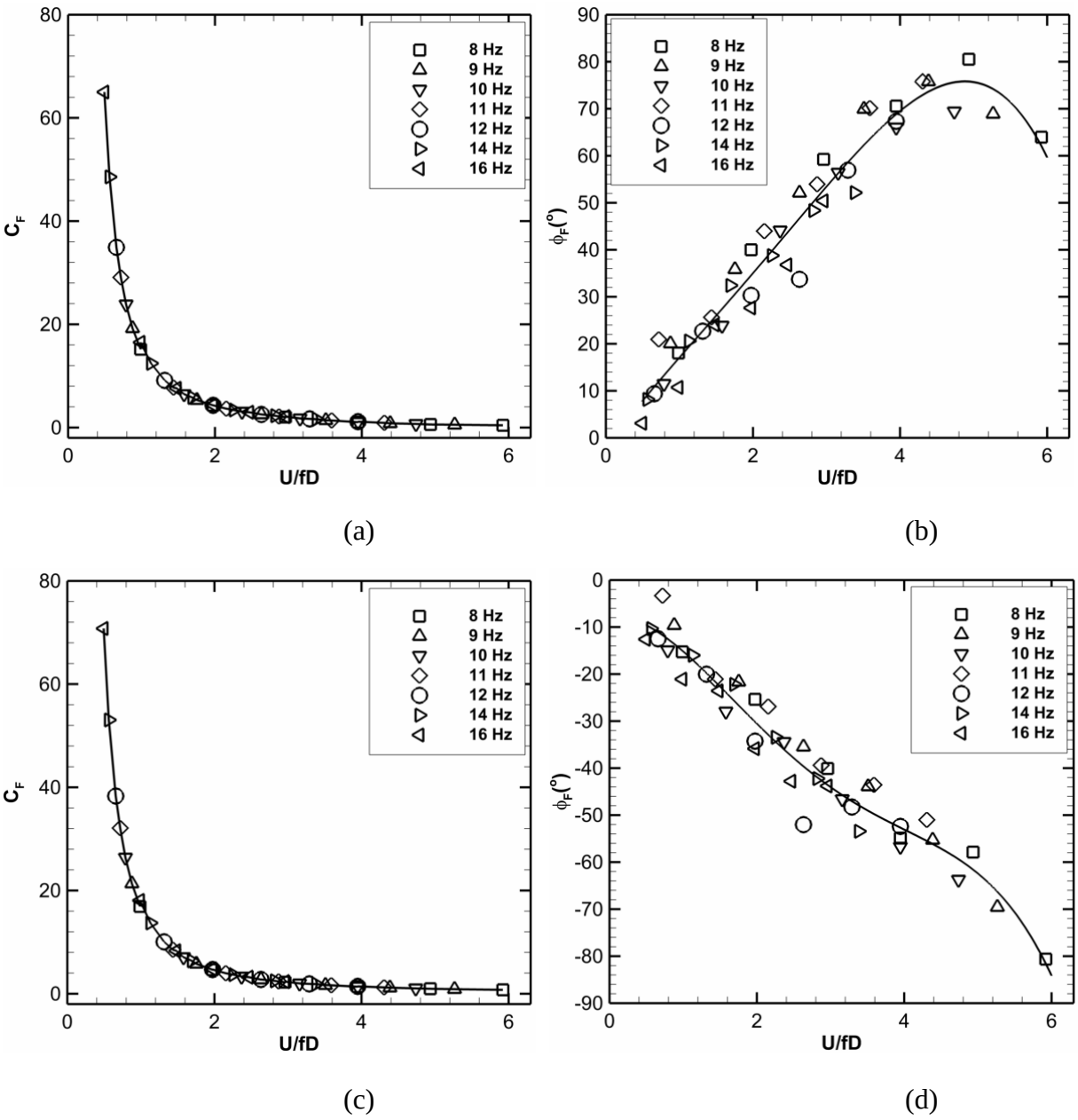


Figure 4-6 : Variation of the unsteady streamwise fluid force coefficient with $U/fD$ for $\beta = 0\%$ (a-b) Tube 2, (c-d) Tube 3

Representative unsteady fluid force measurement results for two-phase flow are presented in Figure 4-7 to Figure 4-12 for 60% and 80% void fractions, respectively. It is seen that the general trends of the unsteady fluid force coefficient magnitude and phase are similar to those in water flow although the magnitudes differ. In addition, Tube 2 forces show different characteristics for two-phase flow. Tube 2 phase is initially positive and increases up to a reduced velocity,

$U/fD \simeq 4$ for the two-phase flows and then decreases approximately linearly to negative values. At $U/fD \simeq 8$, the gradient of the fluid force phase changes, the change being more pronounced for the 80% void fraction. A better collapse of the phase data is obtained for the liquid single phase flow than the two-phase flow. The evident scatter in the two phase data, which increases with void fraction, may be attributed primarily to two phase flow intermittency and turbulence. Clearly for 60% and 80% void fractions (high void fraction two-phase in general) the flow pattern is significantly non-uniform, which reduces the force-displacement correlation or coherence. This is more pronounced in the phases corresponding to the cross-coupling forces (Tubes 1, 2, 3 & 4). Despite the scatter, the trend of the data is consistent. For the moving tube C (Figure 4-7 (b) & Figure 4-8 (b)), the phase scatter is much lower for a specific void fraction.

The force coefficients for tubes 5 and 6 (Figure 4-1) can be deduced from those of tubes 2 and 3 due to the symmetry of the array under consideration. Similarly to Tanaka & Takahara (1980) observation for a normal square array of $P/D = 1.33$ in water flow, the phase between the streamwise dynamic fluid force on tube C and the displacement of the central tube, C, in the flow direction is negative for both water and two-phase flows in the rotated triangular array of $P/D = 1.5$.

The trends of the force coefficient magnitude for the central vibrating tube are also similar to those obtained by Sawadogo & Mureithi (2014b) for the transverse oscillation measurements in the same test section. In Sawadogo & Mureithi (2014b), the central tube was excited at frequencies between 5 Hz-28 Hz with amplitudes set at 3 mm (0.08D) for frequencies up to 11 Hz and 2 mm (0.05D) for higher frequencies. However, the phases differ in both size and sign. Sawadogo & Mureithi (2014b) found the fluid force phase for tube C in the transverse direction to be always positive in two-phase flow with values increasing from 0° for small reduced velocities to 180° for higher values of $U/fD$. In the streamwise direction, however, the fluid force phase for tube C is essentially negative decreasing from 0° to about -50° with increasing reduced velocity.

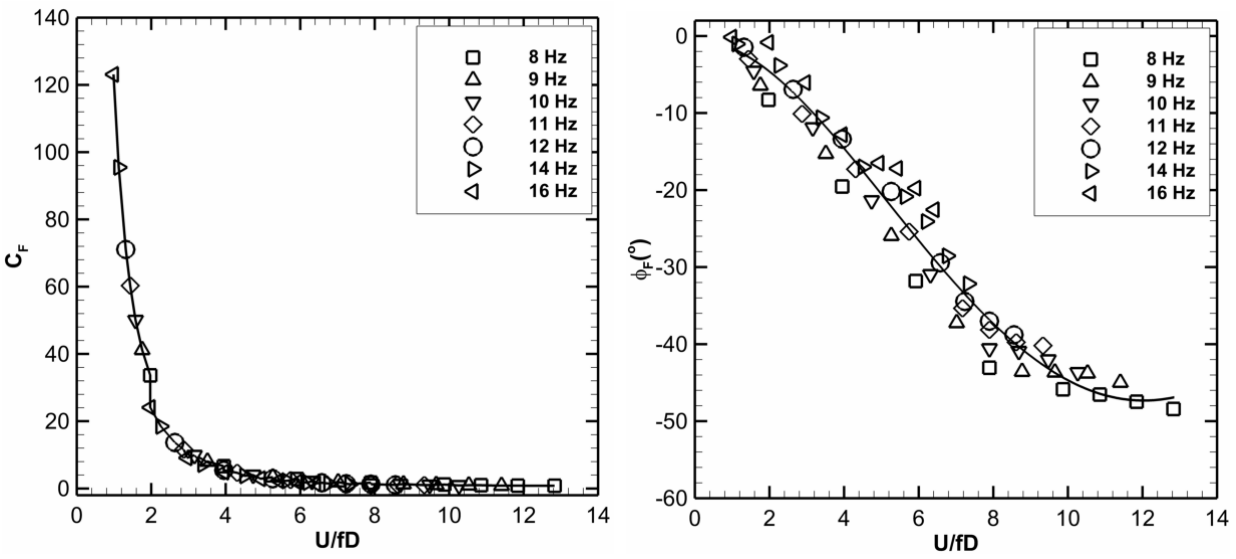


(a) (b)

Figure 4-7 : Variation of the unsteady streamwise fluid force coefficient with $U/fD$ for tube C, $\beta = 60\%$

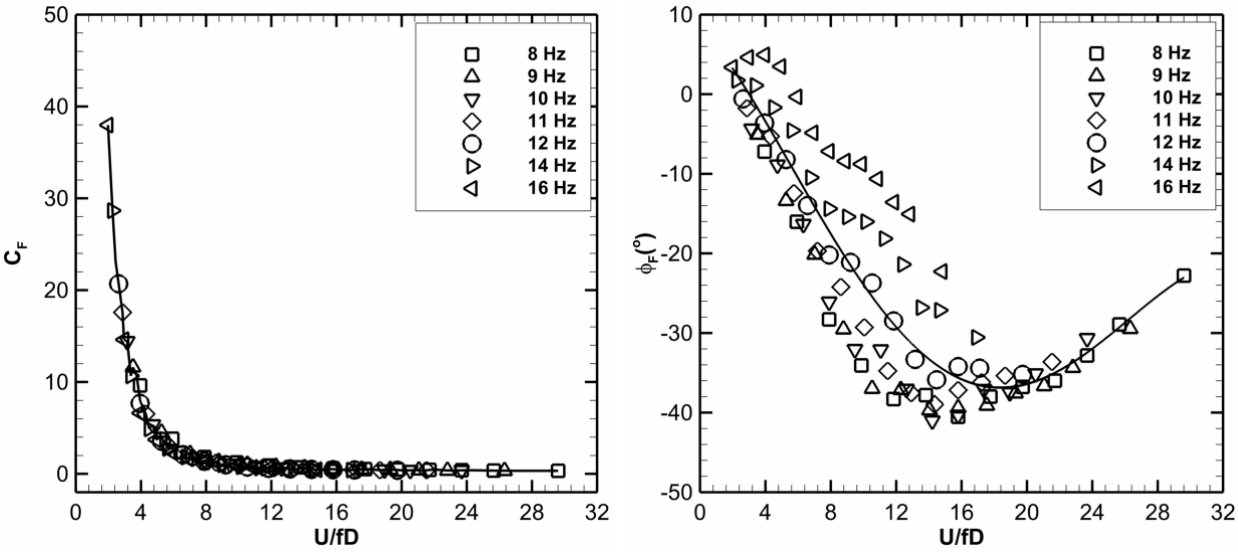


(a) (b)

Figure 4-8 : Variation of the unsteady streamwise fluid force coefficient with $U/fD$ for tube C, $\beta = 80\%$

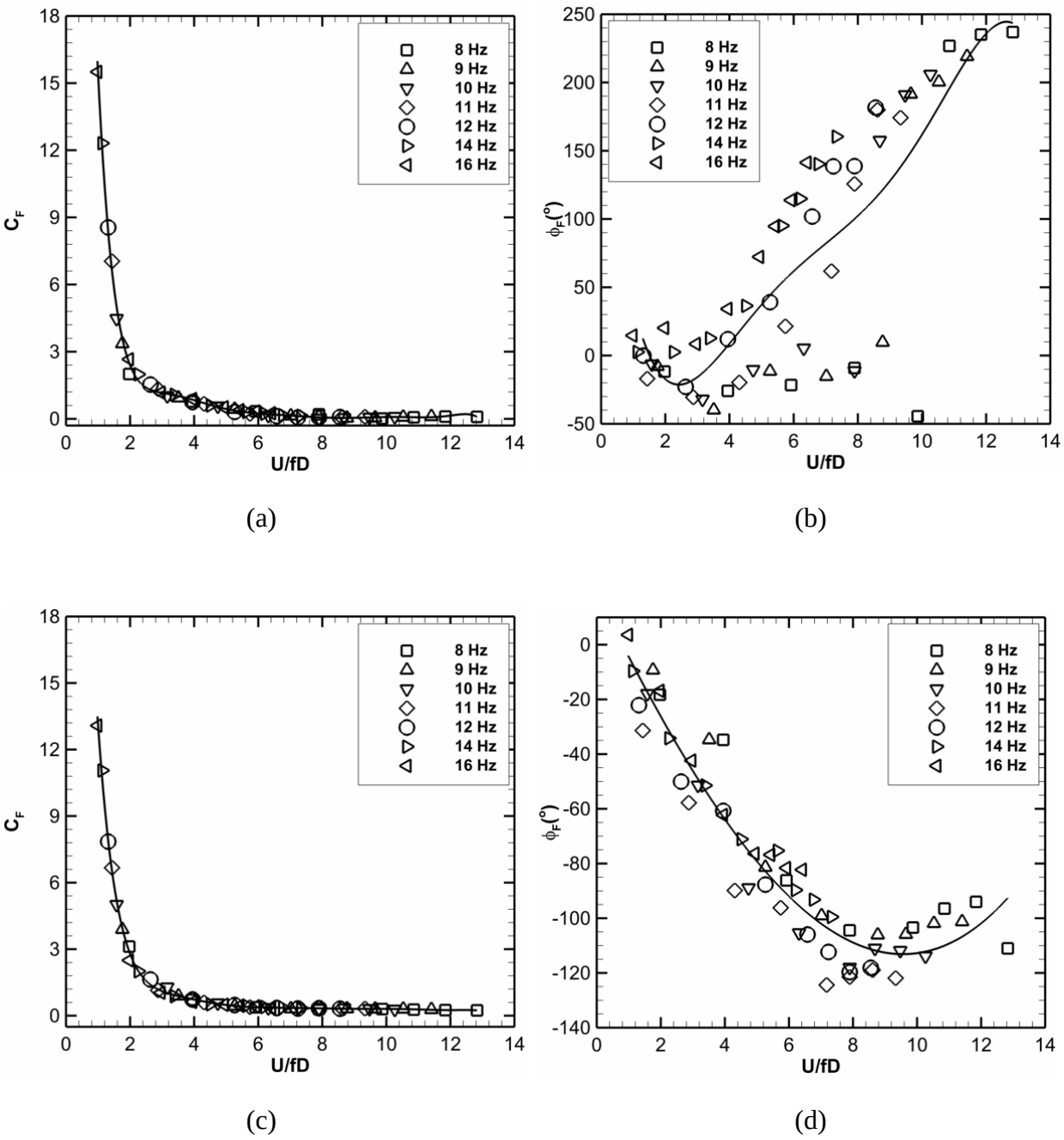


Figure 4-9 : Variation of the unsteady streamwise fluid force coefficient with $U/fD$ for $\beta = 60\%$ (a-b) Tube 1, (c-d) Tube 4

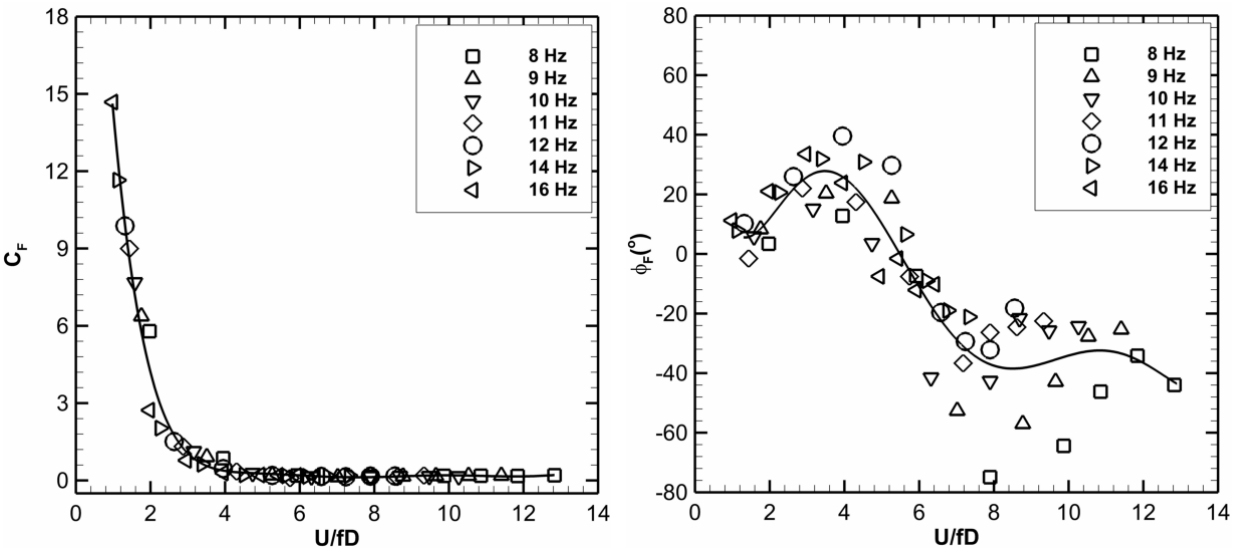


(a) (b)

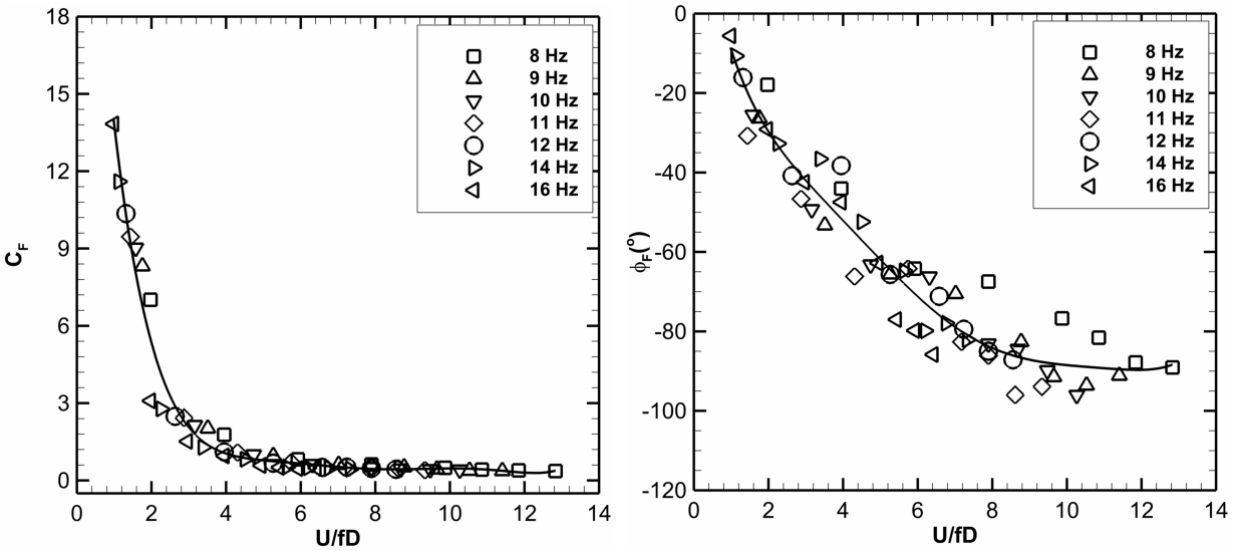


(c) (d)

Figure 4-10 : Variation of the unsteady streamwise fluid force coefficient with $U/fD$ for $\beta = 60\%$ (a-b) Tube 2, (c-d) Tube 3

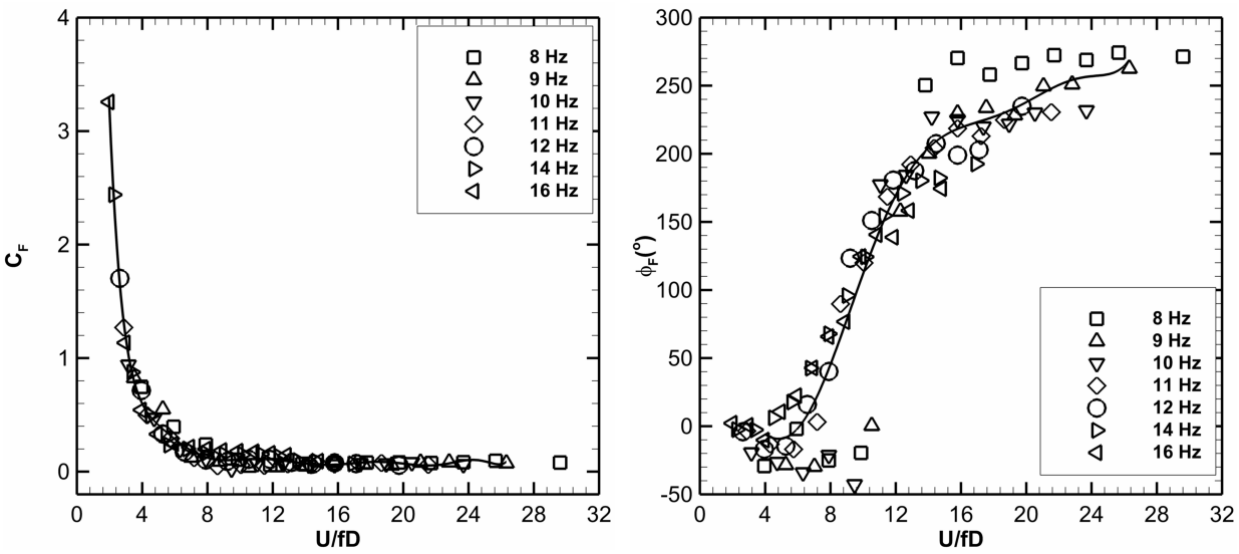


(a) (b)

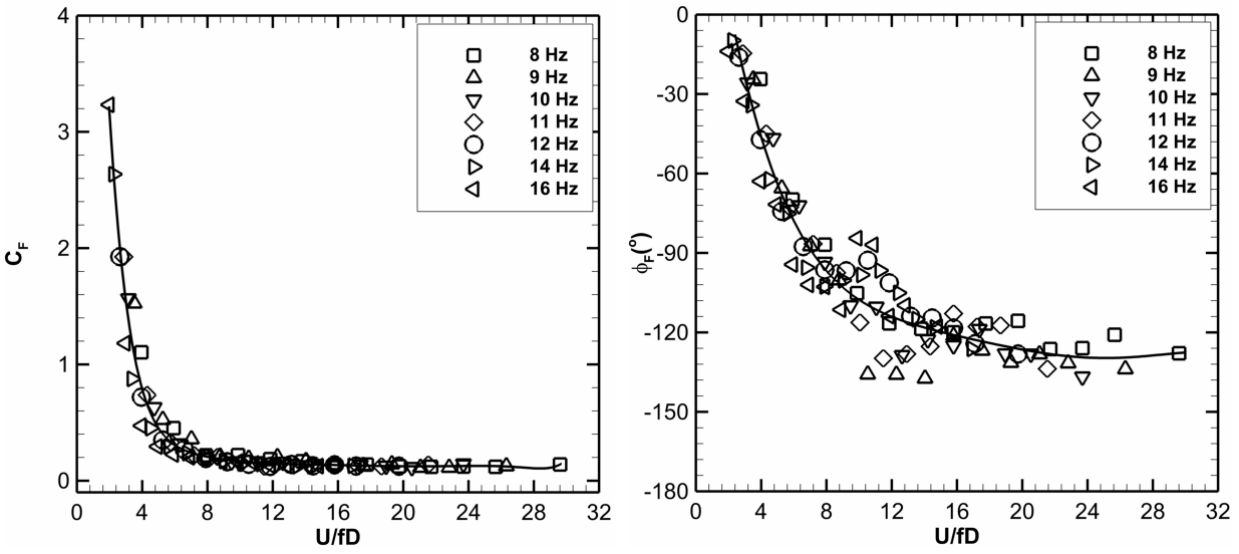


(c) (d)

Figure 4-11 : Variation of the unsteady streamwise fluid force coefficient with $U/fD$ for $\beta = 80\%$ (a-b) Tube 1, (c-d) Tube 4

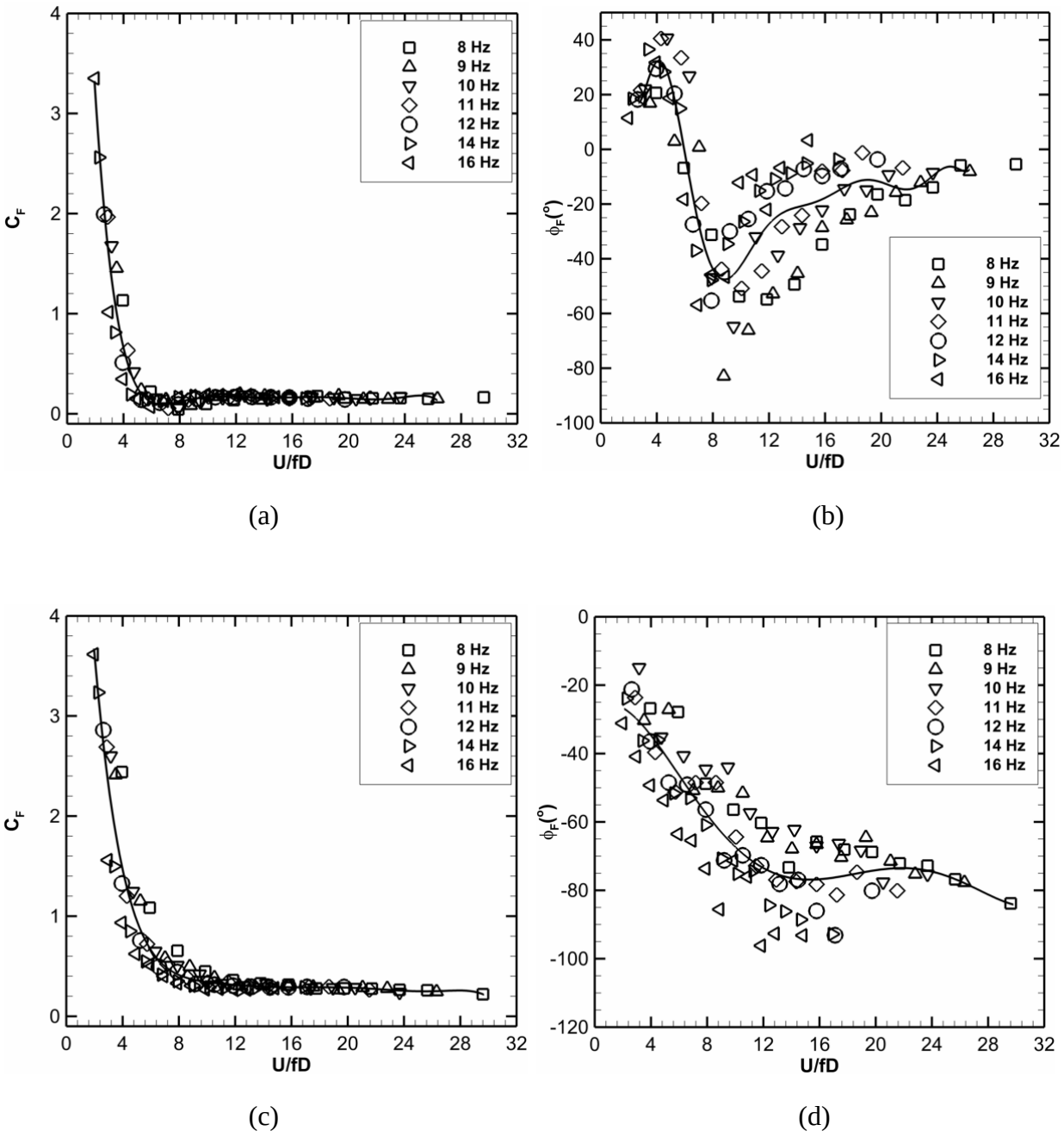


Figure 4-12 : Variation of the unsteady streamwise fluid force coefficient with $U/fD$ for $\beta = 80\%$ (a-b) Tube 2, (c-d) Tube 3

A negative phase means the fluid force imparts positive damping to the system (Mureithi et al., 2002). Since the phase difference between the unsteady fluid force on a tube and the displacement of the same tube is negative in the streamwise direction (Olala et al., 2014; Tanaka & Takahara, 1980), a single flexible tube in an otherwise rigid array has not been observed to

experience dynamic instability in the flow direction. The results of the fluid coupling force measurement for the tubes adjacent to the vibrating tube C, show that some of the phases are positive while others are negative suggesting the possibility of fluidelastic instability for multiple flexible tubes in the streamwise direction. This kind of instability has been confirmed for rotated triangular arrays by the dynamic tests of Violette et al. (2006), and the fluidelastic instability analyses of Nakamura et al. (2014) and Olala & Mureithi (2016a).

### 4.3.1 Effect of Void Fraction on the Measured Fluid Forces

Additional sets of tests were conducted to investigate the effect of void fraction on the unsteady fluid force for the central vibrating tube. Here the tube was excited with an amplitude of 3 mm for frequencies lower than 11 Hz and 2 mm for higher frequencies to improve signal to noise ratio. The data acquisition time was 300 s for frequencies up to 14 Hz, 240 s for 17 Hz-20 Hz and 120 s for 20 Hz-28 Hz.

The void fraction effects on the unsteady fluid force when the central tube is excited at three different frequencies are shown in Figure 4-13 to Figure 4-15. Similarly to observations made by Sawadogo & Mureithi (2014b), the void fraction has no significant effect on the unsteady fluid force magnitude and phase between 0% and 80% void fractions for 8-14 Hz frequencies. The unsteady fluid force phase data for 90% void fraction, however, diverges from the rest, tending to opposite curvature with increasing frequency. At 14 Hz, the 90% void fraction unsteady fluid force phase increases from 0° to a peak value of about 20° at $U/fD \simeq 7.3$ then decreases with increasing $U/fD$. Overall, it appears that in the range 8 Hz-11 Hz (Figure 4-13 and Figure 4-14), the void fraction uncertainty has insignificant influence on the fluid force data. This is important since the fluid force phase is used to extract the time lag. The evidently changing behavior of the dynamic fluid force phase with frequency at high void fractions may be attributed to two-phase flow intermittency (Moran & Weaver, 2013; Noghrehkar et al., 1999).

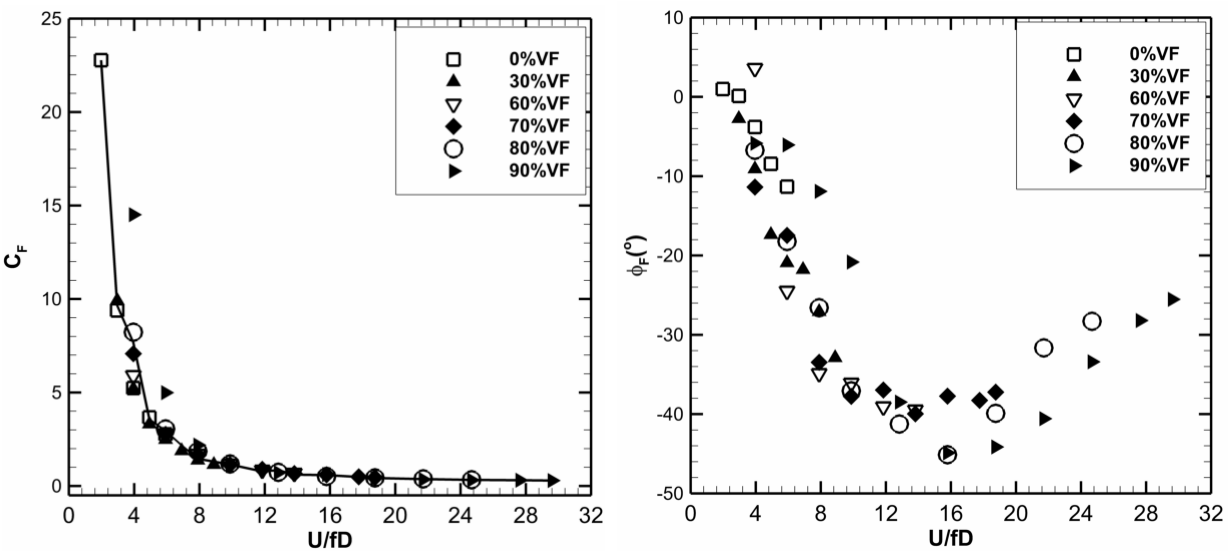


(a) (b)

Figure 4-13 : Effect of void fraction on the unsteady streamwise fluid force for 8 Hz Excitation (Central tube, C)

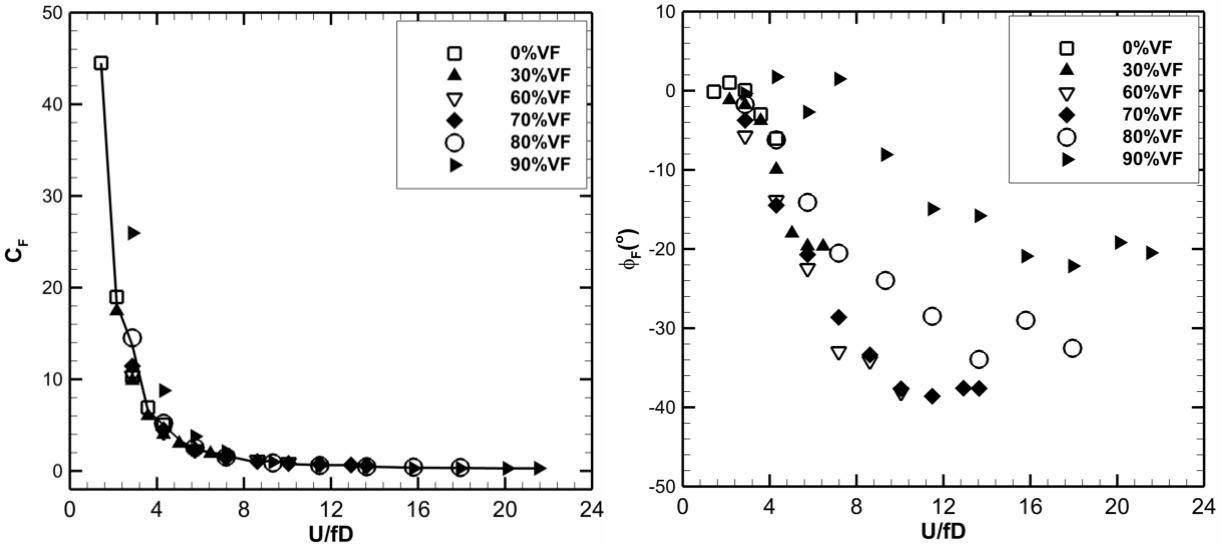


(a) (b)

Figure 4-14 : Effect of void fraction on the unsteady streamwise fluid force for 11 Hz Excitation (Central tube, C)

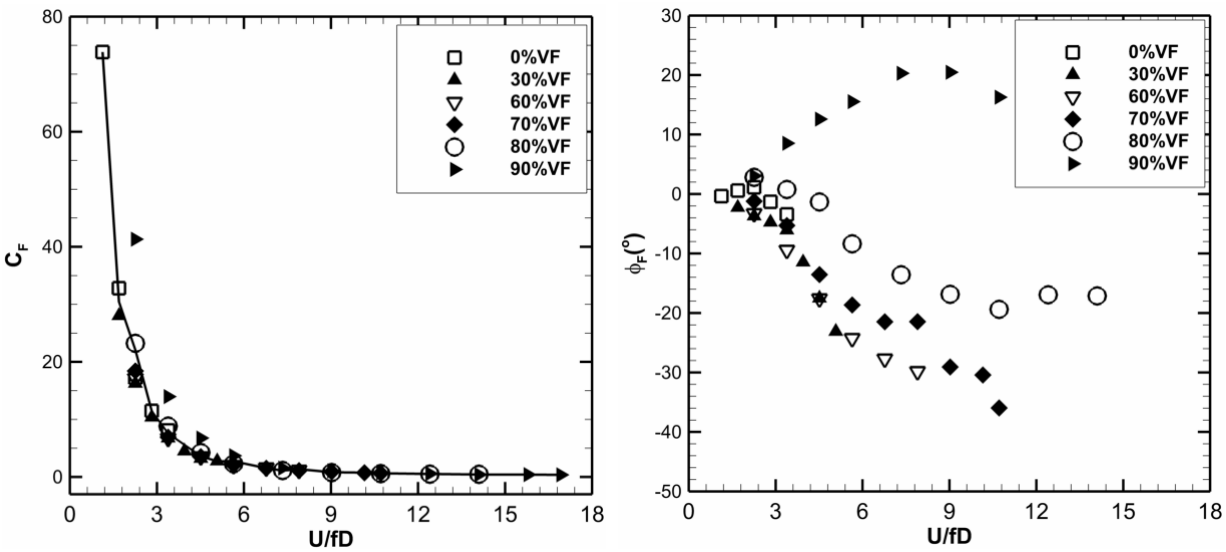


(a) (b)

Figure 4-15 : Effect of void fraction on the unsteady streamwise fluid force for 14 Hz Excitation (Central tube, C)

Two-phase mixtures are hardly uniform across a flow path. Under certain flow conditions, such as vertical flow against gravity, the slip between the phases cannot be neglected. Consolini et al. (2006) have demonstrated that among the existing void fraction models, the Feenstra et al. (2000) model closely reproduces the behavior of two-phase flows. Since the experimental conditions were based on the homogeneous model, the Feenstra et al. (2000) model is used in the current work only for comparison. In this model, void fraction is presented as a function of the velocity ratio, $S$, flow quality, $x$, and density ratio. A semi-empirical correlation is then established between the velocity ratio and other flow parameters. The void fraction, $\alpha$, is given by:

$$\alpha = \left[1 + S\frac{\rho_g}{\rho_l}\left(\frac{1}{x} - 1\right)\right]^{-1} \tag{4-12}$$

where $\rho_l$ and $\rho_g$ are the liquid and gas phase densities. The velocity ratio is expressed as:

$$S = \frac{U_g}{U_l} = 1 + 25.7\left(Ri \times Cap\right)^{0.5}\left(P/D\right)^{-1} \tag{4-13}$$

in which, $U_g$ is the gas phase pitch velocity, $U_l$ the liquid phase pitch velocity, $Ri$ the Richardson number and $Cap$ the capillary number.

$$Ri = \left(\rho_l - \rho_g\right)^2 \left(P - D\right) g \Big/ G_p^2 \tag{4-14}$$

and

$$Cap = \mu_l U_g / \sigma \tag{4-15}$$

where $P$ is the array pitch, $D$ the tube diameter, $G_p$ the pitch mass flux, $g$ the gravitational acceleration, $\mu_l$ the liquid absolute viscosity and $\sigma$ the surface tension. The gas phase pitch velocity, $U_g$, in Eq. (11) and the liquid pitch velocity are then obtained as follows:

$$U_g = \frac{xG_p}{\alpha\rho_g}; \quad U_l = \frac{\left(1-x\right)G_p}{\left(1-\alpha\right)\rho_l} \tag{4-16}$$

The capillary number, $Cap$ depends on the void fraction through the gas phase velocity, $U_g$, as shown in Eq.(4-15). Calculation of $Cap$ is therefore an iterative process in which the velocity ratio is calculated starting from an assumed value and iterated until the assumed and calculated void fractions agree within a desired degree of precision.

The mixture density, $\rho_{tp}$ and the equivalent pitch velocity, $U_{eq}$ are defined as:

$$\begin{aligned} \rho_{tp} &= \left(1-\alpha\right)\rho_l + \alpha\rho_g, \\ U_{eq} &= \sqrt{\left(\alpha\rho_g U_g^2 + \left(1-\alpha\right)\rho_l U_l^2 / \rho_{tp}\right)} \end{aligned} \tag{4-17}$$

and the gas mass quality, $x$ is given by:

$$x = \frac{\rho_g Q_g}{\rho_g Q_g + \rho_l Q_l} \tag{4-18}$$

The data for 60% and 90% void fractions in the second series of tests (Figure 4-16 (a) and Figure 4-17 (a)) were re-analyzed using the Feenstra et al. (2000) model. Due to the limited data points obtained with this model, no correction for the electronic measuring devices and flow independent damping induced phases were done for fluid force phases presented in Figure 4-16 and Figure 4-17. Figure 4-16 (a) and Figure 4-17 (a), which are based on the homogeneous model show marked dispersion in the phase data, though, with data for each flow velocity falling on a single curve and showing similar trends. The frequencies tested for each flow velocity are 8

Hz, 11 Hz, 14 Hz, 17 Hz, 20 Hz, 24 Hz and 28 Hz. The same data, however, when re-plotted with the Feenstra et al. (2000) model (Figure 4-16 (b) and Figure 4-17 (b)) with the reduced velocity presented in the form $Y\left(U_{eq}/fD\right)$, where $Y=\left(f\sqrt{D/g}\right)^{-a}\alpha^{-b}$ show all the data, from all the flow velocities tested collapse approximately onto a single curve. The quantities $a$ and $b$ were obtained by minimization of the variance to obtain the values that best collapsed the data. For Figure 4-16 (b), $a=1.5$ and $b=1$ while for Figure 4-17 (b) $a=1.5$ and $b=6.5$. Each flow velocity used in the homogeneous model essentially represents a void fraction in the Feenstra's model. It is therefore evident that the homogeneous model averages several void fractions thereby masking the true nature of the fluid dynamics. The Feenstra et al. (2000) model accounts for the effect of buoyancy and inertia forces on the dispersed phase in the form of Richardson number, $Ri$. The Capillary number, $Cap$, on the other hand, incorporates the effect of viscous and surface tension forces. A better representation of the two-phase flow physics can therefore be obtained with the Feenstra et al. (2000) model.

It should be noted that no assumption has been made regarding the flow distribution inside the tube array in the current study. The void fraction model used, in this case, the homogeneous model is used only to estimate the void fraction at which the tests are done and the two-phase flow parameters (density, velocity) used for normalizing the fluid force coefficients. Since the physical dimensional values of the forces are used in a typical stability analysis, there is no loss of accuracy (of the measured fluid force data) originating specifically from the use of the homogeneous model.

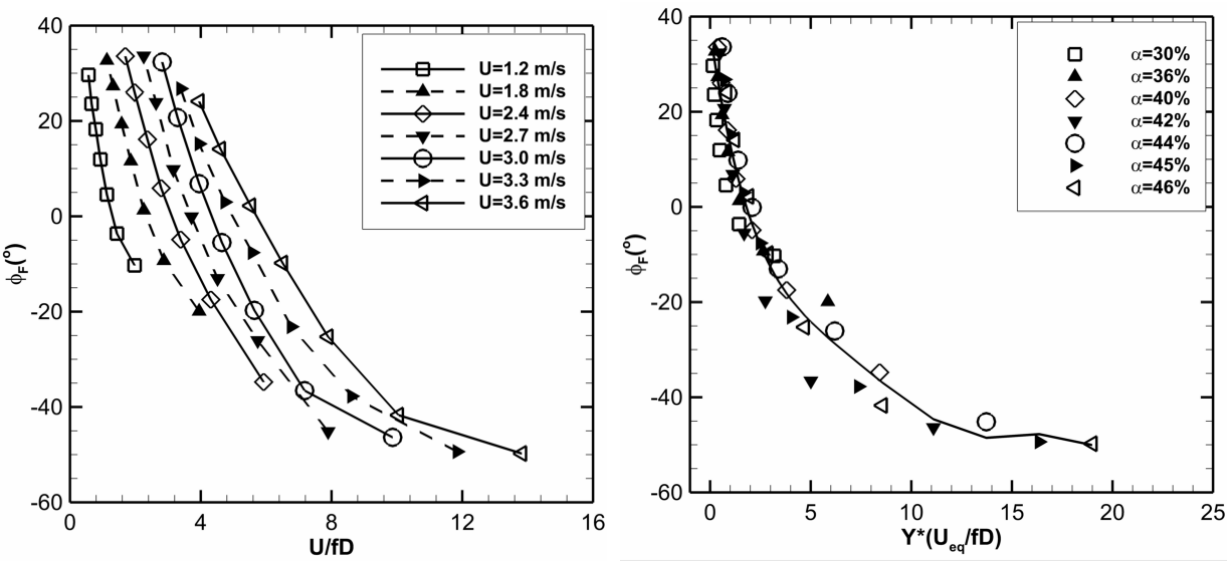


(a) (b)

Figure 4-16 : Unsteady Fluid Force Phase Variation with $U/fD$ for tube C: (a) $\beta = 60\%$ (b) $30 \le \alpha \le 46$

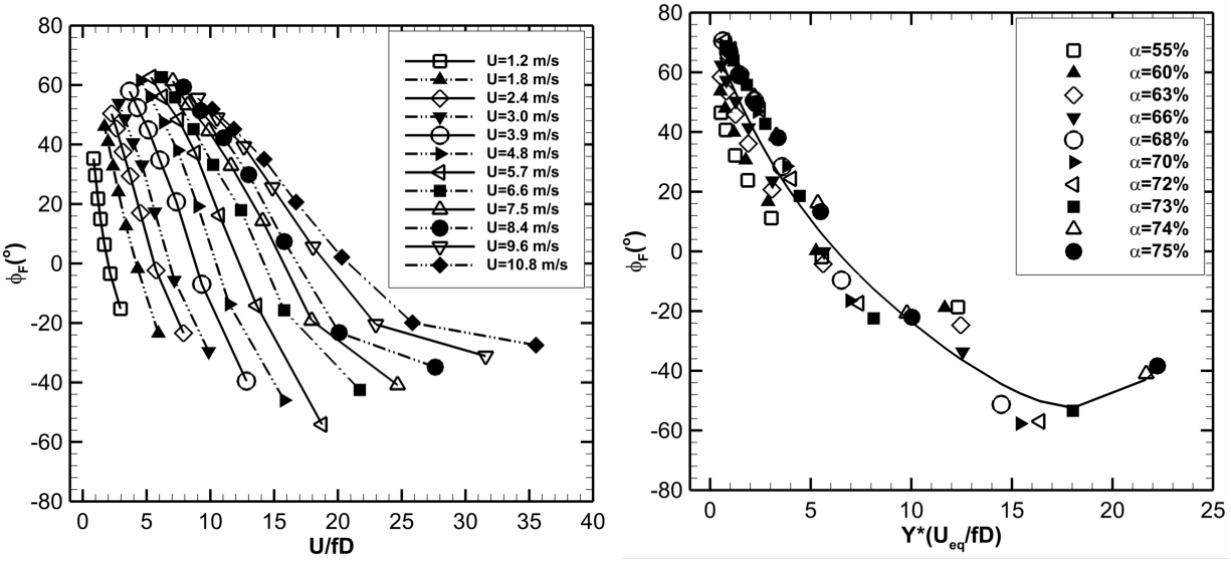


(a) (b)

Figure 4-17 : Unsteady Fluid Force Phase Variation with $U/fD$ for tube C: (a) $\beta = 90\%$ (b) $55 \le \alpha \le 75$

## 4.4 Time delay

The quasi-steady model presupposes that fluid forces acting on an oscillating tube are wholly influenced by its own motion and that of its neighbors. Additionally, two types of time delays are considered. For instance, a time delay, $\tau_i$, exists between the displacement of each of the neighboring tubes and the resulting changes in the fluid force on the central tube. Viewed from the central tube at instant $t$, this time lag results in an apparent displacement of tube, $i$, in the flow direction,

$$\tilde{x}_i(t) = x_i(t-\tau_i) + \tau_i \dot{x}_i(t-\tau_i) \tag{4-19}$$

where $\tau_i$ is the mean time taken by the wake of the upstream tube to travel from its location to the central tube, and $\tau_i \dot{x}_i(t-\tau_i)$ is the distance traversed by tube $i$ between instants $t-\tau_i$ and $t$. As a first approximation, $\tau_i = \mu_t L/U$ for a tube in an adjacent row and $\tau_i = \mu_t 2L/U$ for a tube located two rows away (Price et al., 1990) in which $\mu_t = O(1)$ and $L$ is the distance between tube centers in adjacent rows.

Considering the tube oscillations to be harmonic,

$$x_i(t) = x_{0i} e^{i\omega t} \tag{4-20}$$

where $x_{0i}$ is the amplitude of oscillation, we can therefore write

$$\dot{x}_i(t) = \lambda x_i(t); \quad \dot{x}_i(t-\tau_i) = \lambda x_{0i} e^{(\lambda(t-\tau_i))} = g_i \dot{x}_i(t) \tag{4-21}$$

where $g_i = e^{(-\lambda\tau_i)}$ and $\lambda = i\omega$. Equation (4-19) can thus be re-written for tubes restrained to vibrate only in the streamwise direction as:

$$\tilde{x}_i(t) = g_i \{ x_i(t) + \tau_i \dot{x}_i(t) \} \tag{4-22}$$

The other is the time lag between a tube displacement and the fluidelastic forces generated on itself by its own motion. This time delay is thought to originate from the retardation of the flow as it approaches an oscillating tube (Price & Paidoussis, 1984, 1986b) or to result from the delay in the viscous wake readjusting itself continuously to the boundary condition of the moving tube (Paidoussis & Price, 1988). Together with the variation in inter-tube positions, this time lag may

lead to fluid-dynamic damping force which can either be positive (stabilizing) or negative (destabilizing) (Price & Paidoussis, 1984). Following the work of Simpson & Flower (1977), Price & Paidoussis (1984) have shown that this time lag may be represented as

$$\tau = \mu \frac{D}{U} \tag{4-23}$$

where $\mu$ is a non-dimensional parameter taken to be of order 1.

A similar approach as proposed by Sawadogo & Mureithi (2014b) is used in the current work to estimate both the time delays from corresponding quasi-steady and unsteady fluid forces. Noting the quasi-steady assumption that instantaneous fluid forces acting on an oscillating tube in a flow are equal to those acting on the same tube while in a static state at an identical position, the expression for the time delay is obtained by equating the two forces (unsteady and quasi-steady). This is achieved as follows: The quasi-steady fluid force on a tube purely due to its motion in the streamwise direction (in this case the central tube with the added mass removed) in a rotated triangular array may be expressed as (Paidoussis & Price, 1988),

$$F_{x_c} = \frac{1}{2}\rho_h U^2 D\left( e^{-i\omega\tau}\frac{\partial C_{Dc}}{\partial x_c} - 2i\omega\frac{C_{D0c}}{U}\right)x_c + \frac{1}{2}\rho_h U^2 D C_{D0c} \tag{4-24}$$

while that on a fixed neighboring tube due to the displacement of the central tube would be

$$F_{x_i} = \frac{1}{2}\rho_h D U^2\left( C_{D0i} + \left[x_c + \tau_i \dot{x}_c\right] g_i \frac{\partial C_{Di}}{\partial x_c}\right) \tag{4-25}$$

where $C_{Dc}$ is the drag coefficient, $C_{D0}$ is the drag coefficient at the tube equilibrium position and $\tau$ is the time delay. Subscripts $c$ and $i$ denote central and tube index, respectively.

### 4.4.1 Time delay due to flow retardation

Equating Eq. (4-8) to Eq. (4-24) and considering only the "unsteady effects", that is, ignoring the fluid inertia and the steady drag, respectively, in the expressions for the unsteady and quasi-steady forces yields:

$$\frac{1}{2}\rho_h D U^2\left( e^{-i\omega\tau}\frac{\partial C_{D_c}}{\partial x_c} - 2i\omega\frac{C_{D0_c}}{U}\right) = i\omega\frac{\rho_h U D}{2}C_{dh} + \frac{\rho_h U^2}{2}C_{sh} \tag{4-26}$$

Letting $\chi = x_c/D$ and reorganizing we get:

$$e^{-i\omega\tau} = i\frac{\omega D}{\partial C_{D_c}/\partial\chi}\left[\frac{2C_{D0_c}}{U}+\frac{C_{dh}}{U}\right]+\frac{C_{sh}}{\partial C_{D_c}/\partial\chi} \tag{4-27}$$

$\tau$ can therefore be obtained by either equating the real or imaginary parts of both sides of Eq. (4-27). However, as noted by Sawadogo & Mureithi (2014b), there is considerable uncertainty in the estimation of the fluid added mass, hence in the stiffness coefficient (see Eq. (4-10)). Therefore, equating the imaginary parts on both sides of Eq. (4-27) yields

$$-\sin(\omega\tau) = \frac{\omega D}{\partial C_{D_c}/\partial\chi}\left[\frac{2C_{D0_c}}{U}+\frac{C_{dh}}{U}\right] \tag{4-28}$$

Leading to (for the streamwise direction)

$$\tau = -\sin^{-1}\left(\frac{\omega D}{\partial C_{D_c}/\partial\chi}\left[\frac{2C_{D0_c}}{U}+\frac{C_{dh}}{U}\right]\right)/\omega \tag{4-29}$$

It should, however, be noted that Eq. (4-29) is only valid when the right hand side of Eq. (4-28) is between -1 and 1. Additionally the reduced flow velocity should be high enough ($U/fD >> 1$) to satisfy the quasi-steady model assumption. This condition can be satisfied either by increasing the flow velocity or decreasing the excitation frequency. Since the flow rate that could be attained by the current experimental loop was limited, and to ensure that the accuracy of the data is satisfactory while still meeting the preceding condition, a trade-off was found in the range of 8.7–9.5 Hz. Again, due to limited water pump capacity, this condition could only be fulfilled for void fractions higher than 50%. Therefore, the time delay was only obtained for 60%–90% homogeneous void fraction.

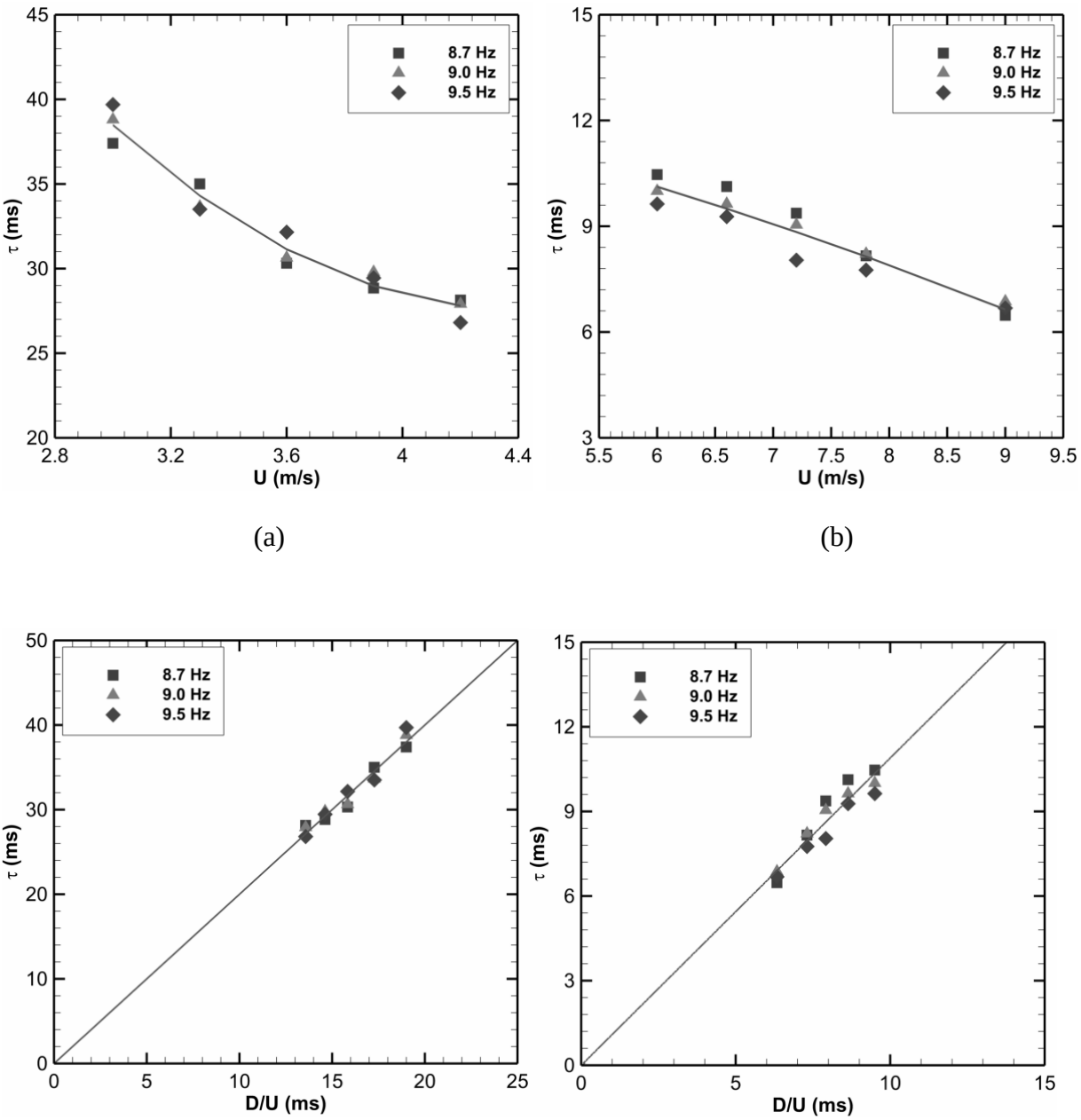


Figure 4-18 : Time delay due to flow retardation for Tube C: (a, c) 60% void fraction (b, d) 80% Void fraction; $\mu = 2.0$ for 60% void fraction and $\mu = 1.1$ for 80% void fraction

Figure 4-18 displays the results for the time delay ($\tau$) due to flow retardation. For brevity, only two void fractions (60% and 80%) results are presented. Figure 4-18 (a-b) shows the variation of the time delay with pitch velocity while Figure 4-18 (c-d) presents the time delay plotted against the convection time ($D/U$). It is seen that the time delay decreases with increasing flow velocity

in Figure 4-18 (a, b), meaning that the time delay will tend to zero as the flow velocity approaches infinity. Similarly to Mahon & Meskell (2010), Price & Paidoussis (1984) and Sawadogo & Mureithi (2014b), it was also assumed in the current work that the time delay would be zero at $D/U = 0$ thus any value of $\tau$ at $D/U = 0$ was attributed to residual time delay produced by measurement electronic devices. This value was therefore, eliminated from all the data presented in the present study. With the stated correction, the time delay was found to vary linearly with the convection time (Figure 4-18 (c-d)), in agreement with the model proposed by Price & Paidoussis (1984); $\tau = \mu D/U$. It was shown earlier that in the frequency range 8 Hz-11 Hz, there was no significant frequency effect on the unsteady fluid force phase data for various void fractions. The effect of frequency on the estimated time delay can thus, as a first approximation, be ignored.

The parameter $\mu$ was found to be $\mu = 2.0$ for 60% void fraction, and $\mu = 1.1$ for 80% void fraction. Similarly for other void fractions, $\mu = 1.1$ for 70% void fraction and $\mu = 1.1$ for 90% void fraction. These values, except for the 90% void fraction show a similar trend as that obtained by Sawadogo & Mureithi (2014b) for measurements in the lift direction and the order of magnitude of $\mu$ is consistent with that suggested by Price & Paidoussis (1984); $\mu = O(1)$. The difference in $\mu$ values for different void fractions is attributed to flow structure evolution that characterizes the two-phase flow fluctuations in the array.

### 4.4.2 Time delay due to apparent tube displacement

A similar procedure is employed for the time delay between the displacement of the central tube, C, and the induced fluid forces on the neighboring tubes. Equating the streamwise direction quasi-steady (Eq. (4-25)) and unsteady forces (Eq. (4-11)) (which represent the fluid cross-coupling effect between the central vibrating tube and the fixed neighboring tubes), with the steady drag in the quasi-steady force and inertia in the unsteady force expressions removed:

$$\left[1 + i\omega\tau_i\right]e^{-i\omega\tau_i} = i\omega \frac{D}{\partial C_{D_i} / \partial \chi} \frac{C_{dh_{cc_i}}}{U} + \frac{C_{sh_{cc_i}}}{\partial C_{D_i} / \partial \chi} \tag{4-30}$$

Equating the imaginary parts on both sides of Eq. (4-30) gives

$$\omega\tau_i \cos\omega\tau_i - \sin\omega\tau_i = \frac{\omega D}{\partial C_{D_i} / \partial\chi} \frac{C_{dhcc_i}}{U} \tag{4-31}$$

Equation (4-31) can be expressed as $f(\tau_i) = 0$, and solved iteratively to obtain the zero of the function $f(\tau_i)$ which will give the desired value of $\tau_i$. However, the solution obtained strongly depends on the initial value, which has to be generally in a narrow basin of attraction. We can therefore choose our initial value as $\tau_{i0} = L/U$ or $\tau_{i0} = 2L/U$ since the flow, if it were to travel in a straight line between tubes, would approximately take this duration to reach a downstream tube depending on whether the tube is one or two rows away, respectively. Thus

$$f(\tau_i) = \omega\tau_i \cos\omega\tau_i - \sin\omega\tau_i - \frac{\omega D}{\partial C_{D_i} / \partial\chi} \frac{C_{dhcc_i}}{U} = 0 \tag{4-32}$$

The dimensionless damping coefficient, ($C_{dh}$) was obtained from the streamwise unsteady fluid forces presented in Figure 4-7-Figure 4-12 using Eq. (4-9). The other necessary parameters for the time delay estimation: the steady drag coefficient ($C_{D0}$) and the quasi-steady fluid force coefficient derivative $\partial C_D/\partial\chi$ were taken from Olala & Mureithi (2016a)

Figure 4-19 to Figure 4-22 present the time delays between the displacement of the central tube, C, and the induced unsteady fluid forces on the neighboring tubes. Here again, the time delay, $\tau$, is plotted against the flow pitch velocity and also against the convection time with the same assumptions as reported in section 4.1. However, the convection time is taken as either $L/U$ or $2L/U$ depending on the streamwise separation distance between the particular tube and the central tube. The apparent displacement time delays for 60% void fraction are shown in Figure 4-19 (Tubes 1 and 4) and Figure 4-20 (Tubes 2 and 3). Similarly, the variation of the time delay with pitch velocity and the convection time for 80% void fraction are displayed in Figure 4-21 (Tubes 1 and 4) and Figure 4-22 (Tubes 2 and 3).

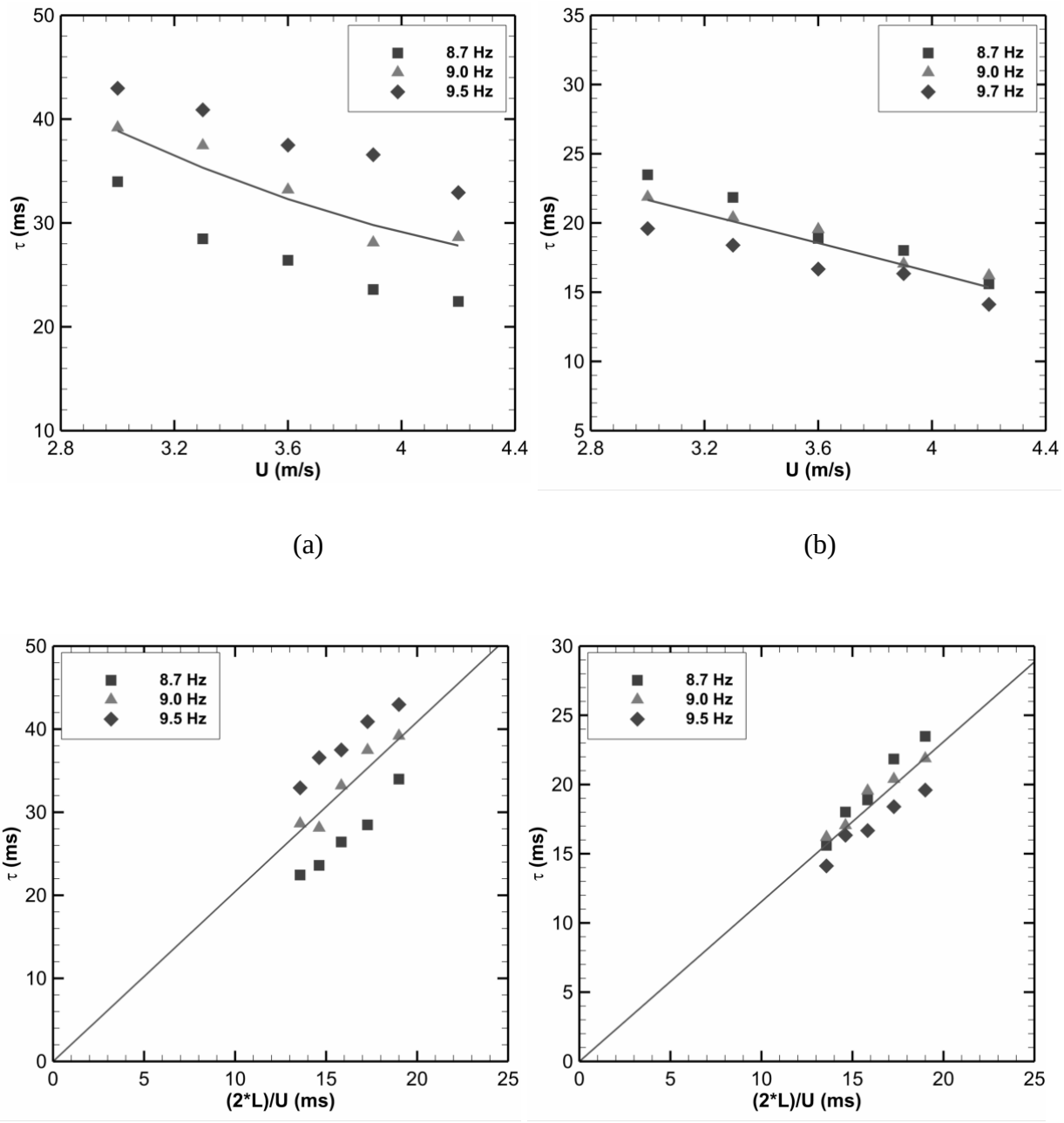


Figure 4-19 : Time delays due to displacement of tube C for 60%VF (a, c) Tube 1 (b, d) Tube 4; $\mu = 2.0$ for tube 1, $\mu = 1.2$ for tube 4

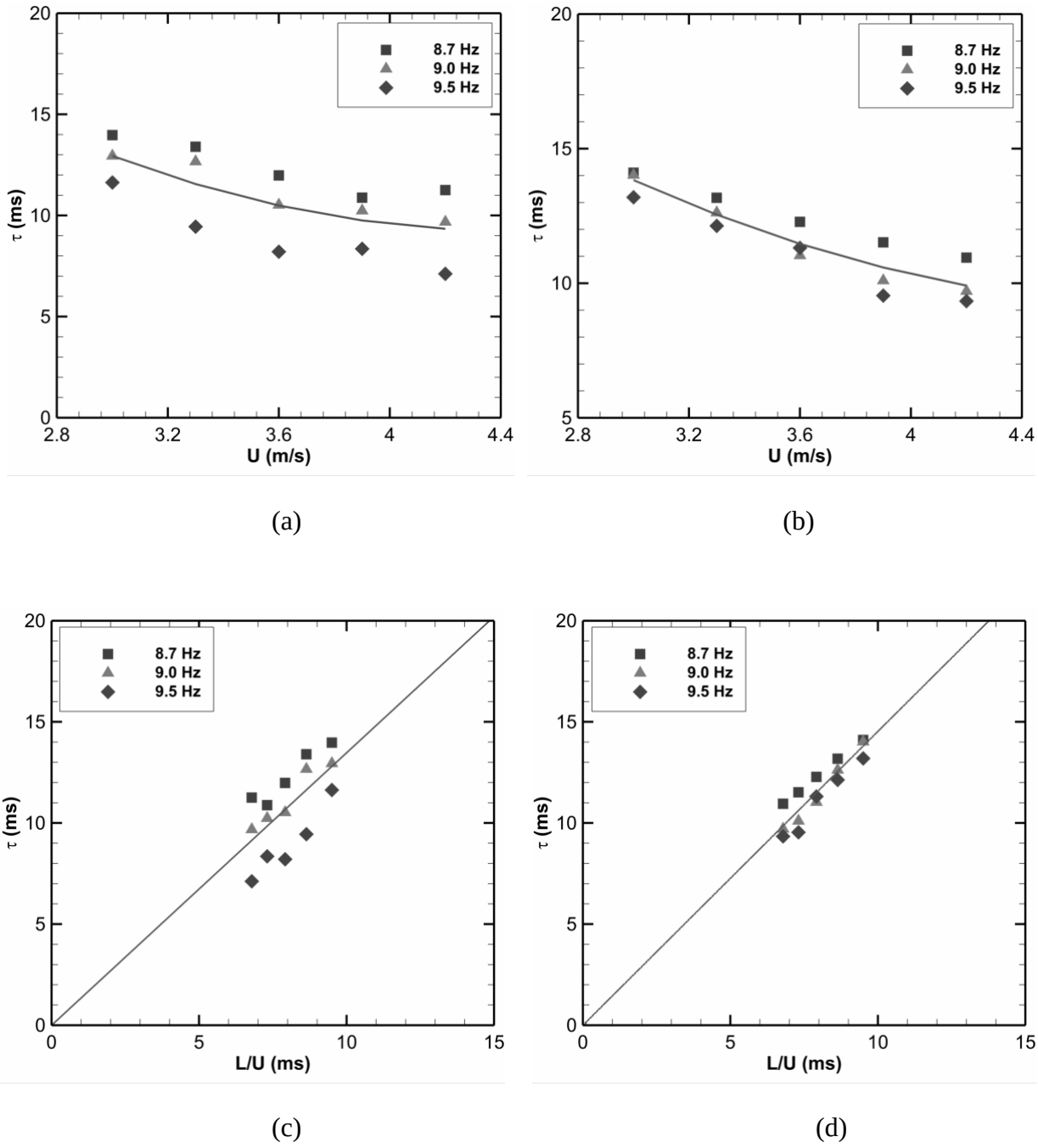


Figure 4-20 : Time delays due to displacement of tube C for 60%VF (a, c) Tube 2 (b, d) Tube 3; $\mu = 1.3$ for tube 2, $\mu = 1.5$ for tube 3

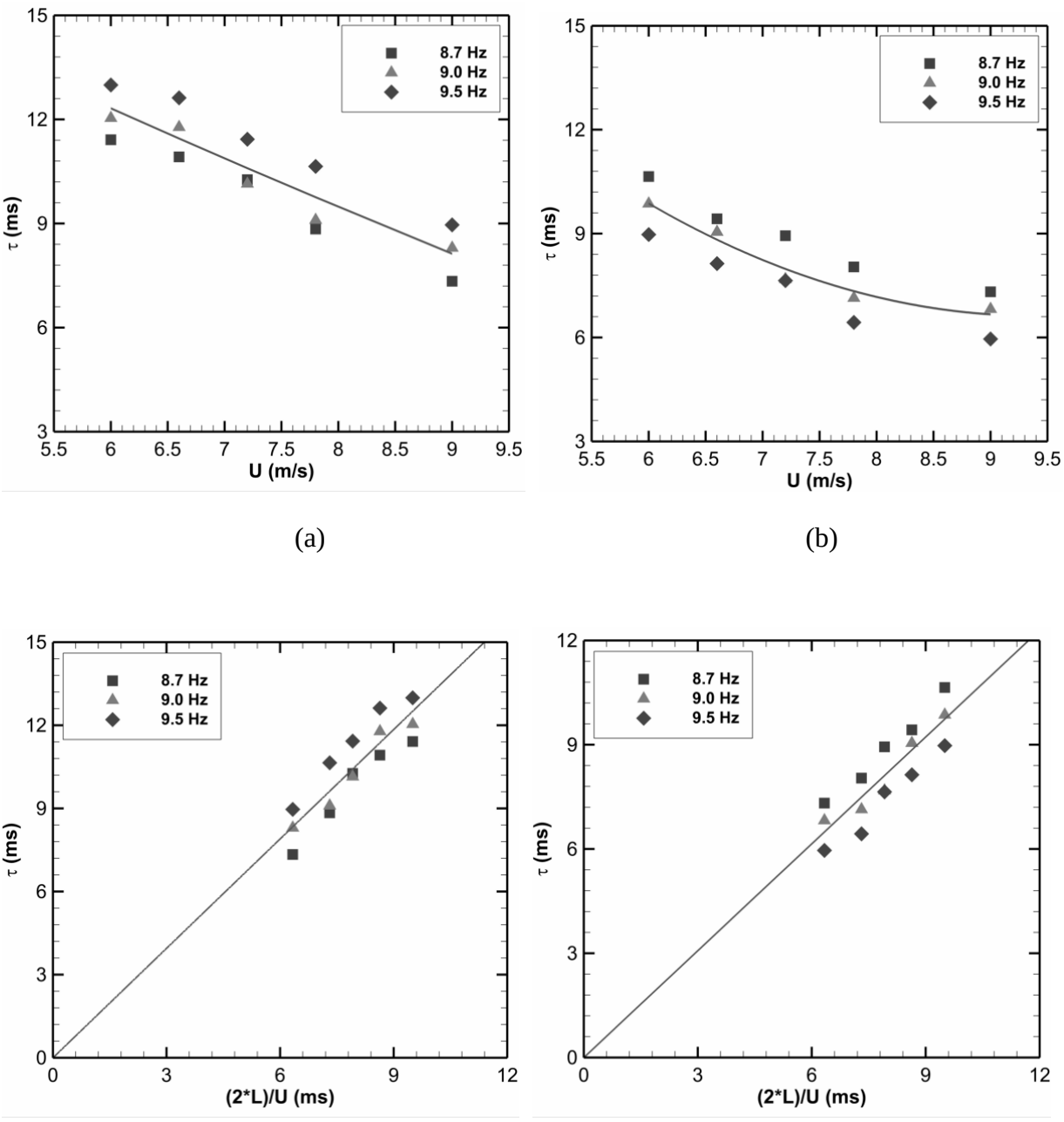


(a) (b)

(c) (d)

Figure 4-21 : Time delays due to displacement of tube C for 80%VF (a, c) Tube 1 (b, d) Tube 4; $\mu = 1.3$ for tube 1, $\mu = 1.0$ for tube 4

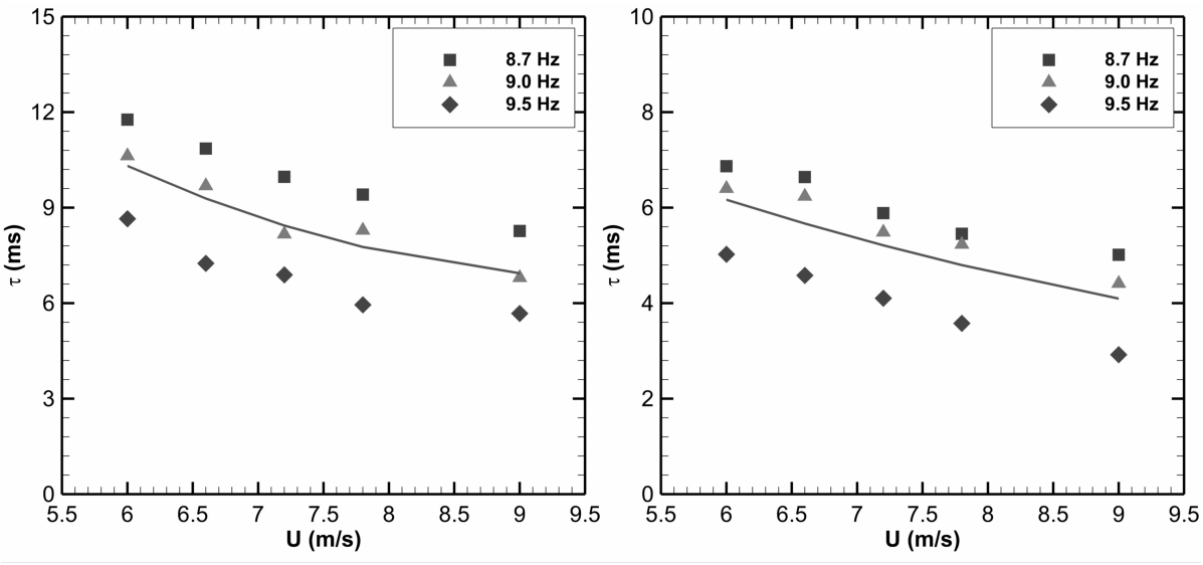


(a) (b)

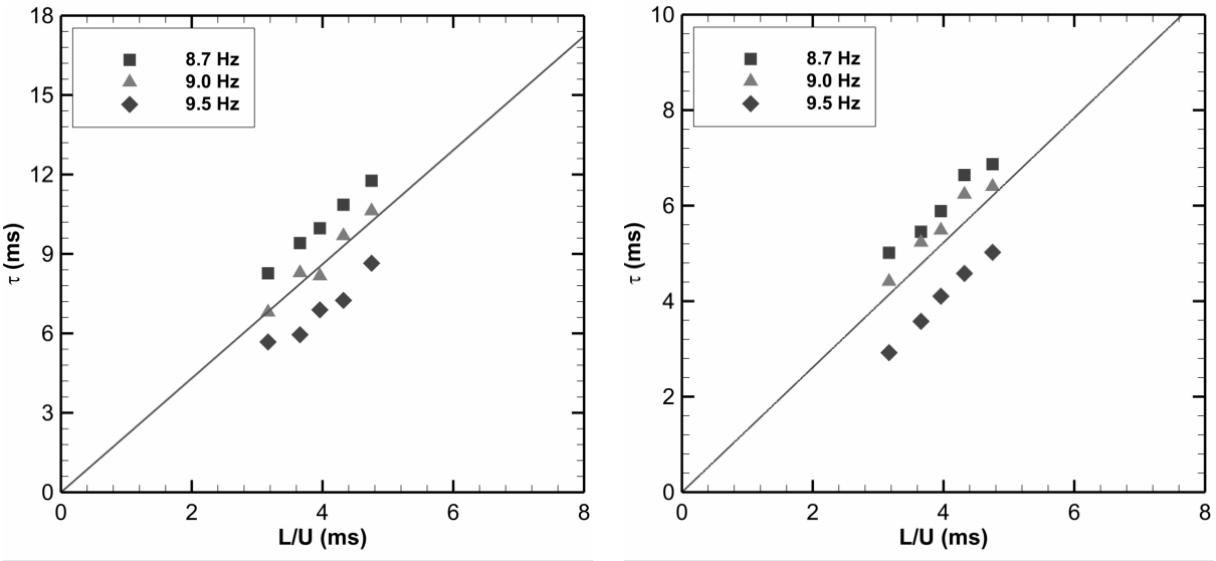


(c) (d)

Figure 4-22 : Time delays due to displacement of tube C for 80%VF: (a, c) Tube 2 (b, d) Tube 3; $\mu = 2.2$ for tube 2, $\mu = 1.3$ for tube 3

The trend of the data remains similar to that of the time delay due to flow retardation shown in Figure 4-18. However, there is marked scatter in the time delay data associated with the cross-coupling forces, more so for the tubes downstream of the vibrating central tube, C. The scatter in $\tau$ follows from the unsteady cross-coupling fluid force phases presented in section 3.3 and

attributed to two-phase flow intermittency. This lowers the coherence between the tube motion and the resulting unsteady forces on the neighboring tubes. Further work is, thus, needed to establish the effect of amplitude and frequency vis-à-vis flow regime to improve the results. Though Price et al. (1990) appreciated that the magnitude of this time delay is unknown, they proposed a correlation, $\tau = L/U$ for a tube one row away. However, in the current study, the expression of Price et al. (1990) is modified to $\tau = \mu L/U$ with $\mu = O(1)$ to account for the flow fluctuation in the rotated triangular array which would generally lower the "mean" streamwise flow velocity between tubes. The parameter ( $\mu$ ) is shown in Table 4-1 for various void fractions and tubes.

The time delays obtained here will be used in determining the fluidelastic instability threshold using the quasi-steady model in the second part of the paper (Olala & Mureithi, 2016c).

Table 4-1 : Time delay parameter ( $\mu$ ) dependence on void fraction and tube position for the adjacent tubes

| Tube | Void fraction | | | |
|---|---|---|---|---|
| | 60% ( $\mu$ ) | 70% ( $\mu$ ) | 80% ( $\mu$ ) | 90% ( $\mu$ ) |
| 1 | 2.0 | 1.4 | 1.3 | 1.6 |
| 2 | 1.3 | 2.4 | 2.2 | 2.7 |
| 3 | 1.5 | 1.2 | 1.3 | 1.4 |
| 4 | 1.2 | 1.0 | 1.0 | 1.3 |

## 4.5 Conclusion

Unsteady fluid forces acting on a kernel of tubes in a rotated triangular tube bundle of $P/D = 1.5$ subjected to liquid (water) single phase and air-water two-phase flows were measured when the

central tube was oscillated in the flow direction. The streamwise unsteady fluid force coefficient magnitude was found to be a single valued function of the reduced velocity ($U/fD$). However, fluid force phase in two-phase flow, especially those related to the cross-coupling forces displayed scatter which increased with void fraction.

The measured unsteady fluid forces were then used, together with previously measured quasi-steady forces (Olala & Mureithi, 2016a), to estimate the time delays for 60%-90% void fractions. The time delay between the tube motion and the resulting fluid forces in the streamwise direction was found to be consistent with Price & Paidoussis (1984) model: $\tau = \mu D/U$, in terms of order of magnitude. However, $\mu$ values as high as double the value proposed by Price & Paidoussis (1984) were found. Additionally, the time delay between the vibration of the central tube and the induced forces on the adjacent tubes was also found to follow the same trend, but with the convection time expressed as $L/U$ or $2L/U$ depending on the separation distance between the tubes. The time delay parameter, $\mu$, obtained was found to also depend on void fraction. The $\mu$ values reported here will be used to perform streamwise fluidelastic stability analysis of multiple flexible tubes using the quasi-steady model in the second part of the paper (Olala & Mureithi, 2016c).

# CHAPTER 5 ARTICLE 3: STREAMWISE FLUIDELASTIC VIBRATION OF A TRIANGULAR TUBE ARRAY IN TWO-PHASE FLOW. PART II: FLUIDELASTIC INSTABILITY ANALYSIS

Olala, S. and Mureithi, N. W. (2016)

Submitted to "Journal of Fluids and Structures" on 20th July 2016

**Abstract**

Experimental tests were performed to determine the hydrodynamic mass and flow independent damping on a tube constrained to vibrate only in the streamwise direction in a rotated triangular array of $P/D = 1.5$ subjected to air-water two-phase flow. The measurements were done for various void fractions with the tube excitation wholly emanating from the fluid flow. Together with previously measured quasi-steady fluid forces and time delay parameters estimated in the first part of the paper, the quasi-steady model was used to predict the critical velocity for streamwise fluidelastic instability of multiple flexible tubes in a rotated triangular tube array in two-phase flow. A single flexible column was found to be more stable than multiple flexible columns. The use of the experimentally determined time delays was found not to significantly affect the reduced critical velocity for fluidelastic instability of the multiple flexible tube configurations analyzed.

The results obtained with the quasi-steady model were in fairly good agreement with experimentally determined critical velocities for specific multiple tubes configurations in the same array. The capability of the quasi-steady model to predict fluidelastic instability for multiple flexible tubes in a triangular tube array subjected to two-phase flow was therefore verified. It was also confirmed that streamwise fluidelastic instability of multiple flexible tubes in a rotated triangular array is strongly dependent on the cross-coupling forces as opposed to damping controlled instability mechanism.

*Key words*: Two-phase flow, tube array, streamwise fluidelastic instability, quasi-steady model, Time delay, cross-flow

## 5.1 Introduction

Flow-induced vibration is a major concern to both designers and operators of tube-and-shell heat exchangers. Excessive vibrations may lead to tube failure due to fatigue or fretting wear at the supports. The "U" bend region of nuclear steam generators is especially susceptible to such failures due to the presence of high speed two-phase cross flow. It is now known that of the several tube excitation mechanisms (Pettigrew & Taylor, 1994; Weaver, D. S. & Fitzpatrick, J. A., 1988), fluidelastic instability (FEI) has the highest potential of causing catastrophic tube damage in the short term. As such, a number of theoretical models (Price, 1995) have been developed to estimate the critical velocity for FEI. It is important to note that these models were primarily formulated for single phase flows, even though a majority of the heat exchangers operate in two-phase flow (Pettigrew & Taylor, 1994). In addition, the design guidelines currently in use were developed using lift direction experimental data. It is therefore necessary to extend the models to two-phase flow and validate their applicability for predicting streamwise FEI in tube bundles.

Streamwise FEI has not been a major concern to steam generator designers since experimental data have typically shown that FEI occurs in the lift direction. However, since the tube failure in a replacement steam generator (SG) at the San Onofre Nuclear Generating Station (SONGS) (S.C.E., 2013), great interest has been shown by a number of researchers who have contributed relevant data in an attempt to better understand the physics of the phenomenon.

Roberts (1962) was probably the first author to report streamwise FEI, at least in tube rows subjected to liquid flow. However, experimental evidence of streamwise FEI in two-phase flow was first reported by Janzen et al. (2005). The authors observed in-plane FEI for a rotated triangular U-tube array of pitch-to-diameter ratio, $P/D = 1.5$ subjected to liquid water flow and for low void fractions (up to 25%) air-water two-phase flow. Violette et al. (2006) conducted a detailed experimental investigation of streamwise FEI for different flexible tube configurations in a rotated triangular tube array of $P/D = 1.5$ in air-water two-phase flow. The authors found FEI to occur for multiple flexible tubes but not for a single tube in the flow direction. Augmenting these efforts is Mureithi et al. (2005) who also demonstrated the occurrence of FEI in the flow direction for a rotated triangular array of $P/D = 1.5$ subjected to air flow. Except for Hassan & Weaver (2016), all the other authors (e.g Nakamura et al. (2014), Violette et al. (2006), Olala et al. (2014), Olala & Mureithi (2016a)) have reported streamwise FEI to only occur for multiple

flexible tubes and not a single tube preferentially flexible in the flow direction. FEI has therefore been considered to be predominantly stiffness controlled, relying on the cross-coupling between tubes due to the fluid flow for its initiation. This is in contrast to tube oscillations in the direction transverse to the flow which experience FEI through damping controlled instability mechanism, generated by fluidelastic force components that are in phase with the tube's velocity. As outlined in the first part of this paper (Olala & Mureithi, 2016b) the current work is a continuation of the work reported in Olala & Mureithi (2016a).

The main objective in this part of the study is to validate the quasi-steady model (Price & Paidoussis, 1982, 1984; Price et al., 1990) for streamwise FEI of multiple flexible tubes subjected to two-phase flow. To that end, hydrodynamic mass and the flow independent damping are measured for a tube in a rotated triangular tube array of $P/D = 1.5$ subjected to two-phase flow and constrained to vibrate only in the flow direction. The damping ratios and the hydrodynamic mass so obtained are then used, together with the time delay parameters obtained in the first part of the paper (Olala & Mureithi, 2016b), and the previously measured quasi-steady force coefficients (Olala & Mureithi, 2016a), to compute the critical velocity for FEI for different multiple flexible tube configurations. The results are then compared with those from the dynamic tests of Violette et al. (2006).

## 5.2 Experimental apparatus and test procedure

### 5.2.1 Experimental setup

The same two-phase flow loop and test section as presented in the first part of the paper (Olala & Mureithi, 2016b) was used for the following measurements. The test loop consists of a water tank, a centrifugal pump, compressed air supply system and connecting piping. The test section is a rotated triangular tube array of $P/D = 1.5$. A complete description of the test set up is presented in the first part of the paper. For the present case, only the central tube shown in Figure 5-1 was instrumented. The instrumented tube assembly consists of a rigid tube attached to a fixed cantilever beam. The beam has a rectangular cross section of $0.00415m \times 0.025m$ and oriented such that the tube assembly is more flexible in the streamwise direction than in the crosswise direction resulting in tube frequencies, in air, of 14 Hz and 81Hz, respectively. A pair of strain gauges mounted close to the clamped end of the beam is calibrated to measure the fluid forces on

the tube. In the present case, the tube excitation is wholly induced by the flow and measurements (hydrodynamic mass and damping) were done for the streamwise direction only.

The strain gauge signals were acquired for each flow condition using a Labview® program via a National Instruments data acquisition card at a sampling rate of 1000 Hz over a period of 40 seconds. The properties of the two-phase flow were estimated using the homogeneous model.

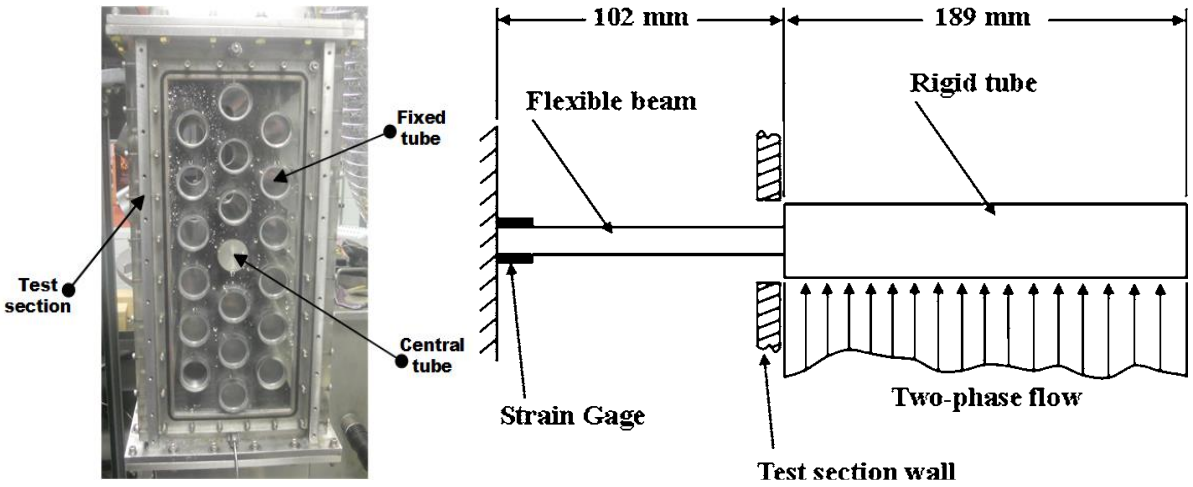


(a) (b)

Figure 5-1 : (a) Test section (b) Flexible tube assembly

## 5.2.2 Hydrodynamic mass

The hydrodynamic mass represents the mass of the external fluid which appears to be accelerated with the tube (Pettigrew et al., 2001). In the present study, the streamwise hydrodynamic mass was determined from the unsteady fluid forces acting on the central vibrating tube presented in part one of the paper (Olala & Mureithi, 2016b) according to $m_h = \Re e\left[G_{Fx}\right]/\omega^2 - m_s$; where $\Re e\left[G_{Fx}\right]$ is the real part of the transfer function, $\omega$ is the angular vibration frequency of the tube, $m_s$ is the mass of the tube per unit length and $m_h$ the hydrodynamic mass per unit length . This was done at low velocities and relatively high frequencies for each void fraction, conditions for which fluidelastic forces are considered negligible (Pettigrew, Tromp, et al., 1989). Additionally, the hydrodynamic mass was estimated for each void fraction, at low velocities, from the variation

of the tube natural frequency in fluid flow using the set-up in Figure 5-1 as follows (Carlucci & Brown, 1983):

$$m_h = m_s\left[\left(\frac{\omega_a}{\omega}\right)^2 - 1\right] \tag{5-1}$$

where $\omega_a$ is the angular natural frequency of tube in air and $\omega$ the frequency of vibration in fluid flow. Results from the two methods were found to be very similar as shown in Figure 5-2(a). Figure 5-2 (b) presents the hydrodynamic mass ratio, $m_R$, which is the ratio of the added two-phase fluid mass to the added mass of the liquid phase ($m_h/m_l$) as a function of the homogeneous void fraction. The continuous line represents the predicted hydrodynamic mass ratio given by (Pettigrew, Taylor, et al., 1989):

$$m_{R,\text{pred}} = \frac{\rho_h}{\rho_l} \tag{5-2}$$

where $\rho_l$ and $\rho_h$ are the homogeneous mass densities of liquid and two-phase mixture, respectively. The measured streamwise hydrodynamic mass ratio $m_R$ decreases with void fraction as expected since the density of the two-phase mixture decreases with increasing void fraction.

From Figure 5-2, it is evident that Eq. (5-2) generally underestimates the hydrodynamic mass in a rotated triangular tube array, more so for high void fractions. This is attributed to the following reasons: (i) homogeneous model overestimates the actual void fraction (Consolini et al., 2006; Feenstra et al., 2000; Moran & Weaver, 2013), leading to a lower two-phase flow mixture density, $\rho_h$, especially for higher void fractions; (ii) distribution of the two phases in the rotated triangular array. In Pettigrew et al. (2005) detailed flow measurements using fiber optic probes in a rotated triangular tube bundle, the authors found the local void fraction around the tubes to be lower than the other regions in the tube array. This localized liquid hold up around the tubes leads to a higher measured hydrodynamic mass than predicted for rotated triangular tube arrays. Figure 5-2(b) shows a comparison between the measured hydrodynamic mass ratios in drag and lift (Sawadogo & Mureithi, 2014a) directions. Similarly to Pettigrew, Taylor, et al. (1989)

observation, the hydrodynamic mass in the streamwise direction was found to have no significant difference to that in the transverse direction for the array studied in the present work.

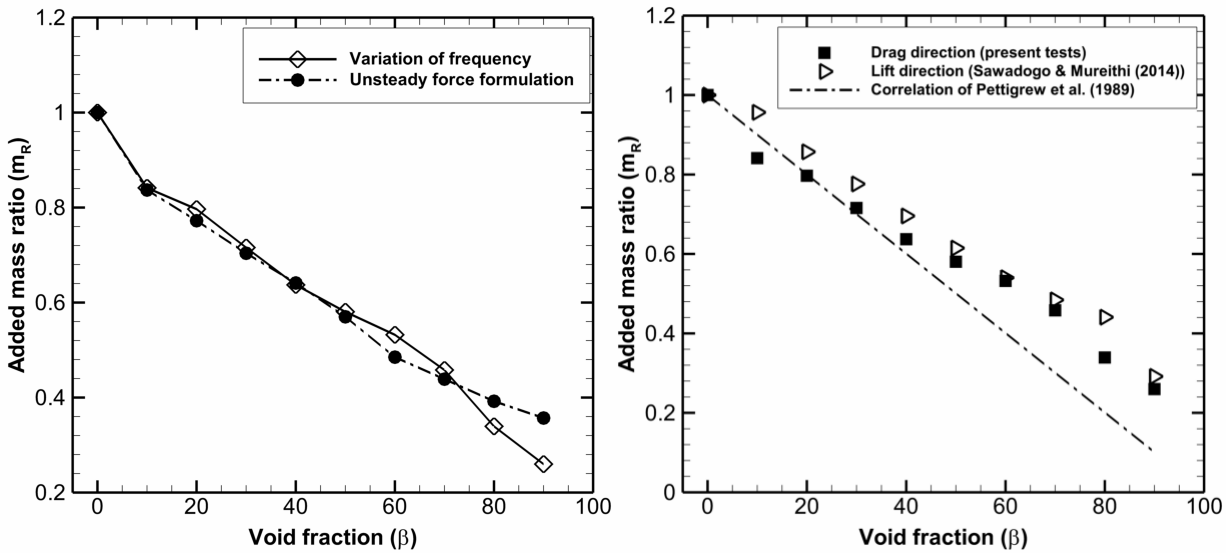


(a) (b)

Figure 5-2 : Variation of the hydrodynamic mass ratio, $m_R$ with void fraction: (a) Drag comparison (b) comparison between drag and lift directions

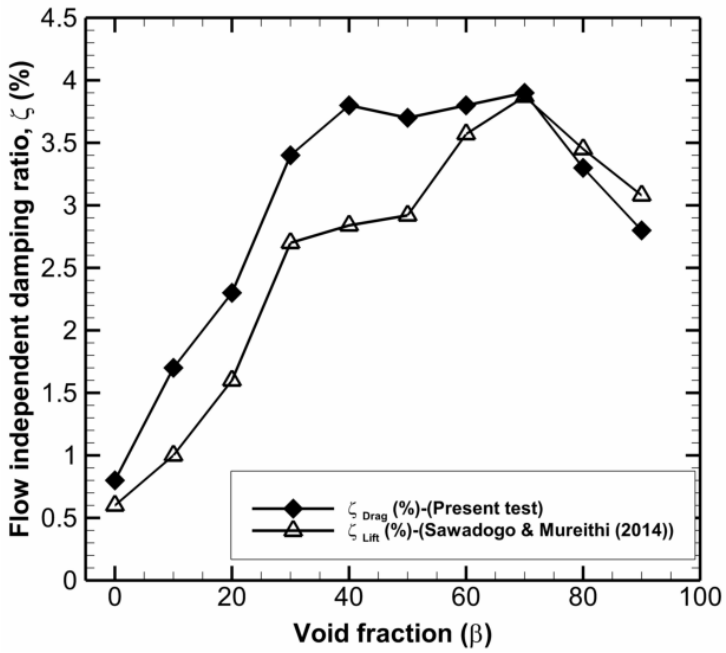


Figure 5-3 : Variation of fluid flow independent damping with void fraction in streamwise and transverse directions

### 5.2.3 Damping

Damping is a measure of the system's ability to dissipate energy from the vibrating tube thereby limiting the tube's vibration response. The tube damping in flow was obtained from its vibration response to turbulence excitation (Figure 5-1). The tube's frequency response spectrum was assumed to be equivalent to that of a single-degree-of-freedom system (Pettigrew et al., 1985) expressed as:

$$\left|X(\omega)\right| = \left\{\left(1-\left(\frac{\omega}{\omega_n}\right)^2\right)^2 + \left(2\zeta\left(\frac{\omega}{\omega_n}\right)\right)^2\right\}^{-0.5} \tag{5-3}$$

where $\left|X(\omega)\right|$ is the normalized vibration amplitude, $\omega$ is the excitation frequency, $\omega_n$ is the tube natural frequency in flow and $\zeta$ the total damping ratio. The total damping ratio, $\zeta$, which includes both tube structural and flow independent damping is then deduced from the best fit of the curve given by Eq. (5-3) to the experimental data by a nonlinear least square regression analysis technique outlined in Marquardt (1963).

Pettigrew et al. (2001) report that damping is fairly constant at flow rates far below the critical velocity for fluidelastic instability where coupling between hydrodynamic forces and the tube motion is negligible (Pettigrew et al., 1985). Thus, since it is impossible to maintain a stagnant two-phase mixture, the total damping in the streamwise direction was measured at three distinct but close and relatively low flow velocities for each void fraction. The difference between the average of these three damping values and the structural damping yielded the flow independent damping. The tube structural damping was measured to be 0.2% in air.

Figure 5-3 presents the flow independent damping as a function of void fraction. The streamwise flow independent damping is seen to increase with void fraction up to about 40% void fraction. The damping then remains fairly constant up to 70%. Beyond 70% void fraction, damping decreases gradually as the flow approaches single-phase gas flow. A similar observation had been made by Pettigrew, Taylor, et al. (1989) for a rotated triangular tube arrays each P/D=1.47 (air-water), and Feenstra et al. (2002) for a rotated triangular tube array of P/D=1.44 (Freon, R-11). Compared to the direction transverse to the flow (Sawadogo & Mureithi, 2014a), damping in the streamwise direction is slightly higher as shown in Figure 5-3.

## 5.3 Stability analysis

The stability analysis performed in the present study is based on the quasi-steady model (Price & Paidoussis, 1982, 1983, 1984, 1986a; Price et al., 1990). This model makes the following key assumptions: the vibration characteristics of an oscillating tube may be approximated by the tube's successive static states; there exists a time delay between the tube displacement and the fluid dynamic forces generated thereby; another time delay exists between the displacement of a tube and the resulting changes on an adjacent tube and that the tube velocity is much smaller than the flow velocity.

Considering a multiple-degree-of-freedom system, the governing equation of motion for a tube bundle with tubes free to vibrate parallel to the flow direction may be written as:

$$\left(\left[\mathbf{M}\right]_s+\left[\mathbf{M}\right]_f\right)\left\{\ddot{\bar{\mathbf{x}}}\right\}+\left(\left[\mathbf{C}\right]_s+\left[\mathbf{C}\right]_f\right)\left\{\dot{\bar{\mathbf{x}}}\right\}+\left(\left[\mathbf{K}\right]_s+\left[\mathbf{K}\right]_f\right)\left\{\bar{\mathbf{x}}\right\}=\left\{\mathbf{0}\right\} \tag{5-4}$$

where

$$\left[\mathbf{M}\right]_s=m_s\left[I\right]_{N\times N};\quad \left[\mathbf{M}\right]_f=m_h\left[I\right]_{N\times N};\quad \left[\mathbf{C}\right]_s=2\omega\zeta m_s\left[I\right]_{N\times N};$$

$$\left[\mathbf{C}\right]_f=\rho_h DUC_{D0}\left[I\right]_{N\times N};\quad \left[\mathbf{K}\right]_s=m_s\omega^2\left[I\right]_{N\times N}$$

Subscripts '$s$' and '$f$', respectively, indicate 'structural' and 'fluid' quantities while $\bar{x}=x/D$ is the reduced displacement parallel to the flow direction and $\left\{\bar{\mathbf{x}}\right\}$ the reduced displacement vector. $C_{D0}$ is the drag coefficients at the tube equilibrium position, $\left[I\right]$ the identity matrix and $N$ the number of flexible tubes. The damping factor, $\zeta$ in Eq.(5-4) includes both the structural and flow-independent damping components.

The fluid stiffness term takes the form:

$$\begin{aligned}\left[\mathbf{K}\right]_{f_{kn}}&=-\frac{1}{2}\rho_h U^2 g\left[\frac{\partial C_{Dk}}{\partial\bar{x}_n}\right]\ for\ k=n\\ \left[\mathbf{K}\right]_{f_{kn}}&=-\frac{1}{2}\rho_h U^2 \bar{g}\left[\frac{\partial C_{Dk}}{\partial\bar{x}_n}\right]\ for\ k\neq n\end{aligned} \tag{5-5}$$

where $C_{Dk}$ is the drag coefficient of tube $k$ and, $x_n$ the displacement of tube $n$ in the drag directions, $g=e^{-\lambda\tau_r}$ and $\bar{g}=e^{-\lambda\tau_i}$; $\tau_r=\mu_r D/U$ is the time delay due to flow retardation and

$\tau_k = \mu_k L/U$ or $\tau_k = \mu_k (2L)/U$ is the time delay due to adjacent tube displacement depending on whether the tube is one or two rows away from the reference tube, $L$ is the row spacing, $\mu$ is the time delay parameter, $\lambda$ is the complex natural frequency of the system while $U$ is the pitch velocity ($=U_\infty P/(P-D)$) and $U_\infty$ is the freestream velocity.

It is evident from Eq. (5-4) that the necessary fluid dynamic parameters in fluidelastic vibration analysis of multiple flexible arrays using the quasi-steady model (Price & Paidoussis, 1982, 1983, 1984) are the derivatives of the drag coefficients which indicate cross-coupling between the tubes due to fluid flow, the equilibrium drag coefficients and the time delays. In the present study, only the effects of the immediate neighboring tubes are considered.

### 5.3.1 Solution method

Expressing Eq.(5-4) in the generalized coordinate system yields:

$$\mathbf{M}\ddot{\mathbf{q}}(t) + \mathbf{C}\dot{\mathbf{q}}(t) + \mathbf{K}\mathbf{q}(t) = \mathbf{0} \tag{5-6}$$

where $\mathbf{M}, \mathbf{C}$ and $\mathbf{K}$ are the $(\mathrm{N}\times N)$ total mass, total damping and total stiffness matrices respectively, and $\mathbf{q}(t)$ is the $(\mathrm{N}\times 1)$ vector of generalized coordinates, whose length, N, in this case corresponds to the number of flexible tubes. By defining the state vector $\bar{\mathbf{q}}(t)$ as:

$$\bar{\mathbf{q}}(t) = \begin{bmatrix} \tilde{\tilde{\mathbf{x}}} \\ \cdots \\ \dot{\tilde{\mathbf{x}}} \end{bmatrix} \tag{5-7}$$

an equivalent first-order state-space differential equation to Eq. (5-6) may be written as (Géradin & Rixen, 1994):

$$\bar{\mathbf{B}}\dot{\bar{\mathbf{q}}}(t) + \bar{\mathbf{A}}\bar{\mathbf{q}}(t) = \mathbf{0} \tag{5-8}$$

where the $(2N\times 2N)$ matrices $\bar{\mathbf{B}}$ and $\bar{\mathbf{A}}$ are defined as:

$$\bar{\mathbf{B}} = \begin{bmatrix} \mathbf{D} & \mathbf{M} \\ \mathbf{M} & \mathbf{0} \end{bmatrix}; \qquad \bar{\mathbf{A}} = \begin{bmatrix} \mathbf{K} & \mathbf{0} \\ \mathbf{0} & \mathbf{-M} \end{bmatrix} \tag{5-9}$$

in which $\mathbf{0}$ is the zero matrix. Assuming a solution of Eq. (5-8) to be in the form $\bar{\mathbf{q}} = e^{\lambda t}\tilde{\mathbf{q}}$ , where $\lambda$ denotes an eigenvalue and $\tilde{\mathbf{q}}$ the corresponding eigenvector transforms Eq. (5-8) to the following generalized eigenvalue problem:

$$\bar{\mathbf{A}}\tilde{\mathbf{q}} = -\boldsymbol{\lambda}\bar{\mathbf{B}}\tilde{\mathbf{q}} \tag{5-10}$$

with the complex eigenvector, $\tilde{\mathbf{q}}$ defined as:

$$\tilde{\mathbf{q}} = \begin{bmatrix} \tilde{\mathbf{x}} \\ \dots \\ -\lambda\dot{\tilde{\mathbf{x}}} \end{bmatrix} \tag{5-11}$$

Here, $\tilde{\mathbf{x}}$ is the $(N \times 1)$ eigenvector of the eigenvalue problem and defines the mode shapes of the system. By incrementally increasing the flow velocity and iteratively solving Eq. (5-10) for each incremental value of the velocity, the lowest velocity at which the real part of any of the eigenvalues vanishes or becomes positive defines the critical velocity for fluidelastic instability. That is, the velocity at which the net system damping becomes zero or negative.

As an illustration, consider a two-degree-of-freedom system (an array with two adjacent tubes constrained to vibrate only in the direction parallel to the flow):

$$\begin{aligned} &\begin{bmatrix} m & 0 \\ 0 & m \end{bmatrix}\ddot{\vec{X}} + \begin{bmatrix} c & 0 \\ 0 & c \end{bmatrix}\dot{\vec{X}} + \begin{bmatrix} k & 0 \\ 0 & k \end{bmatrix}\vec{X} = \\ &-\begin{bmatrix} m_h & 0 \\ 0 & m_h \end{bmatrix}\ddot{\vec{X}} - \rho DU\begin{bmatrix} C_{D01} & 0 \\ 0 & C_{D02} \end{bmatrix}\dot{\vec{X}} + \frac{1}{2}\rho U^2\begin{bmatrix} e^{-\lambda\tau_r}C_{D1,1} & e^{-\lambda\tau_1}C_{D1,2} \\ e^{-\lambda\tau_2}C_{D2,1} & e^{-\lambda\tau_r}C_{D2,2} \end{bmatrix}\vec{X} \end{aligned} \tag{5-12}$$

where the left-hand side is associated with the mechanical structure and the right-hand side represents the fluid-dynamic quantities. $C_{Dk,n} = \partial C_{D_k} / \partial \overline{x}_n$ , is the derivative of the drag coefficient of tube $k$ relative to the streamwise displacement of tube $n$, $c$ and $k$ are the structural damping (including the flow independent damping) and stiffness, respectively, $l$ is the length of the tube while $\lambda$ is one of the complex eigenvalues of the final equations solution, in this case, Eq. (5-10). For a purely stiffness-controlled-instability, the exponents in the last term of Eq. (5-12) are ignored $(\tau_r = 0)$, thus the quasi-steady model (Paidoussis & Price, 1988) reduces to the quasi-static model (Blevins, 1974; Connors, 1970) and assumes that fluidelastic instability originates entirely from the off-diagonal terms in the fluid stiffness component (the last matrix of

Eq. (5-12)), which represent the flow induced cross-coupling between tubes. However, in the current study, both stiffness-controlled instability and damping-controlled instability mechanisms are considered. The presence of the exponential terms ($e^{-\lambda\tau_r}$ and $e^{-\lambda\tau_i}$) make the fluid stiffness part a complex number, hence, may produce the fluid negative damping responsible for damping controlled instability. Substituting the structural and fluid components of Eq. (5-12) into the eigenvalue problem (Eq.(5-10)) yields a complex transcendental function that depends on $\lambda$, $\tau_r$ and $\tau_i$.

An iterative Newton method was used to solve the characteristic equation obtained from Eq. (5-10). Since convergence to the desired solution by this method strongly depends on the initial value chosen for $\lambda$ ($=i\omega$), which, generally has to be in a narrow basin of attraction, the tube natural frequency was taken as the initial value for all the cases. This is because for a tuned tube array in which all the tubes have the same natural frequency, the tube frequency at instability remains close to the zero flow natural frequency. No assumptions have been made regarding the expected tube vibration frequency and vibration modes. These are direct products of the eigenvalue analysis.

In the stability analysis, for each of the void fractions considered, the quasi-steady fluid force coefficients from Olala & Mureithi (2016a) and the time delay parameters from the first part of the paper (Olala & Mureithi, 2016b) are employed. Since the main interest is to determine the critical velocity for fluidelastic instability, the linearized quasi-steady fluid force coefficients may sufficiently be used in the quasi-steady fluid force expression, hence in the system's equation of motion (Eq.(5-4)). The hydrodynamic mass and flow independent damping are as reported earlier in the current paper. The results obtained with the experimentally measured time delay parameters ($\mu = \mu_{\exp}$ and $\mu_i = \mu_{i\exp}$) are compared with those of dynamic stability tests (Violette et al., 2006), those of the classical analysis with $\mu = \mu_i = 1$ proposed by Price & Paidoussis (1984) and the pure stiffness-controlled fluidelastic instability analysis of Olala & Mureithi (2016a).

### 5.3.2 FEI instability analysis results

The configurations of the tube bundle analyzed for fluidelastic instability are shown in Figure 5-4Figure 3-10 for both flexible tubes in a single and multiple columns. These are the same as

those used in both Violette et al. (2006) and Olala & Mureithi (2016a) to enable direct comparison and understanding of the effect of the time delay on streamwise fluidelastic instability for a triangular tube array.

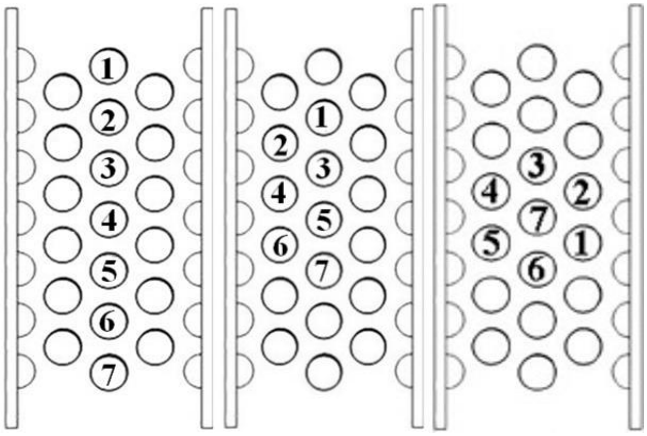


(a) (b) (c)

Figure 5-4 : Flexible tubes configuration for stability analysis (a) single column, (b) two-partial columns, (c) Central cluster

Firstly, the effect of time delay was investigated for the tube configurations considered in the present analysis. Figure 5-5 to Figure 5-7 show the variation of the critical velocity with: (a) void fraction, $\beta$, and (b) mass damping parameter, $2\pi\zeta m/\rho_h D^2$. The mass, $m$, includes both the structural and hydrodynamic mass components (Figure 5-2). Similarly, the damping ratio, $\zeta$, is the sum of structural damping and the flow independent damping given in Figure 5-3. Four different cases of time delays are considered for each configuration: experimentally measured time delay ($\mu_r = \mu_i = \mu_{\exp}$), time delay due to flow retardation experimentally obtained with the delay parameter for adjacent tubes assumed to be 1 ($\mu_r = \mu_{\exp}$, $\mu_i = 1$), all the time delay parameters assumed to be 1 ($\mu_r = \mu_i = 1$), and the case with time delay ignored ($\mu_r = \mu_i = 0$). It is seen in Figure 5-5 that for a column of flexible tubes, except for 60% void fraction, there is no noticeable difference in the critical velocity for the time delay cases considered. This is because the time delays for the tubes upstream and downstream of a vibrating central tube are approximately equal to 1 for 70%-90% void fractions (Olala & Mureithi, 2016b), hence almost the same time delay values are used for each of the cases. The case of $\mu_r = \mu_i = 0$ however,

appears to yield higher reduced critical velocities, more so for 80% and 90% void fractions, the high mass damping parameter cases.

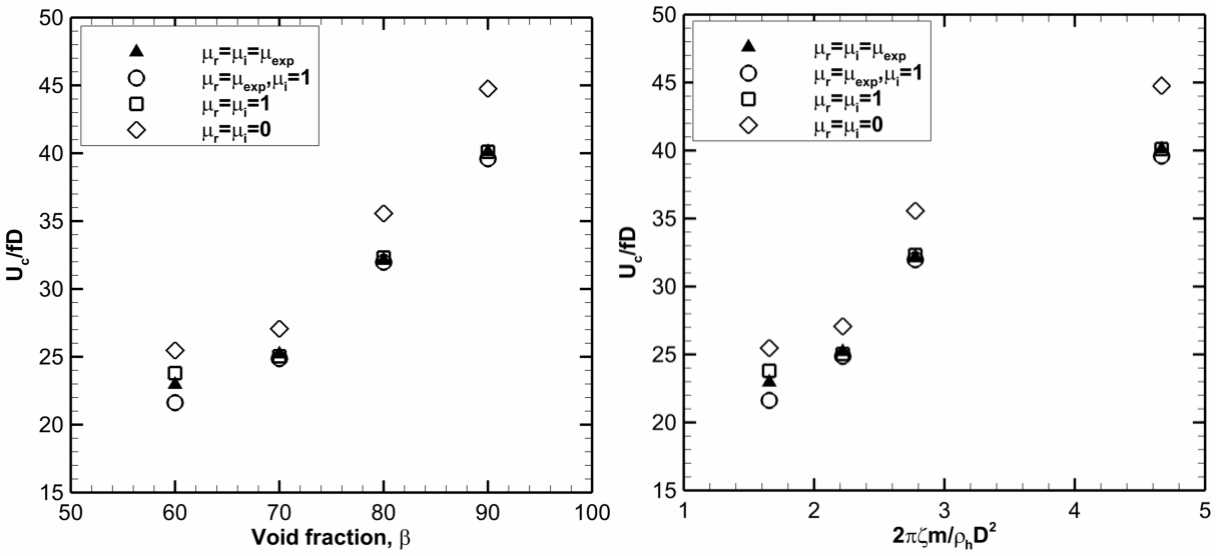


(a) (b)

Figure 5-5 : Effect of the time delay on the reduced critical velocity for a flexible column of tubes (Refer to Figure 5-4(a))

Figure 5-6 displays the time delay effect comparison for the two partially flexible columns. Except for the 70% void fraction case, the reduced critical velocity $(U_c/fD)$ obtained with the experimentally determined time delay parameters and that for the case of zero time delay ($\mu_r = \mu_i = 0$) are practically equal. The two remaining cases, $\mu_r = \mu_{\exp}$, $\mu_i = 1$ and $\mu_r = \mu_i = 1$, also yield equal values of $U_c/fD$ for 70%-90% void fractions. This is not surprising since the time retardation parameters, $\mu_r$, for these void fractions are equal to one, thus the two cases are identical. For the 60% void fraction, $\mu_r = 2.0$. A similar trend is observed for the kernel of flexible tubes (Figure 5-7). Here, again, the $U_c/fD$ obtained with the experimentally measured time delay parameters and those with time delays neglected ($\mu_r = \mu_i = 0$) are approximately equal. It is noted that the configuration of the flexible tubes also influences the critical velocity for each void fraction. For the cases considered, the single flexible column (Figure 5-5) has the highest $U_c/fD$ values followed by the two-partially flexible columns (Figure 5-6) and finally the central cluster of flexible tubes (Figure 5-7). It is therefore evident that the mechanism causing

streamwise instability is dependent on the fluid coupling between tubes, the more the number of neighboring tubes, the stronger the coupling strength.

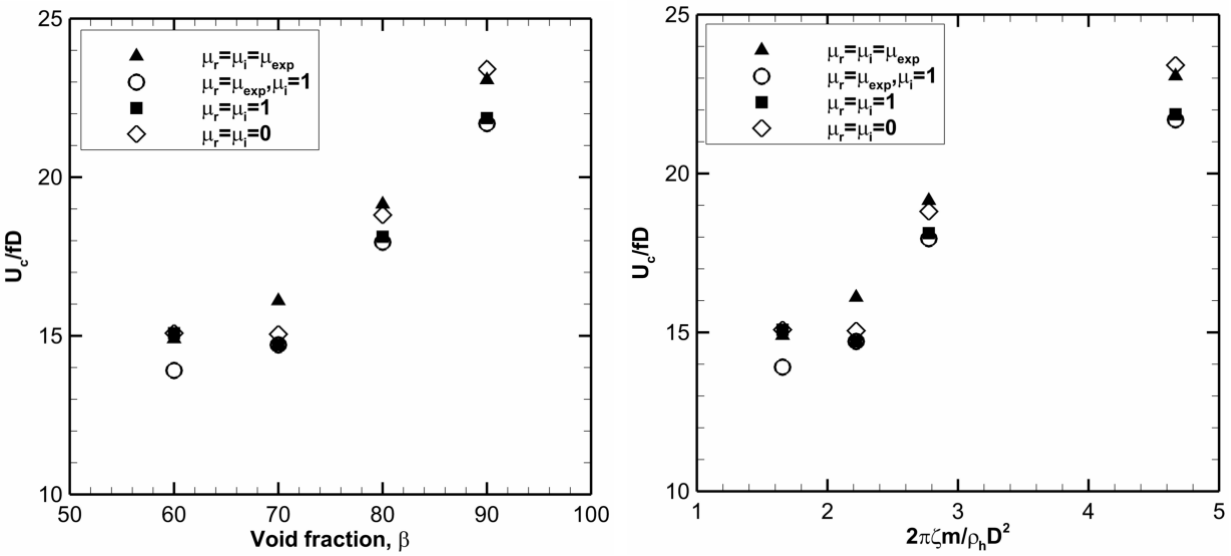


(a) (b)

Figure 5-6 : Effect of the time delay on the reduced critical velocity for two partially flexible columns of tubes (Refer to Figure 5-4(b))

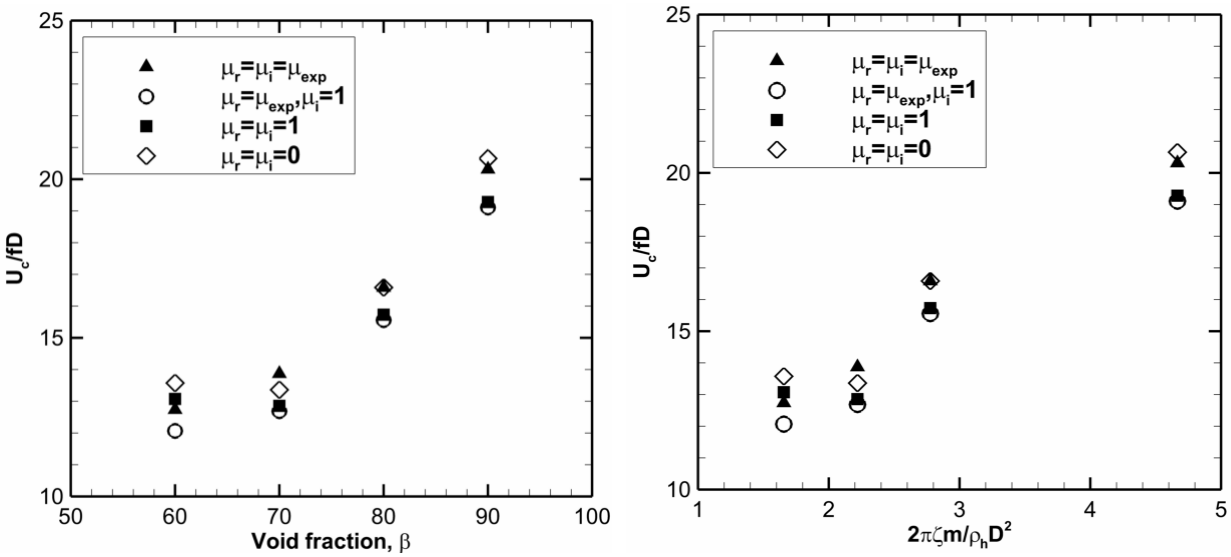


(a) (b)

Figure 5-7 : Effect of the time delay on the reduced critical velocity for a kernel of flexible tubes (Refer to Figure 5-4(c))

### 5.3.3 Model comparison with experiments

Figure 5-8 to Figure 5-11 present the comparison between the results of the current analysis and the experimental tests of Violette et al. (2006). It can be seen that the agreement between the theoretical and experimental data is generally fairly good. The reduced critical velocity predicted by the quasi-steady model with the measured time delay parameters are slightly higher, by up to 24% for the two-partially flexible columns (Figure 5-8) and 13% for the flexible central cluster (Figure 5-10). Similarly, the classical values of the time delay parameters, $\mu_r = \mu_i = 1$, (Price et al., 1990) yield percentage errors up to 17% for the two-partially flexible columns (Figure 5-9(a)) and up to 8% for the flexible kernel (Figure 5-11(a)). A case of purely fluid stiffness controlled instability was also considered. For this particular case where $\mu_r = \mu_i = 0$, the model predicted $U_c / fD$ values which were up to 21% and 15% over the experimental value for the two-partially flexible columns (Figure 5-9(b)) and the flexible central cluster (Figure 5-11(b)), respectively.

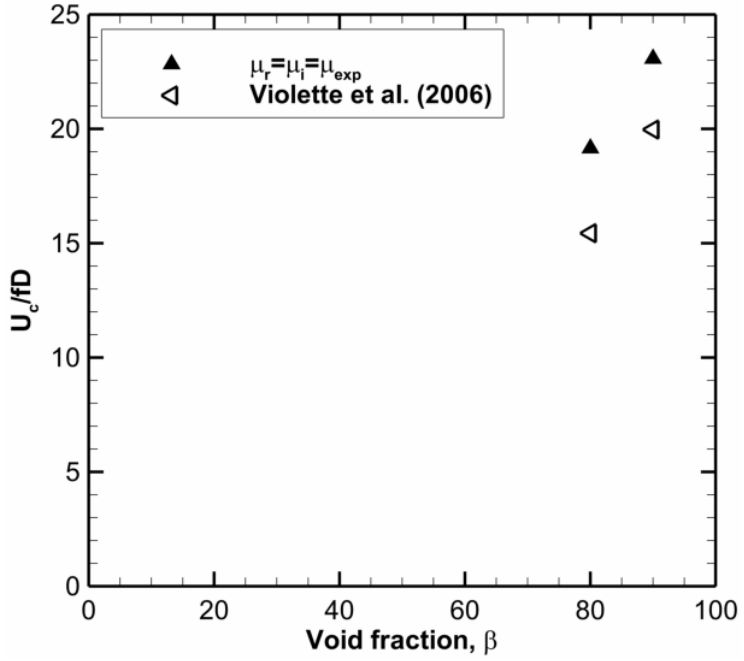


Figure 5-8 : Comparison between theoretical results ($\mu_r = \mu_i = \mu_{\exp}$) and experimental data (Violette et al., 2006) for two partially flexible columns of tubes (Refer to Figure 5-4(b))

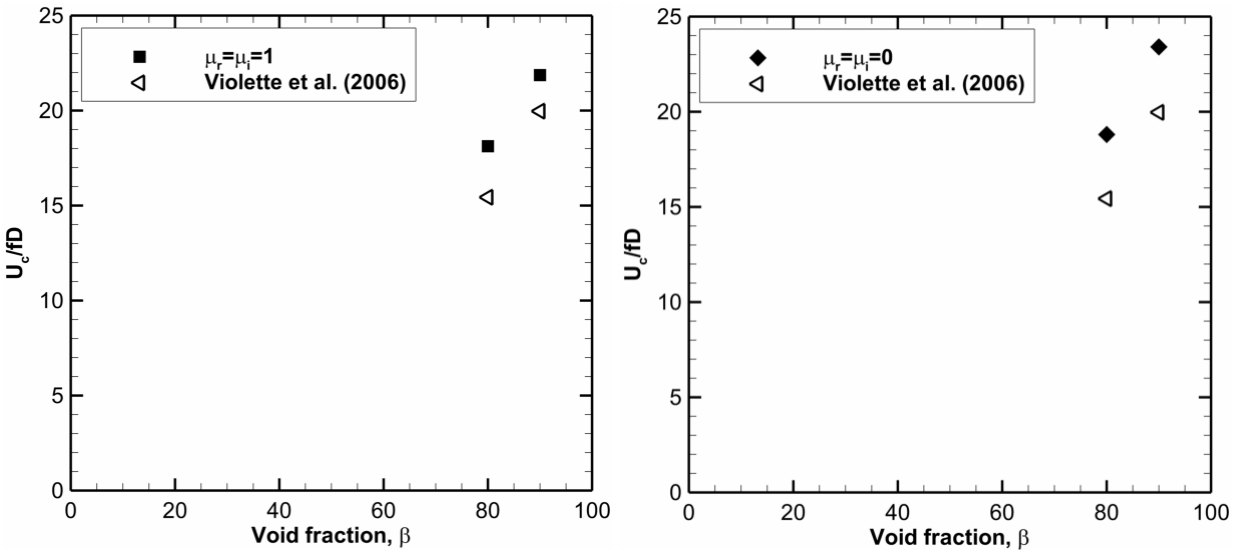


(a) (b)

Figure 5-9 : Comparison between theoretical results and experimental data (Violette et al., 2006) for two partially flexible columns of tubes (Refer to Figure 5-4(b)) (a) $\mu_r = \mu_i = 1$ (b) $\mu_r = \mu_i = 0$

The last case ( $\mu_r = \mu_i = 0$ ) results are an improvement over those obtained by Olala & Mureithi (2016a) who found predicted values higher than the experimental data by up to 22% and 19% for the two-partially flexible columns and the flexible central cluster, respectively. It should be remarked that Olala & Mureithi (2016a) did the same analysis with the same input values as in the present case except for the hydrodynamic mass which was determined from a theoretical relation (Pettigrew, Taylor, et al., 1989).

There is no significant difference in the reduced critical velocity, $(U_c / fD)$, obtained either when the time delay is considered $\left(\mu_r = \mu_i = \mu_{\exp}\right)$ or when the time delay is neglected $\left(\mu_r = \mu_i = 0\right)$. The results obtained from the present analysis, therefore, suggest that fluidelastic instability of multiple tubes in a rotated triangular array purely flexible in the streamwise direction is predominantly stiffness controlled. This is in agreement with the dynamic tests of Violette et al. (2006) and Mureithi et al. (2005). Inclusion of the measured time delay term ( $e^{-i\omega\tau}$ ) in the quasi-steady model formulation for streamwise fluidelastic instability analysis of multiple flexible tubes, thus, appears, in general, not to affect the critical velocity $U_c / fD$.

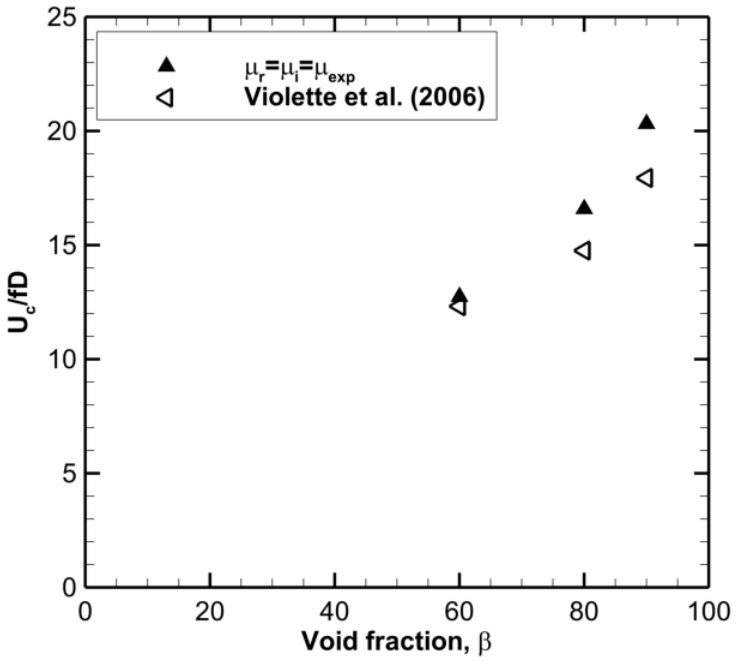


Figure 5-10 : Comparison between theoretical results ( $\mu_r = \mu_i = \mu_{\exp}$ ) and experimental data (Violette et al., 2006) a kernel of flexible of tubes (Refer to Figure 5-4(c))

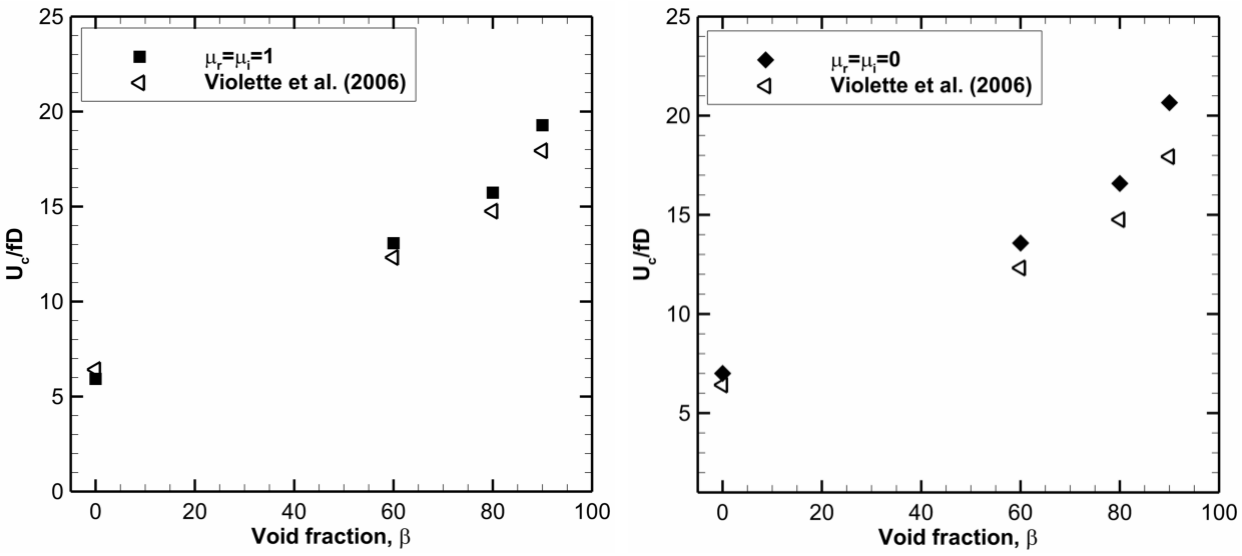


(a) (b)

Figure 5-11 : Comparison between theoretical results and experimental data (Violette et al., 2006) for a kernel of flexible tubes (Refer to Figure 5-4(c)): (a) $\mu_r = \mu_i = 1$ and (b) $\mu_r = \mu_i = 0$

## 5.4 Conclusion

Experimental measurements were performed to determine the hydrodynamic mass and flow independent damping on a tube in a rotated triangular array of $P/D = 1.5$ subjected to air-water two-phase flow. The tube was constrained to vibrate only in the flow direction. Together with previously measured quasi-steady fluid forces and time delay parameters estimated in the first part of the paper, a quasi-steady analysis was conducted to establish the effect of time delay on the critical velocity for streamwise fluidelastic instability of multiple flexible tubes in a rotated triangular tube array in two-phase flow. A single flexible column was found to be more stable than multiple flexible columns in conformity with previous findings.

The results obtained with the quasi-steady model were compared to experimentally determined critical velocities for specific multiple tube configurations in the same array and found to be in fairly good agreement. It was therefore verified that streamwise fluidelastic instability of multiple flexible tubes in a rotated triangular array are strongly dependent on the cross-coupling forces thus stiffness controlled. The present results further demonstrate the capability of the quasi-steady model in predicting fluidelastic instability for multiple flexible tubes. It should, however, be noted that the aforementioned observations are specific to a rotated triangular array of a specific pitch-to-diameter-ratio hence may not necessarily be applicable to other array geometries.

# CHAPTER 6 GENERAL DISCUSSIONS

The work presented in this Thesis was motivated by the need to validate the fluidelastic instability models presented in Chapter 2 in two-phase flow and extend the candidate model, in this case, the quasi-steady model, to analyze fluidelastic instability in the streamwise direction. Following replacement steam generator tube failures at San Onofre Nuclear Generating Station, U.S.A in 2012 (S.C.E., 2013), streamwise fluidelastic instability became a reality and the need to develop predictive tools that would enable design against its occurrence gained prominence.

In the first paper (Chapter 3), the streamwise quasi-steady fluid force coefficients for a kernel of tubes are reported for various void fractions. The steady drag coefficients for different tubes were observed to strongly depend on the position of the central tube. Also, for a given position of the central tube, the drag coefficient, $C_D$, for each tube varied with the void fraction. These drag coefficients together with their derivatives with respect to the streamwise displacement of the central tube are used in the quasi-steady model to predict the critical velocity for fluidelastic instability of multiple flexible tubes free to vibrate in the flow direction. The trend of the steady force derivatives was found to also vary with the tube location relative to the central tube position. This was the case for all the void fractions tested. The effect of the time delay was ignored, as a first step, and streamwise fluidelastic instability assumed to be fluid stiffness controlled. It was found that the number and location of the flexible tubes greatly influenced the array stability. For instance, two flexible tubes on the same column were found to be more stable than two tubes on adjacent columns. A single column of flexible tubes was also found to be more stable than multiple flexible columns. Likewise the fewer the number of flexible tubes the higher the critical velocity estimated. From this analysis, it was observed that the predicted critical velocity did not change when at least five flexible tubes were considered. Overall, the results were in fairly good agreement with dynamic experimental data. Since the time delay was not considered in this analysis, the good agreement between the theoretical and dynamic experimental data indicate that cross-coupling forces, represented by the force derivatives, are more important in generating streamwise fluidelastic instability of multiple flexible tubes in a rotated triangular array.

The first paper also analyzed the effect of frequency detuning on the estimated critical velocity, and in effect, the stability constant used in design. The detuning was introduced artificially by

generating random frequency values with a given variance about the tuned tube frequency. Though detuning generally stabilizes the tube array, the large scatter in the possible values of the stability constant, $K$, makes it a challenge in deciding which value to use in design.

Most importantly, this analysis demonstrated the potential of the quasi-steady model in predicting streamwise fluidelastic instability threshold in tube arrays.

The second paper (Chapter 4) presents results of the unsteady fluid force measurements for the same kernel of tubes used in the work of the first paper and the time delay between the displacement of the central tube and the generated unsteady forces on the neighboring tubes, and on itself. Here the main goal was to estimate the time delay. The unsteady forces on each tube were measured for various void fractions, flow velocities and excitation frequencies of the central tube. Appropriate excitation amplitude for the central tube, was firstly, determined to ensure measurable fluid forces on the adjacent tubes and minimize non-linearity that could appear in the unsteady force due to large amplitude oscillations. The magnitude of the unsteady fluid force coefficient was found to have a single-valued functional relation with the reduced velocity ($U/fD$) for the range of void fractions tested. The fluid force coefficient phases on the other hand could be represented in a similar manner only for low void fractions. For higher void fractions, marked scatter was seen in the phase data, more so for the cross-coupling phases suggesting multi-valued functional relations between the force coefficient phases and $U/fD$. The phase trend for the higher void fractions differ from those presented by Sawadogo & Mureithi (2014b) who found a single valued functional relation for all the void fractions they tested. The authors' tests were done in the same test section as the current case, except that the unsteady forces were measured for a single tube oscillated in the lift direction. The present results (high void fraction), however, resemble those of Mureithi et al. (2002) who did their measurements in an in-line square array subjected to steam-water flow. The observation may be attributed to the level of two-phase intermittency and turbulence which reduces force correlations.

An attempt was made to represent the high void fraction phase data in terms of the Feenstra et al. (2000) void fraction model as opposed to the homogeneous model. It was observed that, with a modified representation of the reduced velocity, $Y^*\left(U_{eq}/fD\right)$, the data could be collapsed onto a single curve suggesting that a better representation of the two-phase flow physics could be

realized with the Feenstra's model. It also became evident that the homogeneous model ('incorrectly') averages a wide range of void fractions, especially for high void fractions.

Next, two forms of the time delay (as already stated) were estimated from the unsteady fluid forces in the current article (Paper 2-Chapter 4) and the quasi-steady fluid forces presented in Chapter 3. This could only be done for void fractions in the range 60%-90% due to water pump limited capacity. The quasi-steady model is only valid for $U/fD \gg 1$, meaning that either $U \gg 1$ or $f \ll 1$. However, there is a limit on how low the excitation frequency can go to maintain reasonable signal-to-noise ratio. A compromise was therefore found in the 60%-90% void fraction range.

The time delay was found to significantly depend on tube position and void fraction. The parameter for the time delay due to flow retardation (the time lag/lead between the displacement of a tube and the unsteady fluid forces generated on itself) showed similar trend to the results by Sawadogo & Mureithi (2014b) for the lift direction except for the 90% void fraction. Similarly, the form of the time delay expression was found to agree with the one suggested by Price & Paidoussis (1984) , $\tau = \mu D/U$ . The time delay parameter for the time lag due to apparent displacement of an adjacent tube could also be expressed in the form $\tau = \mu_i L/U$ or $\tau = \mu_i (2L)/U$ depending on whether it is one or two rows away, respectively. The values of the time delay parameters were then used in the third part of the project to verify the validity of the quasi-steady model.

In the third paper (Chapter 5), the parameters obtained in the earlier sections of the work were used to estimate the critical velocity for fluidelastic instability. Additional measurements were done to determine the flow independent damping and the hydrodynamic mass. It should be noted that, in the fluidelastic instability analysis performed in the first paper (Chapter 3), the added mass was estimated from a semi-empirical formula by Pettigrew, Taylor, et al. (1989). The hydrodynamic mass showed a decreasing trend with void fraction. There seemed also to be no significant difference between the hydrodynamic mass in the drag and lift (Sawadogo & Mureithi, 2014a) directions. However, the formulation by Pettigrew, Taylor, et al. (1989) was found to generally underestimate the added mass, as had earlier been observed by the same authors. To enable validation of the analysis results, the same flexible tube configurations as those tested by Violette et al. (2006) were analysed. With the experimentally obtained time delay

parameters, the quasi-steady model yielded critical velocities in fairly good agreement with dynamic instability tests of (Violette et al., 2006). An error of 24% was found for two-partially flexible configuration (80% void fraction) and 13% for the flexible central cluster (90% void fraction). With the classical values of the time delay parameter, $\mu = \mu_i = 1$ (Price & Paidoussis, 1984; Price et al., 1990), the errors were 17% and 8% respectively; while for the case of $\mu = \mu_i = 0$, when the effect of the time delay is ignored, the error became 21% and 15% respectively. It appears that the instability of multiple flexible tubes in the flow direction depends almost entirely on the fluid stiffness as opposed to the damping mechanism. However, more analysis of different flexible tube configurations and re-examination of the time delay extraction procedure may be necessary.

# CHAPTER 7 CONCLUSION AND RECOMMENDATIONS

## 7.1 Contributions

The following are the main contributions from this work:

- Measurement and comprehensive study of the streamwise quasi-steady and the unsteady fluid forces on a kernel of tubes in a rotated triangular array subjected to air-water two-phase flow. The quasi-static analysis (quasi-steady model with the time delay ignored) using the measured quasi-steady forces confirmed the predominance of the cross-coupling fluid forces in causing streamwise fluidelastic instability of a rotated triangular array. The study on frequency detuning revealed the uncertainty in the use of the Connors stability constant indicating that the use of an average stability constant may be misleading due to the strong dependence of $K$ on the frequency variance.

- Another important outcome of the study is that the phase of the unsteady fluid force in the streamwise direction, for high void fractions, in a rotated triangular array subjected to air-water flow is not a single valued function of the reduced velocity $\left(U/fD\right)$. Using the Feeenstra's void fraction model, the scattered unsteady fluid force phase data could be collapsed onto a single curve as a function of a modified reduced velocity $Y*\left(U_{eq}/fD\right)$; $Y=\left(f\sqrt{D/g}\right)^{-a}\alpha^{-b}$ , taking into account the "true" void fraction and effect of gravity .

- The present work was the first attempt to measure the unsteady cross-coupling fluid forces in a rotated triangular array subject to air-water two-phase flows. This was also the first attempt to experimentally determine both the time delay due to flow retardation and that due to apparent displacement of an adjacent tube for the streamwise direction oscillations of a rotated triangular array in air-water two-phase flow. The phase of the unsteady cross-coupling force for high void fractions displayed marked scatter possibly due to weak coherence. This remains a challenge.

- The extraction of the time delays made it possible to apply the quasi-steady model to two-phase flow and demonstrate the potential of the model in analysing the stability of multiple tubes preferentially flexible in the flow direction.

## 7.2 Limitations and challenges

A number of challenges and limitation were experienced in the course of the project:

- The pump capacity did not permit the estimation of the time delay for void fractions lower than 60%. High velocities that would permit the quasi-steady assumption to be fulfilled, $U/fD \gg 1$, could not be achieved, for low void fractions, with the current water pump.
- Air flow rate control valve required close attention during high velocity air flow rate (case of high speed high void fraction) since it tended to incrementally open. Whenever such discrepancy was noticed, the specific data was discarded.
- The cross-coupling unsteady fluid force phase exhibited considerable scatter for the high void fractions. This could have introduced errors in the estimated time delay, especially for tubes downstream of the oscillating central tube. Further investigation is thus necessary.
- The use of the Feenstra's model enabled collapsing of the unsteady fluid force phase for the oscillating tube in high void fraction. Due to limited data ((since the tests were based on the homogeneous void fraction model) it was not possible to do a complete analysis based on Feenstra's model.

## 7.3 Recommendations for future work

- Increase the pump capacity to realize higher flow velocity for low void fractions. This would allow measurement of the time delay for these void fractions using the method employed in this work
- Replace the manual air flow rate control valve with a self acting automatic control valve to improve on the precision of the estimated void fraction.
- Examine the flow structure around the vibrating tube to provide insight on the physical nature of the time delay.
- Measure the cross-coupling forces in the lift direction to provide complete data for fluidelastic instability of a rotated triangular tube bundle of the pitch ratio used in the current study.

- Repeat the force measurements with the void fraction based on the Feenstra's model to determine the effect of "true" void fraction on the fluid forces.
- Examine other possible dimensionless parameters representative of the two-phase flow physics, e.g Weber number $(We)$ , Womersley number $(\alpha)$ etc.
- Extend the investigation to arrays of other geometric configurations.

## Publications

This PhD project has led to four conference papers and three journal articles. The papers submitted to journals are listed as follows:

OLALA, S & MUREITHI, N. W. (2016a). Prediction of Streamwise Fluidelastic Instability of a Tube Arrays in Two-Phase Flows and Effect of Frequency Detuning (Paper accepted) *Journal of Pressure Vessels Technology, Transactions of the ASME.*

OLALA, S & MUREITHI, N. W. (2016b). Streamwise Fluidelastic Vibration of a Triangular Tube Array in Two-Phase Flow. Part I: Unsteady fluid forces and time delay estimation (Paper submitted to) *Journal of Fluids and Structures.*

OLALA, S & MUREITHI, N. W. (2016c). Streamwise Fluidelastic Vibration of a Triangular Tube Array in Two-Phase Flow. Part II: Fluidelastic Instability Analysis (Paper submitted to) *Journal of Fluids and Structures.*

# BIBLIOGRAPHY

Austermann, R., & Popp, K. (1995). Stability Behavior of a Single Flexible Cylinder in Rigid Tube Arrays of Different Geometry Subjected to Cross-Flow. *Journal of Fluids and Structures, 9*(3), 303-322. doi: 10.1006/jfls.1995.1017

Bearman, P. W. (1984). Vortex Shedding from Oscillating Bluff Bodies. *Annual Review of Fluid Mechanics, 16* 195-222. doi: 10.1146/annurev.fl.16.010184.001211

Blevins, R. D. (1974). Fluidelastic Whirling of a Tube Row. *ASME Journal of Pressure Vessel Technology, 96*(4), 263-267. doi: 10.1115/1.3454179

Blevins, R. D. (1977). Fluidelastic Whirling of Tube Rows and Tube Arrays. *Journal of Fluids Engineering, 99*(3), 457 -460. doi: 10.1115/1.3448811

Blevins, R. D. (1979a). Fluid Damping and the Whirling Instability of Tube Arrays. In S. S. Chen & M. D. Bernstein (Eds.), *Flow Induced Vibrations* (pp. 35 -39). New York: ASME.

Blevins, R. D. (1979b). *Formulas for Natural Frequency and Mode Shape*. New York: Van Nostrand Reinhold co.

Blevins, R. D. (1990). *Flow-Induced Vibrations* (2nd ed.). New York: Van Nostrand Reinhold.

Carlucci, L. N. (1980). Damping and Hydrodynamic Mass of a Cylinder in Simulated Two-Phase Flow. *ASME Journal of Mechanical Design, 102*(3), 597-602. doi: 10.1115/1.3254791

Carlucci, L. N., & Brown, J. D. (1983). Experimental Studies of Damping and Hydrodynamic Mass of a Cylinder in Confined Two-Phase Flow. *Journal of Vibration, Acoustics, Stress, and Reliability in Design, 105*(1), 83-89. doi: 10.1115/1.3269073

Chen, S. S. (1983a). Instability Mechanisms and Stability Criteria of a Group of Circular Cylinders Subjected to Cross-Flow. Part I:Theory. *Journal of Vibration, Acoustics, Stress and Reliability in Design, 105*(1), 51-58. doi: 10.1115/1.3269066

Chen, S. S. (1983b). Instability Mechanisms and Stability Criteria of a Group of Circular Cylinders Subjected to Cross-Flow. Part II: Numerical Results and Discussion. *Journal of Vibration, Acoustics, Stress and Reliability in Design, 105*(2), 253-260. doi: 10.1115/1.3269095

Chen, S. S. (1987). A General Theory for Dynamic Instability of Tube Arrays in Cross-Flow. *Journal of Fluids and Structures, 1*(1), 35-53. doi: 10.1016/S0889-9746(87)90170-8

Chen, S. S., & Jendrzejczyk, J. A. (1983). Stability of Tube Arrays in Crossflow. *Nuclear Engineering and Design, 75*(3), 351-373. doi: 10.1016/0029-5493(83)90004-3

Chen, S. S., & Srikantiah, G. S. (2001). Motion-Dependent Fluid Force Coefficients for Tube Arrays in Crossflow. *ASME Journal of Pressure Vessel Technology, 123*(4), 429-436. doi: 10.1115/1.1401022

Cheng, B. (1994). *The Mechanisms Underlying Flow-Induced Instability of Cylinder Arrays in Cross-Flow : An Investigation of System Parameters.* (Ph.D. Thesis, McGill University, Montréal, QC, Canada).

Connors, H. J. (1970). Fluidelastic Vibration of Tube Arrays Excited by Cross Flow. In D. D. Reiff (Ed.) *Flow-Induced Vibrations in Heat exchangers* (pp. 42-56). New York: ASME.

Consolini, L., Robinson, D., & Thome, J. R. (2006). Void fraction and Two-Phase Pressure Drops for Evaporating Flow over Horizontal Tube Bundles. *Heat Transfer Engineering, 27*(3), 5-21. doi: 10.1080/01457630500453832

Eisinger, F. L., Rao, M. S. M., Steininger, D. A., & Haslinger, K. H. (1995). Numerical-Simulation of Cross-Flow-Induced Fluidelastic Vibration of Tube Arrays and Comparison with Experimental Results. *ASME Journal of Pressure Vessel Technology, 117*(1), 31-39. doi: 10.1115/1.2842087

Feenstra, P. A., Janzen, V. P., & Smith, T. (2014). *In-Plane Vibration Damping of a U-Tube with Wet and Dry Flat-Bar Supports.* Paper presented at ASME 2014 Pressure Vessels & Piping Conference, Anaheim, California, U.S.A. (Vol. 4, pp. V004T004A043). doi: 10.1115/PVP2014-28429

Feenstra, P. A., Judd, R. L., & Weaver, D. S. (1995). Fluidelastic Instability in a Tube Array Subjected to 2-Phase R-11 Cross-Flow. *Journal of Fluids and Structures, 9*(7), 747-771. doi: 10.1006/jfls.1995.1042

Feenstra, P. A., Weaver, D. S., & Judd, R. L. (2000). An Improved Void Fraction Model for Two-Phase Cross-Flow in Horizontal Tube Bundles. *International Journal of Multiphase Flow, 26*(11), 1851-1873. doi: 10.1016/S0301-9322(99)00118-4

Feenstra, P. A., Weaver, D. S., & Judd, R. L. (2002). Modelling Two-Phase Flow-Excited Damping and Fluidelastic Instability in Tube Arrays. *Journal of Fluids and Structures, 16*(6), 811-840. doi: 10.1006/Jfls.442

Géradin, M., & Rixen, D. (1994). *Mechanical Vibrations - Theory and Application to Structural Dynamics* (1st ed.). Chichester: John Wiley.

Gorman, D. J. (1976). Experimental Development of Design Criteria to Limit Liquid Cross-Flow-Induced Vibration in Nuclear Reactor Heat Exchange Equipment. *Nuclear Science and Engineering, 61*(3), 324-336.

Granger, S., Campistron, R., & Lebret, J. (1993). Motion-Dependent Excitation Mechanisms in a Square In-Line Tube Bundle Subject to Water Cross-Flow : An Experimental Modal Analysis. *Journal of Fluids and Structures, 7*(5), 521-550. doi: 10.1006/jfls.1993.1032

Granger, S., & Paidoussis, M. P. (1996). An Improvement to the Quasi-Steady Model with Application to Cross-Flow-Induced Vibration of Tube Arrays. *Journal of Fluid Mechanics, 320* 163-184. doi: 10.1017/S0022112096007495

Grant, I. D. R., & Chishom, D. (1979). Two-Phase Flow on the Shell-Side of a Segmentally Baffled Shell-and-Tube Heat Exchanger. *ASME Journal of Heat Transfer, 101*(1), 38-42. doi: 10.1115/1.3450927

Grant, I. D. R., & Murray, I. (1972). *Pressure Drop on the Shell Side of a Segmentally Baffled Shell-and-Tube Heat Exchanger with Vertical Two-Phase Flow* (Report No. NEL-500). National Engineering Laboratory, East Kilbride, Glasgow.

Gross, H. G. (1975). *Untersuchung Aerodynamischer Scwingungs-Mechanismen und deren Berucksichtigung bei der Auslegung von Rohrbundelwarmetauschern.* (Ph.D. Thesis, Technical University of Hannover).

Hassan, M., Gerber, A., & Omar, H. (2010). Numerical Estimation of Fluidelastic Instability in Tube Arrays. *ASME Journal of Pressure Vessel Technology, 132*(4), Art. 041307. doi: 10.1115/1.4002112

Hassan, M., & Weaver, D. S. (2014). *The Effect of Flat Bar Supports on Streamwise Fluidelastic Instability in Heat Exchanger Tube Arrays.* Paper presented at ASME 2014 Pressure Vessels and Piping Conference Anaheim, California, U.S.A. (Vol. 4, pp. V004T004A079). doi: 10.1115/PVP2014-29038

Hassan, M., & Weaver, D. S. (2016). Modeling of Streamwise and Transverse Fluidelastic Instability in Tube Arrays. *ASME Journal of Pressure Vessel Technology, 138*(5), Art. 051304. doi: 10.1115/1.4032817

Hassan, M., Weaver, D. S., & Dokainish, M. A. (2003). The Effects of Support Geometry on the Turbulence Response of Loosely Supported Heat Exchanger Tubes. *Journal of Fluids and Structures, 18*(5), 529-554. doi: 10.1016/j.jfluidstructs.2003.08.011

Inada, F., Kawamura, K., Yasuo, A., & Yoneda, K. (2002). An Experimental Study on the Fluidelastic Forces Acting on a Square Tube Bundle in Two-Phase Cross-Flow. *Journal of Fluids and Structures, 16*(7), 891-907. doi: 10.1006/jfls.2002.0460

Inman, D. J. (2001). *Engineering Vibration* (2nd ed.). New Jersey: Prentice-Hall, Inc.

Janzen, V. P., Hagberg, E. G., Pettigrew, M. J., & Taylor, C. E. (2005). Fluidelastic Instability and Work-Rate Measurements of Steam-Generator U-Tubes in Air-Water Cross-Flow. *ASME Journal of Pressure Vessel Technology, 127*(1), 84-91. doi: 10.1115/1.1849229

Khalifa, A., Weaver, D. S., & Ziada, S. (2011, July 17-21, 2011). *An Experimental Study of the Phase Lag Causing Fluidelastic Instability in Tube Bundles.* Paper presented at ASME 2011 Pressure Vessels and Piping Conference, Baltimore, Maryland, USA (Vol. 4, pp. 211-218). doi: 10.1115/PVP2011-57263

Kuppan, T. (2000). *Heat Exchanger Design Handbook*. New York: Marcel Dekker, Inc.

Lever, J. H., & Weaver, D. S. (1982). A Theoretical Model for the Fluidelastic Instability in Heat Exchanger Tube Bundles. *ASME Journal of Pressure Vessel Technology, 104*(3), 147-158. doi: 10.1115/1.3264196

Lever, J. H., & Weaver, D. S. (1986a). On the Stability Behaviour of Heat Exchanger Tube Bundles. Part I: Modified Theoretical Model. *Journal of Sound and Vibration, 107*(3), 375-392. doi: 10.1016/S0022-460X(86)80114-6

Lever, J. H., & Weaver, D. S. (1986b). On the Stability Behaviour of Heat Exchanger Tube Bundles. Part II - Numerical Results and Comparison with Experiments. *Journal of Sound and Vibration, 107*(3), 393-410. doi: 10.1016/S0022-460X(86)80115-8

Little, J. (2003). *The Effect of Damping on Fluidelastic Instability in Heat Exchanger Tube Array.* (Master's thesis, McMaster University, Hamilton, Ontario, Canada).

Mahon, J., & Meskell, C. (2010). *Measurement of the Time Delay Associated with Fluid Damping Controlled Instability in a Normal Triangular Tube Array.* Paper presented at ASME 2010 3rd Joint US-European Fluids Engineering Summer Meeting, FEDSM 2010 - ASME 2010 7th International Symposium on Fluid-Structure Interactions, Flow-Sound

Interactions, and Flow-Induced Vibration and Noise, FSI2 and FIV+N, Montreal, QC, Canada (Vol. 3, pp. 553-563). doi: 10.1115/FEDSM-ICNMM2010-30495

Marn, J., & Catton, I. (1990). Flow-Induced Vibration Problem in a Simple Cylinder Array - One Dimensional Unsteady Integral Approach In P. H. Rotih (Ed.) *ASME Forum on Unsteady flow* (Vol. FED-Vol. 102, PVP-Vol. 204, pp. 19-21). New York: ASME.

Marn, J., & Catton, I. (1991). Flow Induced Vibrations in Cylindrical Bundles: Two Dimensional Analysis into Normal Modes. In F. B. Cheung & L. E. Hochreiter (Eds.), *Numerical Modelling of Basic Heat Transfer Phenomena in Nuclear Systems* (Vol. HTD-Vol.165, pp. 9-14). New York: ASME.

Marn, J., & Catton, I. (1992). *On the Instability of Two Phase Cross Flow through a Staggered Cylinder Array.* Paper presented at International Symposium on Flow-Induced Vibrations and Noise, New York, U.S.A (Vol. 2, pp. 57-68).

Marquardt, D. W. (1963). An Algorithm for Least-Squares Estimation of Nonlinear Parameters. *Journal of the Society for Industrial and Applied Mathematics, 11*(2), 431-441.

McAdams, W. H., Woods, W. K., & Heroman, L. C. (1942). Vaporization Inside Horizontal Tubes - II: Benzene-Oil Mixtures. *Transactions of ASME, 64*(3), 193-200.

Moran, J. E., & Weaver, D. S. (2013). On the Damping in Tube Arrays Subjected to Two-Phase Cross-Flow. *ASME Journal of Pressure Vessel Technology, 135*(3), Artn 030906. doi: 10.1115/1.4023421

Mureithi, N. W., Nakamura, T., Hirota, K., Murata, M., Utsumi, S., Kusakabe, T., & Takamatsu, H. (2002). Dynamics of an In-Line Tube Array Subjected to Steam-Water Cross-Flow. Part II: Unsteady Fluid Forces. *Journal of Fluids and Structures, 16*(2), 137-152. doi: 10.1006/jfls.2001.0407

Mureithi, N. W., Zhang, C., Ruel, M., & Pettigrew, M. J. (2005). Fluidelastic Instability Tests on An Array of Tubes Preferentially Flexible in the Flow Direction. *Journal of Fluids and Structures, 21*(1), 75-87. doi: 10.1016/j.jfluidstructs.2005.03.010

Nakamura, T., Fujita, Y., & Sumitani, T. (2014). Study on In-Flow Fluidelastic Instability of Triangular Tube Arrays Subjected to Air Cross Flow. *ASME Journal of Pressure Vessel Technology, 136*(5), Artn 051302. doi: 10.1115/1.4027618

Naudascher, E., & Rockwell, D. (2005). *Flow-Induced Vibrations: An Engineering Guide*. New York: Dover Publications.

Noghrehkar, G. R., Kawaji, M., & Chan, A. M. C. (1999). Investigation of Two-Phase Flow Regimes in Tube Bundles under Cross-Flow Conditions. *International Journal of Multiphase Flow, 25*(5), 857-874. doi: 10.1016/S0301-9322(98)00075-5

Olala, S., Mureithi, N., Sawadogo, T., & Pettigrew, M. J. (2014). *Streamwise fluidelastic forces in tube arrays subjected to two-phase flows.* Paper presented at ASME 2014 Pressure Vessels & Piping Conference (PVP2014-28153), Anaheim, California, USA (Vol. 4, pp. V004T004A014). doi: doi:10.1115/PVP2014-28153

Olala, S., & Mureithi, N. W. (2014). *Streamwise Fluidelastic Instability of Tube Arrays in Two-Phase Cross-Flow.* Paper presented at ASME 2014 International Mechanical Engineers Congress and Exposition Montréal, QC, Canada (Vol. 4A, pp. V04AT04A079). doi: 10.1115/IMECE2014-39234

Olala, S., & Mureithi, N. W. (2016a). Prediction of Streamwise Fluidelastic Instability of Tube Array in Two-Phase Flows and Effect of Frequency Detuning (Paper submitted) *ASME Journal of Pressure Vessel Technology*. doi: 10.1115/1.4034467

Olala, S., & Mureithi, N. W. (2016b). Streamwise Fluidelastic Vibration of a Triangular Tube Array in Two-Phase Flow. Part I: Unsteady Fluid Forces and Time Delay Estimation (paper submitted). *Journal of Fluids and Structures*.

Olala, S., & Mureithi, N. W. (2016c). Streamwise Fluidelastic Vibration of a Triangular Tube Array in Two-Phase Flow. Part II: Fluidelastic Instability Analysis (paper submitted). *Journal of Fluids and Structures*.

Paidoussis, M. P. (1982). A review of Flow-Induced Vibrations in Reactors and Reactor Components. *Nuclear Engineering and Design, 74*(1), 31-60. doi: 10.1016/0029-5493(83)90138-3

Païdoussis, M. P., de Langre, E., & Price, S. J. (2011). *Fluid-Structure Interactions : Cross-Flow-Induced Instabilities*. New York: Cambridge University Press.

Paidoussis, M. P., Mavriplis, D., & Price, S. J. (1984). A potential Flow Theory for the Dynamics of Cylinder Arrays in Cross-Flow. *Journal of Fluid Mechanics, 146* 227-252. doi: 10.1017/S002211208400183X

Paidoussis, M. P., & Price, S. J. (1988). Mechanisms Underlying Flow-Induced Instabilities of Cylinder Arrays in Cross-Flow. *Journal of Fluid Mechanics, 187* 45-59. doi: 10.1017/S0022112088000333

Paidoussis, M. P., Price, S. J., & Mureithi, N. W. (1996). On the Virtual Nonexistence of Multiple Instability Regions for Some Heat-Exchanger Arrays in CrossFlow. *ASME Journal of Fluids Engineering 118*(1), 103-109. doi: 10.1115/1.2817486

Pettigrew, M. J., Carlucci, L. N., Taylor, C. E., & Fisher, N. J. (1991). Flow-Induced Vibration and Related Technologies in Nuclear Components. *Nuclear Engineering and Design, 131*(1), 81-100. doi: 10.1016/0029-5493(91)90319-D

Pettigrew, M. J., Rogers, R. J., & Axisa, F. (1986). *Damping of Multispan Heat Exchanger Tubes - Part 2: In Liquids.* Paper presented at ASME 1986 Pressure Vessel and Piping Conference, Chicago, IL, U.S.A (Vol. 104, pp. 89-98).

Pettigrew, M. J., & Taylor, C. E. (1991). Fluidelastic Instability of Heat-Exchanger Tube Bundles - Review and Design Recommendations. *ASME Journal of Pressure Vessel Technology, 113*(2), 242-256. doi: 10.1115/1.2928752

Pettigrew, M. J., & Taylor, C. E. (1994). Two-Phase Flow-Induced Vibration: An Overview (Survey Paper). *ASME Journal of Pressure Vessel Technology, 116*(3), 233-253. doi: 10.1115/1.2929583

Pettigrew, M. J., & Taylor, C. E. (1997). *Damping of Heat Exchanger Tubes in Two-Phase Flow.* Paper presented at Fourth International Symposium on FSI, AE & FIV+N, ASME International Congress, Dallas, Texas, U.S.A (Vol. 53.2, pp. 407-418).

Pettigrew, M. J., & Taylor, C. E. (2003). Vibration Analysis of Shell-and-Tube Heat Exchangers: An Overview - Part 1: Flow, Damping, Fluidelastic Instability. *Journal of Fluids and Structures, 18*(5), 469-483. doi: 10.1016/j.jfluidstructs.2003.08.007

Pettigrew, M. J., & Taylor, C. E. (2009). Vibration of a Normal Triangular Tube Bundle Subjected to Two-Phase Freon Cross Flow. *ASME Journal of Pressure Vessel Technology, 131*(5), Artn 051302. doi: 10.1115/1.3147985

Pettigrew, M. J., Taylor, C. E., Jong, J. H., & Currie, I. G. (1995). Vibration of a Tube Bundle in Two-Phase Freon Cross-Flow. *ASME Journal of Pressure Vessel Technology, 117*(4), 321-329. doi: 10.1115/1.2842130

Pettigrew, M. J., Taylor, C. E., & Kim, B. S. (1989). Vibration of Tube Bundles in Two-Phase Cross-Flow: Part 1—Hydrodynamic Mass and Damping. *ASME Journal of Pressure Vessel Technology, 111*(4), 446-477. doi: 10.1115/1.3265705

Pettigrew, M. J., Taylor, C. E., & Kim, B. S. (2001). The Effects of Bundle Geometry on Heat Exchanger Tube Vibration in Two-Phase Cross Flow. *ASME Journal of Pressure Vessel Technology, 123*(4), 414-420. doi: 10.1115/1.1388236

Pettigrew, M. J., Tromp, J. H., & Mastorakos, J. (1985). Vibration of Tube Bundles Subjected to Two-Phase Cross-Flow. *ASME Journal of Pressure Vessel Technology, 107*(4), 335-343. doi: 10.1115/1.3264461

Pettigrew, M. J., Tromp, J. H., Taylor, C. E., & Kim, B. S. (1989). Vibration of Tube Bundles in Two-Phase Cross-Flow: Part 2 - Fluidelastic Instability. *ASME Journal of Pressure Vessel Technology, 111*(4), 478-487. doi: 10.1115/1.3265706

Pettigrew, M. J., Zhang, C., Mureithi, N. W., & Pamfil, D. (2005). Detailed Flow and Force Measurements in a Rotated Triangular Tube Bundle Subjected to Two-Phase Cross-Flow. *Journal of Fluids and Structures, 20*(4), 567-575. doi: 10.1016/j.jfluidstructs.2005.02.007

Price, S. J. (1995). A Review of Theoretical Models for Fluidelastic Instability of Cylinder Arrays in Cross-Flow. *Journal of Fluids and Structures, 9*(5), 463-518. doi: 10.1006/jfls.1995.1028

Price, S. J., & Paidoussis, M. P. (1982). *A Theoretical Investigation of the Parameters Affecting the Fluidelastic Instability of a Double Row of Cylinders Subject to Cross-Flow.* Paper presented at 3rd International Conference on Vibrations in Nuclear Plant, Keswick, U.K. (Vol. 1, pp. 107-119).

Price, S. J., & Paidoussis, M. P. (1983). Fluidelastic Instability of an Infinite Double Row of Circular Cylinders Subject to a Uniform Cross-Flow. *ASME Journal of Vibration, Acoustics, Stress and Reliability in Design, 105*(1), 59-66. doi: 10.1115/1.3269067

Price, S. J., & Paidoussis, M. P. (1984). An Improved Mathematical Model for the Stability of Cylinder Rows Subject to Cross-Flow. *Journal of Sound and Vibration, 97*(4), 615-640. doi: 10.1016/0022-460X(84)90512-1

Price, S. J., & Paidoussis, M. P. (1985). Fluidelastic Instability of a Full Array of Flexible Cylinders Subject to Cross-Flow. In E. H. Dowell & M. K. Au-Yang (Eds.), *Fluid-Structure Interaction and Aerodynamic Damping* (pp. 171-192). New York: ASME.

Price, S. J., & Paidoussis, M. P. (1986a). A Constrained-Mode Analysis of the Fluidelastic Instability of a Double Row of Flexible Circular Cylinders Subject to Cross-Flow: A

Theoretical Investigation of System Parameters. *Journal of Sound and Vibration, 105*(1), 121-142. doi: 10.1016/0022-460X(86)90225-7

Price, S. J., & Paidoussis, M. P. (1986b). A Single-Flexible-Cylinder Analysis for the Fluidelastic Instability of an Array of Flexible Cylinders in Cross-Flow. *ASME Journal of Fluids Engineering 108*(2), 193-199. doi: 10.1115/1.3242562

Price, S. J., Paidoussis, M. P., & Giannias, N. (1990). A Generalized Constrained-Mode Analysis for Cylinder Arrays in Cross-Flow. *Journal of Fluids and Structures, 4*(2), 171-202. doi: 10.1016/0889-9746(90)90072-D

Rao, S. S. (2004). *Mechanical Vibrations* (4th ed.). Upper Saddle River, New Jersey: Pearson Education, Inc.

Roberts, B. W. (1962). *Low Frequency, Self-Excited Vibration in a Row of Circular Cylinders Mounted in an Airstream.* (Ph.D Thesis, University of Cambridge, Cambridge, UK).

Roberts, B. W. (1966). *Low Frequency, Aeroelastic Vibrations in a Cascade of Circular Cylinders*. Mechanical Engineering Science Monograph, (No.4). Institution of Mechanical Engineers, London.

Rogers, R. J., Taylor, C., & Pettigrew, M. J. (1984). *Fluid Effects on Multi-Span Heat Exchanger Tube Vibration.* Paper presented at ASME 1984 Pressure Vessels and Piping Conference, San Antonio, Texas, U.S.A. (Vol. H00316, pp. 17-26).

S.C.E. (2013). *San Onofre Nuclear Generating Station Unit 2 Return To Service Report*. Southern California Edison. Retrieved from http://www.nrc.gov/docs/ML1228/ML12285A263.pdf

Sawadogo, T. (2016). *Modelling of Fluidelastic Instability in Tube Arrays Subjected to Two-Phase Freon Flow using Air-Water Quasi-Static Force Coefficients*. Paper presented at 11th International Conference on Flow-Induced Vibration, Hague, Netherlands.

Sawadogo, T., & Mureithi, N. (2014a). Fluidelastic Instability in a Rotated Triangular Tube Array Subjected to Two-Phase Cross-Flow. Part II: Experimental Tests and Comparison with Theoretical Results. *Journal of Fluids and Structures, 49* 16–28. doi: 10.1016/j.jfluidstructs.2014.04.013

Sawadogo, T., & Mureithi, N. (2014b). Fluidelastic Instability Study in a Rotated Triangular Tube Array Subjected to Two-Phase Cross-Flow. Part I: Fluid Force Measurements and

Time Delay Extraction. *Journal of Fluids and Structures, 49* 1–15. doi: 10.1016/j.jfluidstructs.2014.02.004

Schroder, K., & Gelbe, H. (1999a). New Design Recommendations for Fluidelastic Instability in Heat Exchanger Tube Bundles. *Journal of Fluids and Structures, 13*(3), 361-379. doi: 10.1006/jfls.1999.0208

Schroder, K., & Gelbe, H. (1999b). Two- and three-dimensional CFD-simulation of flow-induced vibration excitation in tube bundles. *Chemical Engineering and Processing, 38*(4-6), 621-629. doi: Doi 10.1016/S0255-2701(99)00063-X

Seitanis, S. A., Anagnostpoulos, P., & Bearman, P. W. (2005). An Experimental Study of the In-Line Oscillations of a Closely Spaced Row Of Cylinders in Cross-Flow. *Journal of Fluids and Structures, 21*(2), 211-226. doi: 10.1016/j.jfluidstructs.2005.07.004

Shahriary, S., Mureithi, N. W., & Pettigrew, M. J. (2007). *Quasi-Static Forces and Stability Analysis in a Triangular Tube Bundle Subjected to Two-Phase Cross-Flow*. Paper presented at ASME 2007 Pressure Vessels and Piping Conference (Vol. 4, pp. 245-252). doi: 10.1115/PVP2007-26017

Simpson, A., & Flower, J. W. (1977). An Improved Mathematical Model for The Aerodynamic Forces on Tandem Cylinders with Aeroelastic Applications. *Journal of Sound and Vibration, 51*(2), 183-217. doi: 10.1016/S0022-460X(77)80032-1

Tanaka, H., & Takahara, S. (1980). Unsteady Fluid Dynamic Force on Tube Bundle and Its Dynamic Effect on Vibration. In M. K. Au-Yang (Ed.) *Flow-Induced Vibration of Power Plant Components* (Vol. 41, pp. 77-92). New York: ASME.

Tanaka, H., & Takahara, S. (1981). Fluid Elastic Vibration of Tube Array in Cross Flow. *Journal of Sound and Vibration, 77*(1), 19-37. doi: 10.1016/S0022-460X(81)80005-3

Tanaka, H., Takahara, S., & Ohta, K. (1982). Flow-Induced Vibration of Tube Arrays with Various Pitch-to-Diameter Ratios. *ASME Journal of Pressure Vessel Technology, 104*(3), 168-174. doi: 10.1115/1.3264199

Taylor, C. E., Currie, I. G., Pettigrew, M. J., & Kim, B. S. (1989). Vibration of Tube Bundles in Two-Phase Cross-Flow: Part 3—Turbulence-Induced Excitation. *ASME Journal of Pressure Vessel Technology, 111*(4), 488-500. doi: 10.1115/1.3265707

Thome, J. R. (2010). *Engineering Data Book III*. Retrieved from http://www.wlv.com/products2/databook/db3/DataBookIII.pdf

Ulbrich, R., & Mewes, D. (1994). Vertical, Upward Gas-Liquid 2-Phase Flow across a Tube Bundle. *International Journal of Multiphase Flow, 20*(2), 249-272. doi: 10.1016/0301-9322(94)90081-7

Violette, R., Pettigrew, M. J., & Mureithi, N. W. (2006). Fluidelastic Instability of an Array of Tubes Preferentially Flexible in the Flow Direction Subjected to Two-Phase Cross Flow. *ASME Journal of Pressure Vessel Technology, 128*(1), 148-159. doi: 10.1115/1.2138064

Weaver, D. S. (1993). Vortex Shedding and Acoustic Resonance in Heat Exchanger Tube Arrays. In M. K. Au-Yang (Ed.) *Technology of the 90's* (pp. 776-810). New York: ASME

Weaver, D. S. (2008). *Some Thoughts on the Elusive Mechanism of Fluidelastic Instability in Heat Exchanger Tube Arrays.* Paper presented at The 9th International Conference on Flow-Induced Vibrations FIV-2008, Prague, Czech Republic (pp. 21-28).

Weaver, D. S., & Elkashlan, M. (1981a). The Effect of Damping and Mass Ratio on the Stability of a Tube Bank. *Journal of Sound and Vibration, 76*(2), 283-294. doi: 10.1016/0022-460X(81)90355-2

Weaver, D. S., & Elkashlan, M. (1981b). On the Number of Tube Rows Required to Study Cross-Fow Induced Vibrations in Tube Banks. *Journal of Sound and Vibration, 75*(2), 265-273. doi: 10.1016/0022-460X(81)90344-8

Weaver, D. S., & Fitzpatrick, J. A. (1988). A Review of Cross-Flow Induced Vibrations in Heat Exchanger Tube Arrays. *Journal of Fluids and Structures, 2*(1), 73-93. doi: 10.1016/S0889-9746(88)90137-5

Weaver, D. S., & Fitzpatrick, J. A. (1988). A review of cross-flow induced vibrations in heat exchanger tube arrays. *Journal of Fluids and Structures, 2* 73-93.

Weaver, D. S., Fitzpatrick, J. A., & Elkashlan, M. (1987). Strouhal numbers for heat exchanger tube arrays in cross flow. *Journal of pressure vessel technology, 109*(2), 219-223.

Weaver, D. S., & Koroyannakis, D. (1982). The Cross-Flow Response of a Tube Array in Water—A Comparison With the Same Array in Air. *ASME Journal of Pressure Vessel Technology, 104*(3), 139-146. doi: 10.1115/1.3264195

Weaver, D. S., & Koroyannakis, D. (1983). Flow-Induced Vibrations of Heat Exchanger U-Tubes: A Simulation to Study the Effects of Asymmetric Stiffness. *ASME Journal of Vibration, Acoustics, Stress and Reliability in Design 105*(1), 67-75. doi: 10.1115/1.3269069

Weaver, D. S., & Schneider, W. (1983). The Effect of Flat Bar Supports on the Crossflow Induced Response of Heat Exchanger U-Tubes. *Journal of Engineering for Power, 105*(4), 775-781. doi: 10.1115/1.3227481

Weaver, D. S., Ziada, S., Ay-Yang, M. K., Chen, S. S., Paidoussis, M. P., & Pettigrew, M. J. (2000). Flow-Induced Vibrations in Power and Process Plant Components—Progress and Prospects. *ASME Journal of Pressure Vessel Technology, 122*(3), 339-348. doi: 10.1115/1.556190

Yetisir, M., & Weaver, D. S. (1993a). An Unsteady Theory For Fluidelastic Instability in an Array of Flexible Tubes in Cross-Flow. Part I: Theory. *Journal of Fluids and Structures, 7*(7), 751-766. doi: 10.1006/jfls.1993.1044

Yetisir, M., & Weaver, D. S. (1993b). An Unsteady Theory for Fluidelastic Instability in an Array of Flexible Tubes in Cross-Flow. Part II: Results and Comparison With Experiments. *Journal of Fluids and Structures, 7*(7), 767-782. doi: 10.1006/jfls.1993.1045

Ziada, S. (2006). Vorticity Shedding and Acoustic Resonance in Tube Bundles. *Journal of the Brazilian Society of Mechanical Sciences and Engineering, 28*(2), 186-189. doi: 10.1590/S1678-58782006000200008

Ziada, S., & Oengoren, A. (1992). Vorticity Shedding and Acoustic Resonance in an In-Line Tube Bundle - Part I: Vorticity Shedding. *Journal of Fluids and Structures, 6*(3), 271-292. doi: 10.1016/0889-9746(92)90010-Z

Ziada, S., & Oengoren, A. (1993). Vortex Shedding in an In-line Tube Bundle with Large Tube Spacings. *Journal of Fluids and Structures, 7*(6), 661-687. doi: 10.1006/jfls.1993.1039